Doctoral Dissertation

FREE ACCESS TRANSMISSION LINE USING COPLANAR WAVEGUIDE FOR ON-BODY COMMUNICATION

人体近傍通信用コプレーナ線路を用いた

フリーアクセス伝送線路

Graduate School of Engineering

Yokohama National University

Tran Thi Lan

August 2018

This dissertation was reviewed and approved by the following:

Hiroyuki Arai
Professor
Research advisor
Chair of Committee

Takehiko Adachi
Professor
Review Committee Member

Toshihiko Baba
Professor
Review Committee Member

Nobuhiro Kuga
Associate Professor
Review Committee Member

Koichi Ichige
Associate Professor
Review Committee Member

ABSTRACT

We propose an approach to enhance transmission quality between on-body sensors or antennas by using a free access segmented coplanar waveguide (SCPW).

The utilization of supplementary waveguides embed into garments such as “smart suit” to enhance transmission characteristics between on-body antennas or sensors has been previously presented. The supplementary waveguides create a coverage area around themselves, and wireless devices can electromagnetically couple with them at any discretionary position. Moreover, users of on-body wireless communication devices utilize their personal waveguides freely, and therefore, a high security level can be acquired. Thus, the idea of use of supplementary waveguides for improving the transmission on body is a new, much simpler, and high security solution as compared to other solutions like wired connections, diversity reception or increment of ground plane size to lessen body impacts, that making on-body system become more complex, less adaptable and sensitive to body postures.

Getting from this thought, we propose a novel single-layer transmission line or SCPW with non-contact coupling for antennas to improve NLOS links of on-body wireless communication. The SCPW is associated electromagnetically by two half-wavelength resonators put in an order on both sides of the center line. The resonators equip the function to couple the SCPW with top and bottom antennas at arbitrary positions along the transmission line, which is a unique feature of the proposed geometry.

The fundamental effectiveness of SCPW is affirmed at 5.12 GHz by a thin dielectric substrate and at 2.45 GHz by a flexible paper substrate and a silver-ink conductor. The propagation loss is greatly reduced more than 20 dB by this SCPW in on-body communication between abdomen and back sides, which is confirmed by measured results on the PEC plane, a phantom and a real body. In addition, the specific absorption rate (SAR) is fulfilled when SCPW are set close human body.

Finally, the execution of the SCPW is compared with a conductive strip line (CSL) which has a good performance in improving on-body communication in some particular cases. Thus, the CSL can be a simple answer for paths on body.

TABLE OF CONTENTS

LIST OF FIGURES

LIST OF TABLES

LIST OF ABBREVIATIONS

SCPW	Segmented Coplanar Waveguide
CSL	Conductive Strip Line
TL	Transmission Line
EMPro	Electromagnetic Professional
CST	Computer Simulation technology
ADS	Advanced Design System
LOS	Line-Of-Sight
NLOS	Non-Line-Of-Sight
3D	3 Dimensional
CAD	Computer Aided Design
FEM	Finite Element Method
FDTD	Finite=Difference Time-Domain method

CHAPTER 1

INTRODUCTION

This chapter talks about motivations and novelties of our study in Section 1.1. We propose a solution to reduce the propagation loss between on-body antennas by utilizing a subsidiary waveguide or a free access segmented coplanar waveguide. Besides, simulation tools are introduced in Section 1.2. In Section 1.3, the flow of the thesis is presented.

1.1 Motivation and novelty

Wireless body area networks (WBANs) have a great deal of uses from human services and telemedicine up to wellness and sports training, intelligent gaming, and individual data sharing and validation. WBANs can likewise be sent in hazardous situations to help secure unwavering troopers, specialists on call and remote ocean or space adventurers. In this manner, innovations to enhance the reliability for WBANs are constantly pulled in by analysts [1].

Some communication standards are deployed for WBANs, for example, Bluetooth, Zigbee, and UWB. A standout amongst the most crucial issues is the reliability of the propagation path between two antennas/ sensors in non line-of-sight (NLOS) due to the heavy attenuation by human body. An easy answer for this issue is by applying flexible cables. But, the system becomes complex by numerous connectors and cables, which causes users of the sensors uncomfortable, particularly for moving users. Thus, wireless connections are more

adaptable for the on-body sensors, and the propagation loss decline between the sensors is robustly demanded for low power operation.

The researches of propagation loss of the on-body paths suggest that the loss relies upon the position of antennas on body and body posture [2]-[4]. For instance, the belt-to-chest connection gives low loss whereas higher losses are in the connections of belt-to-head and belt-to-wrist. In addition, losses of NLOS paths are at least 45dB [28]. To decrease these body effects, the ground plane size is stretched out to decouple the antennas with the body [5], [6], resulting in less flexibility in applications on body. Another way is the diversity reception [2], [7]-[9] to mitigate fading effects of the propagation channels using more than two antennas at the receiver, which is valuable for dynamic surroundings like moving bodies.

The use of supplementary waveguides is considered as a new method for on-body communication [10]. These waveguides produce a coverage area around themselves and electromagnetically couple with wireless devices at any arbitrary position. They reduce propagation losses between on-body antennas as compared to those in free space. The users use their own waveguides independently, and therefore, a high security level can be obtained. In this manner, the application of supplementary waveguides for enhancing the transmission characteristics on body is a new, much simpler, and high security solution as compared to other solutions such as wired connections, diversity reception or increment of ground plane size to lessen body effects, that causes the on-body system turn out more entangled, less flexible and unstable to body postures.

The wearable sheet-shaped waveguide [10] consisting of double-layered patch resonators as a smart suit makes an autonomous low-loss channel for on-body wireless devices. But, a disadvantage of this smart suit is the utilization of a metallic ground plane which is less convenient and less breathable when it is integrated into a wearable fabric. Its double-layered structure makes the mass production process difficult and expensive. To simplify this sheet waveguide, a periodic bandpass-filter microstrip transmission line is also proposed for on-body links [11], [12], [26]. However, due to the substrate ground plane for the transmission line, its flexibility is still restricted.

This thesis proposes a novel single layer transmission line or a free-access segmented coplanar waveguide (SCPW) with non-contact coupling for antennas to improve links of on-body wireless communication, particularly for NLOS links. This transmission line not just has the previously mentioned benefits of supplementary waveguides, yet additionally high flexibility because it is fabricated by paper substrate with silver-ink conductor. The ground plane layer at the bottom of the transmission line is removed by applying a segmented coplanar structure. It can be effectively embedded into clothes at any position and can be bent around waist or shoulder of any bodies with little effect by bending. In addition, contrasted with the transmission line by a microstrip line in [11], [12], [26], the proposed transmission line has a 5-times wider bandwidth and the 10-times thinner substrate thickness. Because of applying the coplanar waveguide, the transmission line is called another name - ***a segmented coplanar waveguide (SCPW)***.

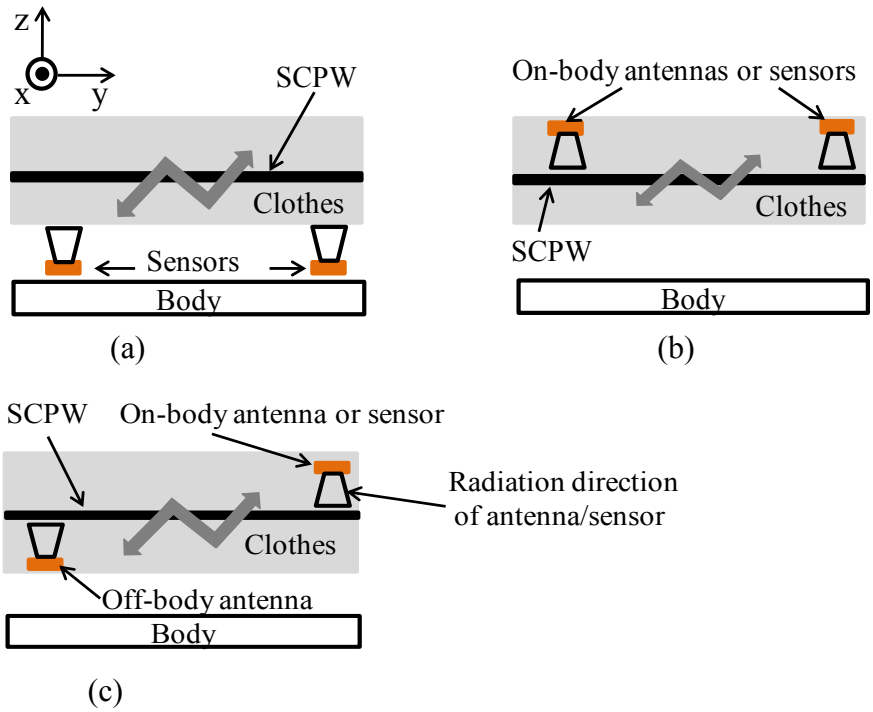

Fig. 1.1. Types of on-body paths are aided by SCPW (Side-view): (a) Between on-body sensors (b) Between antennas/ sensors on the cloth surface; (c) between an off-body antenna and a sensor at the other side of the SCPW.

Communication paths presented in this thesis are (a) between sensors or (b) amongst sensors and antennas. The sensors are appended on the body to monitor vital information or

on the surface of clothes to obtain outside environment data. All sensors are included antennas to transmit or receive data. The antennas for on/off-body communications are installed into clothes or outside surface of clothes, which is very difficult to connect sensors on the body with antenna-feeding cables. Non-contact coupling between transmission lines and antennas are unequivocally asked for on-body communication systems. To analyze on-body propagation, three cases are considered as illustrated in Fig. 1.1, where antennas and the transmission line are implanted inside clothes, sensors are attached on the body or the cloth surface. The antennas radiate toward the transmission line in all the cases. It is proposed as a typical application of the SCPW, vital sensors in the front side of the body and the antennas placed the back as shown in Fig. 1.2 can communicate with each other through the SCPW. Non-contact communication paths are given by the proposed transmission line. This enables the on-body sensors/ antennas to be deployed easily and flexibly in practice. The sensors antennas can communicate to each other, even at different sides of the transmission line, which cannot be implemented by a microstrip line [11], [12]. Especially, more than two sensors/ antennas can be concurrently excited on the transmission line. This is more effective compared to wired connections when the number of sensors is increased. The transmission line greatly reduces the transmission loss between the on-body sensors/ antennas up to more than 20 dB for the NLOS scenario. The terminology “non-contact” means that the on-body sensors/ antennas wirelessly connect with each other through electromagnetic waves in the transmission line without being connected to the transmission line whereas the term “free access” indicates that on-body wireless devices can couple with the SCPW at any arbitrary positions above it.

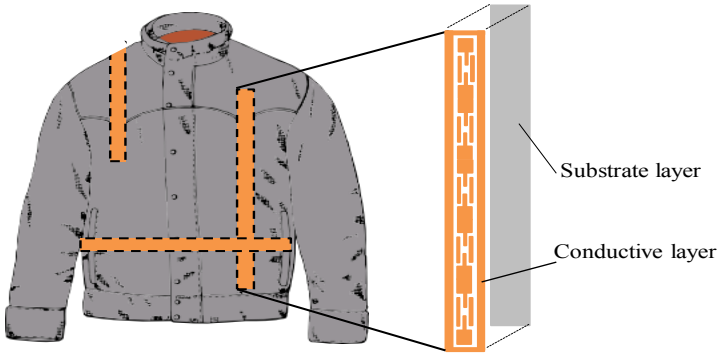

Fig. 1.2. A new smart suit with the single layer non-contact coupling transmission line by a coplanar waveguide.

1.2 Simulation tools

This section introduces simulation software used in our study. Both CST software [16] and EMPro software [17] are used. These tools are popular and strong tools for designing antennas or waveguides.

1.2.1 EMpro software

EMPro (Electromagnetic Professional) is a three-dimensional full wave electromagnetic solver. The following key abilities are provided by the EMPro:

- **Modern and effective 3D solid modeling medium**

EMPro gives the flexibility of creating arbitrary 3D models and the usefulness of importing existent CAD files. You can draw 3D models, include material properties, install simulations, and observe results—all inside the EMPro medium.

- **Simulation technology in both time-domain and frequency-domain**

We can analyze 3D structures in EMPro using the similar FEM simulator accessible in ADS. FEM is a frequency-domain technology generally utilized for RF/microwave applications. For electrically vast issues like antennas, we can use the finite difference time domain (FDTD) simulator.

- **Integration with ADS**

Parameterized 3D elements can be draw in EMPro and put in a layout design in ADS. Then, we can use 3D FEM simulator in ADS to simulate the mix of the 2D layout and the 3D EM elements.

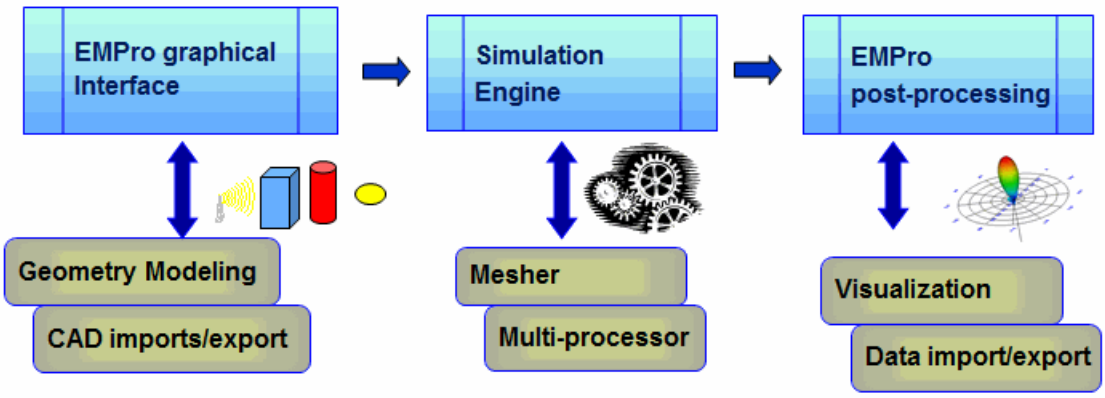

Fig. 1.3 EMPro design flow [17].

Fig. 1.3 illustrates the EMPro design flow. To run an EMPro project, we start with the creation of the physical geometry. In the Geometry window, objects or models can be created from scratch or imported from external files. The Specify Orientation tab window gives exceptional functionality for situating physical parts in the simulation space. Then, we can set material definitions in the Material Editor and store in the Project tree so that we can easily apply to geometry objects by drag-and-drop.

After the geometry objects are drawn and set valid material definitions, discrete circuit components can be included within the Component Tools dialog of the Geometry workspace window. Circuit component definitions are provided within the Circuit Component Definition Editor and saved as Definition objects in the Project Tree. By drag-and-drop, a definition can be applied easily to the appropriate components. In addition to discrete sources and external excitation sources can be included within the External Excitation Editor. Waveform definitions are modified in the Waveform Editor as Definition objects within the Project Tree, and are applied by drag-and-drop to objects that require waveform definitions.

The project can be meshed now. During the meshing operation, materials are applied to the appropriate cell edges. Meshing runs automatically in EMPro as soon as the project is viewed within Mesh View. In the FDTD and FEM simulations, applying the outer boundary conditions which regulate how EMPro treats the boundaries of the project is modified within the Outer Boundary Editor. This editor is approached by double-clicking on the corresponding branch in the Project Tree. For FDTD simulations, define grid settings. For FEM simulations, the FEM padding settings is applied.

Once various components of the project are defined, Sensor objects can be added. Sensors are simply objects that acquire data. There are several different kinds of sensors depending on what type of data they require. Calculation criteria are adjusted within the Simulations workspace window when sensors have been added to get all desired results. Specifications such as source type, parameter sweep definitions, S-parameter feeds, frequencies, total/scattered field interfaces, and termination criteria are defined for each simulation. After running the calculation, we can view the results from the Results workspace window.

Mesh Setup

After the geometry objects are drawn and set the material, the grid can be started within the Grid Tools interface.

- In FDTD simulations, a rectangular mesh is produced depending on the shapes of the objects. Initial mesh is naturally produced to enhance accuracy and running time. Fixed point meshing automatically aligns the mesh with object boundaries. The mesh size can be adjusted to make additionally trade-offs between accuracy and running speed.
- In a similar way, a tetrahedral mesh is created for FEM simulations. The mesh is upgraded for speed/accuracy through a procedure of automatic adaptive refinement.

While selecting a suitable cell size for the mesh, we need to take into account the primary limitation on cell size. A cell cannot be bigger than 1/10 of the smallest wavelength utilized to excite the model. Subsequently, the maximum cell size can be resolved from:

$$L_{max} = c/(10*f) \tag{1.1}$$

where

L_{max} : the maximum cell dimension,

c: the speed of light, 3×10^8 m/s in free space,

f : the frequency of excitation (Hz).

1.2.2 CST MWS software

CST MICROWAVE STUDIO (CST MWS) is an expert instrument for the 3D EM simulation of high frequency objects. CST MWS' incomparable execution makes it the first selection in principal R&D centers.

CST MWS empowers the quick and precise investigation of high frequency (HF) devices such as antennas, filters, couplers, planar and multi-layer structures and SI and EMC effects. Particularly easy to understand, CST MWS rapidly gives you knowledge into the EM conduct of your high frequency projects.

CST advances Complete Technologies for 3D EM. Users of our software are given extraordinary adaptability in tackling a wide application scope through the diversity of accessible solver technologies. Other than the lead module, the comprehensively material Time Domain solver and the Frequency Domain solver, CST MWS offers advance solver modules for particular applications. Filters for the import of particular CAD files and the extraction of SPICE parameters improve design possibilities and reduces running time. What's more, CST MWS can be installed in different industry standard work processes through the CST STUDIO SUITE UI.

CST MICROWAVE STUDIO at present offers various types of solver modules. The accessibility of these solvers relies upon your permit record. Our permit bolsters two sorts of solver:

Time Domain Solver

There are two solvers in time domain. Both of them use hexahedral meshes. These solvers are strikingly effective for most high frequency applications, for examples, connectors, transmission lines, filters, antennas and so forth and can get the whole wideband frequency results of the simulated object from a single calculation run.

Transient solver: The Transient solver is used the Finite Integration Technique (FIT). In blend with the Perfect Boundary Approximation (PBA) aspect and the Thin Sheet Technique (TST) expansion, this solver can increment the exactness of the simulation considerably in contrast with simulation techniques employing a traditional hexahedral mesh.

TLM solver: The TLM solver utilizes the Transmission Line Matrix (TLM) technique to furnish you with exact wideband results and provides an exceptionally proficient octree-based meshing algorithm which effectively diminishes the overall cell count. This solver is particularly appropriate to EMC/EMI/E3 applications.

Frequency Domain Solver

Similar to the transient solver, the primary function of the frequency domain solver module is to compute S-parameters. Because of this way, each frequency sample demands another condition system to be set up and solved, the ratio between simulation time and frequency samples is linear if not unique techniques are used to quicken runs of subsequent frequency domain solver. Therefore, the smaller number of frequency samples is calculated,

the faster the frequency domain solver is. Subsequently, a wideband S-parameter simulation with adaptively picked frequency samples is carried out to underrate the total of equation systems which need to be solved. A reduced-order model technique is alternatively accessible to proficiently generate wideband results. Particularly for lower frequency issues with a reasonable number of mesh cells, the frequency domain solver is extremely appropriate. If a direct equation system solver can be used for the certain issue depending on the amount of memory available, the running time does not increment essentially when the quantity of ports and modes increases. Besides, the frequency domain solver is a decent decision for robustly resonant models because these are set apart by long settling times of the time domain signals. Moreover, electric and monitors of magnetic fields can be computed in a post-processing step very fast at a specific frequency.

1.3 Outline of Contents

The flow of the thesis is shown in Fig. 1.3. The thesis comprises of six chapters. Chapter 1 is "Introduction", where presents the motivation and novelties of our study in Section 1.1, simulation tools used for simulation in Section 1.2, and the main contents of each chapters in Section 1.3. To understand comprehensively the proposed transmission line, it is very important to get basic knowledge on characteristics of coplanar waveguide (CPW) and wireless body area network (WBAN), which are presented in Section 2.1 and 2.2, respectively. In Section 2.1, we discuss about characteristics, applications of CPW, especially considerations when designing CPW. Although tissue characteristics of human body is not too important in this study, but we still discuss about it to get idea to simplify human body model for simulation results in Section 2.2. Moreover, propagation mechanisms on body, challenges for on-body communication are presented in this Section.

Chapter 3 shows details of the design process of the proposed transmission line. First, a summary of free-access mediums where the idea of use of the supplementary waveguides for WBAN comes from is presented in Section 3.1. The design process of the transmission line is presented in Section 3.2. The effect of body on the transmission line is considered in Section 3.3 while bent transmission lines are considered in Section 3.4. Section 3.5 presents

the coupling between the transmission line and external antennas. Chapter 3 is ended by Section 3.6, where some concerns are discussed.

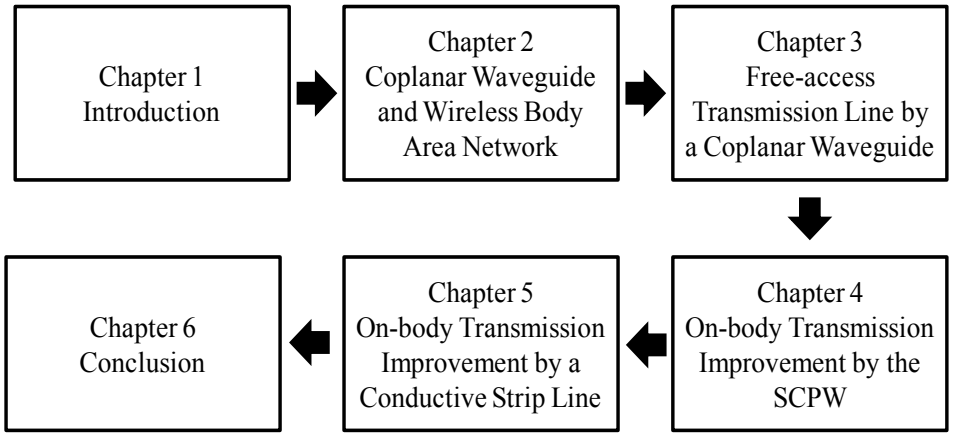

Fig. 1.4. The flow of the thesis.

Chapter 4 is the main content of this thesis. The transmission improvement by the proposed transmission line is presented in this chapter. As discussed in Section 1.1, the transmission line has a flexible structure, and therefore, on-body antennas or sensors can be deployed flexibly in three ways. Thus, the performance of SCPW is also considered following these cases. First, transmission characteristics between two antennas with the transmission line are evaluated on a PEC (Perfect Electric Conductor) plane in both simulation and measurement in Section 4.1. Next, the performance of SCPW is verified by measurement on a phantom and real bodies in Section 4.2. In Section 4.3, SAR (Specific Absorption Rate) is calculated in detail to make sure that the use of the SCPW is safe for human body. Finally, some concerns related to the deployment of antennas are discussed in Section 4.4 such as radiation direction of antennas, radiation loss of the transmission line or orientation of antennas.

Chapter 5 proposes a simple solution for on-body communication in some specific cases by using a conductive strip line (CSL). The performance of the SCPW is compared with that of the CSL which has dimension equivalent to SCPW in Section 5.1. The comparison is done on the PEC plane and a simplified liquid phantom model. From the results in Section 5.1, we find the specific case, where CSL has a good performance as the SCPW. The optimal dimension parameters of the CSL are discussed in Section 5.2 on both the PEC plane and the simplified phantom model. Then, the performance of the CSL with optimal parameters is

verified by measurement on both the PEC plane and the real phantom in Section 5.3 and 5.4, respectively. The calculation of SAR when the CSL is deployed on body is presented at the end of this chapter.

Chapter 6 summarizes the contents which are presented and addressed in this thesis. Besides, future works are discussed in this final chapter.

CHAPTER 2

COPLANAR WAVEGUIDE AND WIRELESS BODY AREA NETWORK

To design the proposed transmission line, it is important to understand about coplanar waveguide (CPW) structures. Thus, this chapter gives a review of CPW and wireless body area network (WBAN) to find advantages of CPW as well as challenges of WBAN. In Section 2.1, we discuss about characteristics, applications and design considerations of CPW. A general architecture, applications, and challenges of WBAN are presented in Section 2.2. Especially, the specific absorption rate (SAR) requirement for human safety is also discussed in Section 2.2.1. Human body characteristics, propagation mechanisms on body, on-body channel model are given in Section 2.2.2.

2.1 Coplanar Waveguide (CPW)

A coplanar waveguide (CPW) manufactured on a dielectric substrate was first exhibited by C. P. Wen in 1969 [15], [27]. An enormous advancement has been made in CPW as of recently. Coplanar waveguides can be widely divided into three types: Conventional CPW, Conductor backed CPW and Micromachined CPW.

In a conventional CPW, there are two semi-infinite ground planes on either side. But, they size are usually finite in a practical circuit. The conductor-backed CPW has an extra ground plane at the base surface of the substrate. This lower ground plane gives mechanical aid to the substrate as well as works as a heat sink for circuits with active devices. The micromachined CPWs are of two kinds, in paticular, the microshield line and the CPW suspended by a silicon dioxide layer over a micromachined groove. However, in our study, we just spotlight on the conventional CPW with finite ground planes. Thus, from here until the end of this thesis the CPW means the conventional CPW.

2.1.1 Characteristics of CPW

Design

A CPW on a dielectric substrate comprises of a center strip line and two ground planes on the two sides as appeared in Fig. 2.1. This geometry supports a quasi-TEM propagation mode. Fig. 2.2 illustrates electric field and magnetic field distributions of the CPW. The CPW has some strong points contrasted with a microstrip line like simple fabrication; shunt and series surface attaching of active or passive devices are made easily; no need to feed via holes; radiation loss is reduced. Additionally, the characteristic impedance is decided by the proportion of *a*/*b*, so size miniaturization is conceivable unbounded, the main punishment being higher attenuation. CPW circuits can be fabricated denser than microstrip line on account of exceptionally powerless cross talk impacts between adjoining lines.

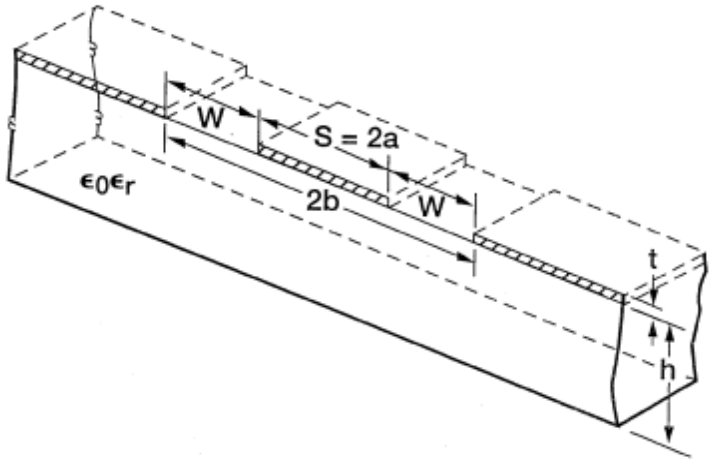

Fig. 2.1. Conventional CPW [15].

Fabricating

Main strong points in fabrication are that CPW fits the utilization of automated pick-and-place and bond assembly devices for surface-mount component placement and interconnection of parts, respectively. In addition, CPW permits the application of computer controlled on-wafer measurement techniques for the equipments and circuit characterization up to a few many GHz. These benefits make CPW based microwave integrated circuits (MICs) and (monolithic microwave integrated circuits) MMICs practical in vast volume.

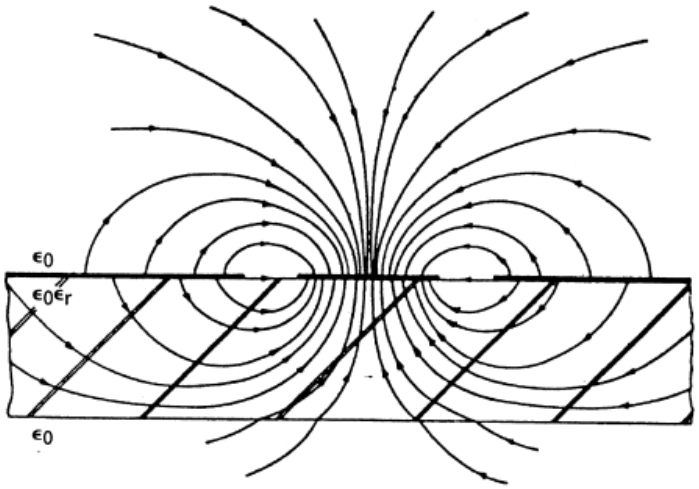

(a) Electric field

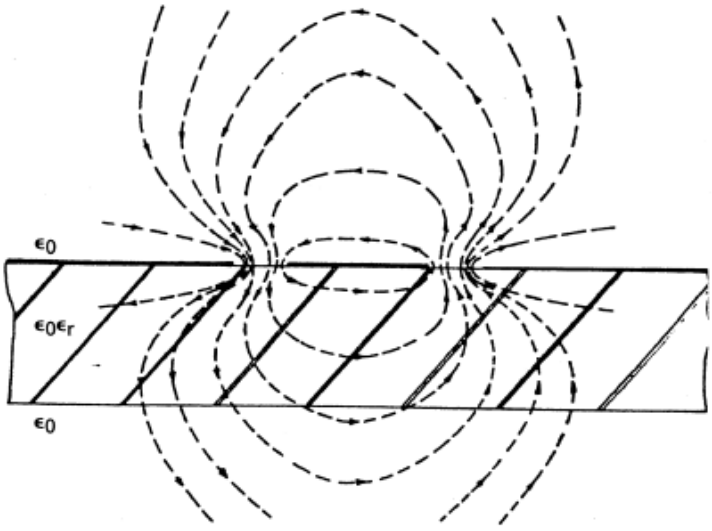

(b) Magnetic field

Fig. 2.2. Electric field and magnetic field distributions [15].

Performance

The quasi-TEM propagation mode on a CPW has low scattering. Hence, it provides the possibility to develop wideband circuits and components. In CPW amplifier circuits, by taking out via holes and its associated parasitic source inductance, the gain can be improved.

2.1.2 Applications of CPW

Coplanar waveguide has typical applications as follows:

- Amplifiers, active combiners, frequency doublers, mixers, and switches: a variety of amplifiers can be made by CPW such us millimeter-wave amplifiers, cryogenically cooled amplifiers, transimpedance amplifiers, cascade amplifiers and so on.
- Microelectromechanical systems (MEMS) metal membrane capacitive witches: In a CPW the conductors are situated on the top surface of a substrate which makes it in a perfect world suited for manufacturing metal membrane, capacitive, shunt-type switches. CPW MEMS shunt switches with good insertion loss characteristics, reasonable switching voltages, fast switching speed, and excellent linearity have recently been proved. These switches provide the possibility to build new age of low-loss high-linearity radio circuits for phased array antennas and communication networks.
- Thin film high-temperature superconducting/ Ferroelectric, tunable Circuits and components: the benefit of utilizing CPW is that just a single surface of the substrate should be covered with high temperature superconducting (HTS) material before designing. HTS low-pass and band-stop CPW filters have been presented.
- Photonic bandgap structures: Since an electromagnetic wave travel along a conductor backed CPW, a significant volume of energy leakage occurs. The leaked energy propagates along the horizontal directions away from the line, and feeds a parallel plate mode between the top and the bottom ground plane. The parasitic parallel plate mode is the leading reason for interference between neighboring circuits. The interference can be cancelled by adding a photonic bandgap grid on the CPW top ground planes.
- Printed antennas: A resonant component is formed from a conventional CPW by broadening the center strip line to shape a rectangular or square patch. This patch creates a single-lobe, linearly polarized pattern toward the plane of the conductors. The benefit

compared to traditional microstrip patch antennas is that cross-polarized radiation from the feed is reduced. In a conductor backed CPW, a series gap in the center strip conductor is utilized to couple power to a patch via an aperture in the shared ground plane. This design provides inserting-semiconductor equipments with the flexibility to control the coupling.

2.1.3 Design Consideration

This section presents some considerations and equations when design CPW with finite grounds, finite substrate. CWP is analyzed by the quasi-static and the fullwave methods [27]. The following equations are applied to design a CPW. Parameters of a, b, h, t, ε_r are shown in Fig. 2.1, and c is the width of waveguide with finites ground planes. The effective dielectric constant, characteristic impedance, effect of metallic thickness, effect of finite substrate thickness, losses, and effect of tolerances are considered, respectively.

Effective Dielectric Constant ε_{re}

The effective dielectric contant is calculated by Eq. (2.1) while impedance characteristic is given by Eq. (2.6).

$$\varepsilon_{re} = 1 + \frac{\varepsilon_r - 1}{2} \frac{K(k_4)}{K'(k_4)} \frac{K'(k_3)}{K(k_3)} \tag{2.1}$$

where

$$k_4 = \frac{\sinh(\pi a / 2h)}{\sinh(\pi b / 2h)} \sqrt{\frac{1 - \sinh^2(\pi b / 2h) / \sinh^2(\pi c / 2h)}{1 - \sinh^2(\pi a / 2h) / \sinh^2(\pi c / 2h)}} \tag{2.2}$$

$$k_3 = \frac{a}{b} \sqrt{\frac{1 - b^2 / c^2}{1 - a^2 / c^2}} \tag{2.3}$$

$$\frac{K(k)}{K'(k)} = \frac{\pi}{\ln[2(1 + \sqrt{k'}) / (1 - \sqrt{k'})]} \quad \text{for } 0 \le k \le 0.707 \tag{2.4a}$$

$$\frac{K(k)}{K'(k)} = \frac{1}{\pi} \ln[2(1 + \sqrt{k}) / (1 - \sqrt{k})] \quad \text{for } 0.707 \le k \le 1 \tag{2.4b}$$

$$k' = \sqrt{1 - k^2} \tag{2.5}$$

Characteristic Impedance Z_{0cp}

$$Z_{0\mathrm{cp}} = Z_{0cp} = \frac{30\pi}{\sqrt{\varepsilon_{re}}} \frac{K'(k_3)}{K(k_3)} \tag{2.6}$$

Effect of Metallization Thickness

The impact of metallization thickness on the characteristics of CPW is getting significant when the dielectric constant of the substrate ϵ_r is large and the ratio *a/b* is small. For example, for $\varepsilon_r = 20$ and $t/W = 0.1$ ($w = 2a$), the decrease in ε_{re} is about 11 percent and the decrease in Z_0 is about 7 percent. For $\varepsilon_r = 2.6$ and for the same value of t/W, the decrease in is about 5 percent and the decrease in is about 10 percent.

Effect of Finite Thickness Substrate

The leakage can occur with a CPW having limited thickness substrate. Although the mechanism of radiation is similar to the infinite thickness case, the substrate modes are different. They are the surface wave modes that cause the leakage. Appearance of substrate modes relies upon the polarizations and symmetries of the transmission line mode and the substrate mode. For instance, it has been demonstrated scientifically that a CPS (Coplanar Strips) with narrow strips can lose power to TM substrate modes simply because the transverse current on the strips is exceptionally powerless to energize the TE type modes [29]. When wider strips are utilized in the investigation, both TE-type and TM-type modes can be excited. Coupling to the substrate modes is realized to be stronger when the substrate thickness is equivalent to the wavelength in dielectric λ_d.

Power leakage causes an attenuation increase as well as cross talk with adjacent parts of the circuit. The power leakage can be canceled if a thin substrate is utilized so that the cut-off frequency of the surface modes is placed above the operating frequency. To meet this condition, the substrate thickness h should be selected such that $h\sqrt{\varepsilon_r} \le 0.12\lambda_d$ [30].

Losses

Two kinds of losses are considered in this part: Dielectric loss and conductor loss.

Dielectric Loss α_d

$$\alpha_d = 2.73 \frac{\varepsilon_r}{\sqrt{\varepsilon_{re}}} \frac{\varepsilon_{re} - 1}{\varepsilon_r - 1} \frac{\tan\delta}{\lambda_0} \; dB/unit\ length \tag{2.7}$$

Conductor Loss

$$\alpha_c^{cw} = 4.88 \times 10^{-4} R_s \varepsilon_{re} Z_{0cp} \frac{P'}{\pi W} \left(1 + \frac{S}{W}\right) \left\{ \frac{1 + 1.25t/\pi S + (1.25/\pi)\ell n(4\pi S/t)}{\left[2 + S/W - (1.25t/\pi W)(1 + \ell n(4\pi S/t))\right]^2} \right\}$$

dB/unit length (2.8)

where

$$P' = \left[\frac{K(k_1)}{K'(k_1)} \right]^2 P \tag{2.9}$$

$$P = \begin{cases} \dfrac{k_1}{\left(1 - \sqrt{1 - k_1^2}\right)\left(1 - k_1^2\right)^{3/4}} & For\ 0 \le k_1 \le 0.707 \\ \dfrac{1}{(1 - k_1)\sqrt{k_1}} \left(\dfrac{K'(k_1)}{K(k_1)} \right)^2 & For\ 0.707 \le k_1 \le 1.0 \end{cases} \tag{2.10}$$

$$k_1 = a/b \tag{2.11}$$

Radiation and Surface Wave Losses

Beside the dielectric and ohmic losses, power coupling to surface waves and radiation from unexpected (parasitic) modes adds to the total loss of CPW. The parasitic mode in a CPW is the odd mode with anti-phase voltages in the two slots. This mode can be fed at the discontinuities, and radiation may take place. Radiation from this mode can be limited by keeping the symmetry of the circuits and thus preventing its excitation or by applying air bridges at regular periods to short it out [31]. In a conductor-backed CPW, the parallel plate waveguide mode is another unwanted mode. The substrate modes can excite a radiation [29]. Some of these losses are important at microwave frequencies, while others become significant in the mm-wave frequency region only.

Effect of Tolerances

The effect of dimensional tolerances becomes important when the fabrication limit for very narrow strips and slots is approached.

Almost considerations and equations mentioned above couldn't applied directly to design our proposed transmission line. But it is valuable to guide our design process.

2.1.4 Comparison with Microstrip Line

CPW has been contrasted with a microstrip line in [32], [33]. A few hightlights are recorded in Table 2.1. We can see that CPW has some advagtages compared to a microstrip line such as low dispersion, small circuit size, high design flexibility. Besides, CPW has a wide range of impedance values (20Ω ÷ 250Ω), is not very sensitive to substrate thickness like microstrip line. In a CPW, there is always a ground plane between any two neighboring lines, subsequently cross talk impacts between nearby lines are exceptionally powerless. Accordingly, CPW circuits can be fabicated denser than traditional microstrip circuits.

Table. 2.1. A comparison between a CPW and a microstrip line [32].

Characteristics	Microstrip line	CPW
Dispersion	High	Low
Losses	Low	High
Coupling	High	Low
Design flexibility	Low	High
Circuit size	Large	Small
Backside processing	Yes	No
Via Holes	Yes	No

2.2 WBAN

WBAN is emerging as a technology for future life with many applications. However, it still faces some challenges. This section will provide general information on it to see its advantages as well as problems need to be solved like the reliability of on-body communication.

2.2.1 Overview of WBAN

2.2.1.1 General Architecture of WBAN

A general architecture is shown in Fig. 2.3 [1], where has three parts: Intra-WBAN, inter-WBAN and beyond-WBAN. There are two kinds of communications in intra-WBAN: between on-body sensors and between on-body sensors and a portable Personal Device (PD) or Body Gateway or Central Node. On-body sensors gather information on physical stimuli, and then process and report this information wirelessly to the PD, which can connect to other networks (Internet or cellular networks) through one or more access points (Inter-WBAN). Some communication standards are deployed for the inter-WBAN such as Bluetooth/Bluetooth Low Energy, Zigbee, UWB, Cellular and WLAN. A gateway equipment interfaces the in-ter WBAN to the beyond-WBAN, which permits authorized health-care personnel to access remotely the patient's medical data through Internet or broadband networks.

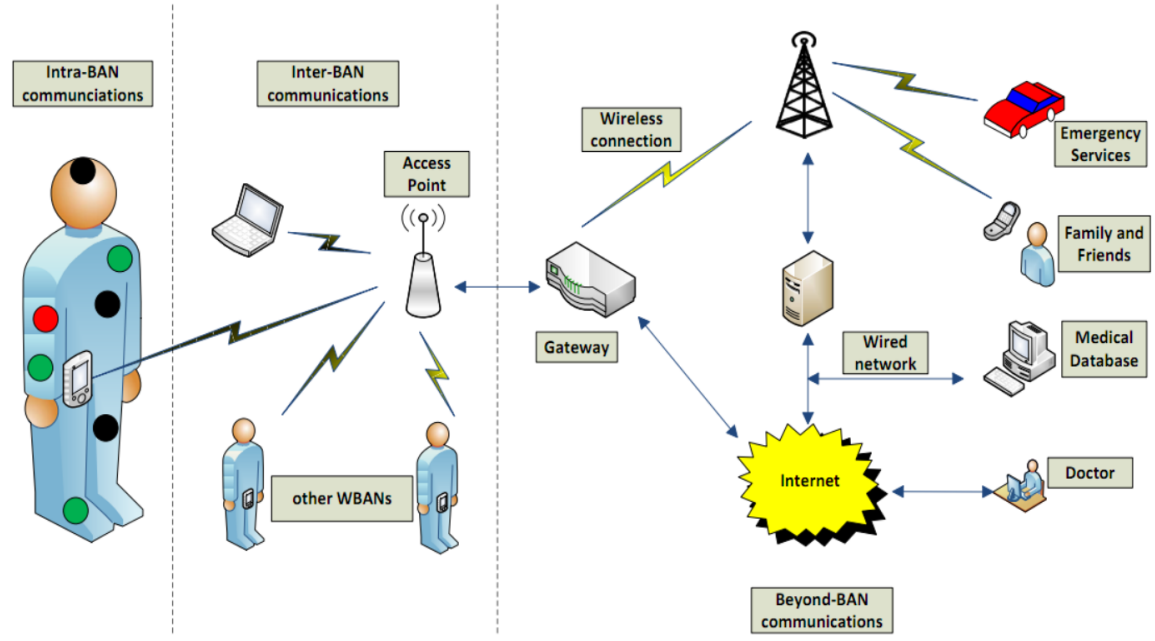

Fig. 2.3. A general architecture for WBANs [1].

Some frequency bands are reserved for WBAN as shown in Fig. 2.4 [34]. The first band licensed and utilized for implant communication in almost over the world is Medical Implant Communications Service (MICS) band (402-405 MHz). The second band is Wireless

Medical Telemetry Services (WMTS) for medical telemetry system. But wideband applications are not supported by both MICS and WMTS. Another band which is available worldwide for high data speed applications is the Industrial, Scientific and Medical (ISM) band. However, many wireless devices use this band including IEEE 802.1 and IEEE 802.15.4, this leads to of interference between devices or systems. The IEEE 802.15.6 standardizes three PHY layers: Narrowband (NB), Ultra wideband (UWB), and Human Body Communications (HBC) layers. The choice of each PHY relies upon the specific requirements. In this thesis, we focus on the in-tra WBAN communication and the ISM band.

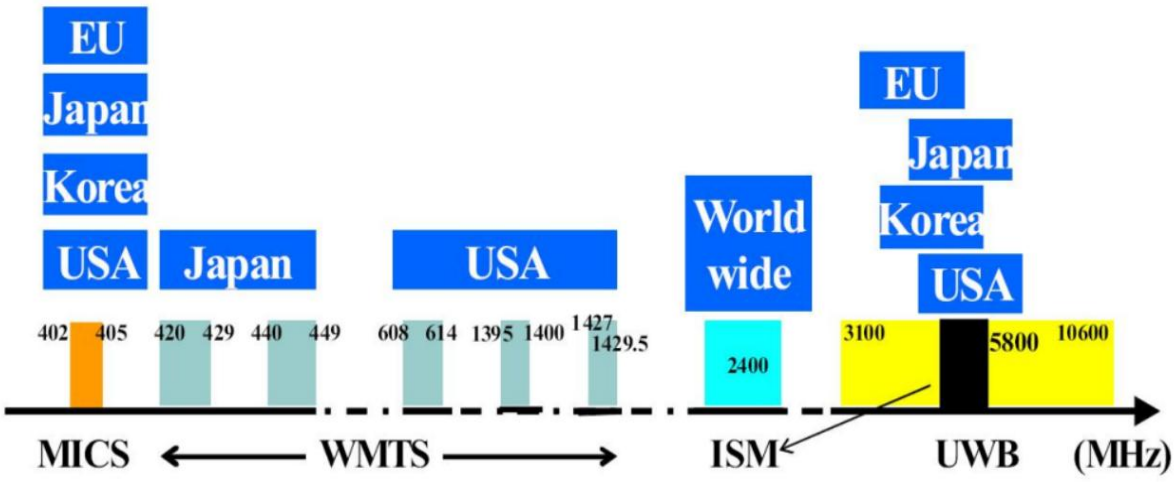

Fig. 2.4. Frequency bands for WBAN [34].

2.2.1.2 Applications of WBAN

Wireless Body Area Networks (WBAN) has developed as a key innovation to give real-time health monitoring of a patient and to analyze and cure many life threatening diseases. But, the WBAN targeted applications by the IEEE 802.15.6 standard comprise of medical and non-medical applications as shown in Fig. 2.5. Medical applications consist of achieving vital data of a patient continuously and transfer it to a remote monitoring center for further investigation. This enormous measure of information can be utilized to keep the occurrence of myocardial infarction and cure various diseases, for example, gastrointestinal tract, cancer, asthma, and neurological disorder. WBAN can likewise be utilized to assist individuals with incapacities. For instance, retina prosthesis chips can be embedded in the human eye to see at

a sufficient level. Non-medical applications consist of monitoring abandoned things, information file transfer, gaming, and social interaction applications. In gaming, sensors in WBAN can gather postures or movements of different parts of the body and create the corresponding movements of a character in the game like moving football player or catching the power of a ball in table tennis. Applying WBAN in interpersonal communication enables individuals to trade computerized profile or business card only by shaking hands.

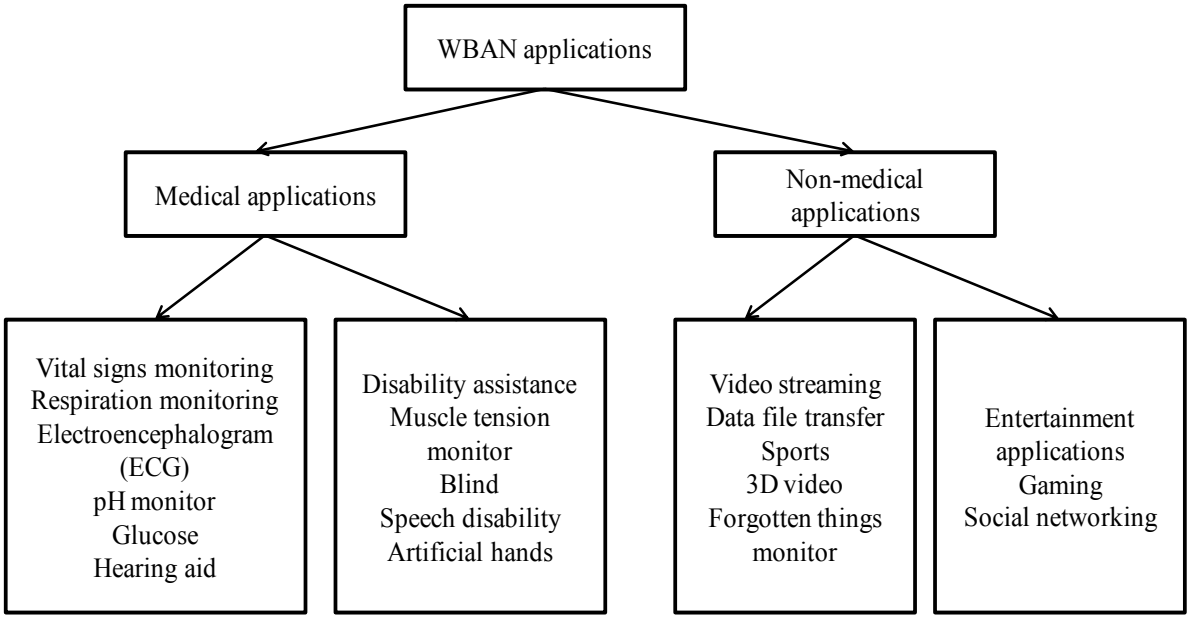

Fig. 2.5. WBAN applications [34].

2.2.1.3 Challenges and Requirements of Devices for WBAN

There are still a few of challenges to employ components of WBAN such as design of on-body sensors, signal processing time, communication between sensors or between sensors and other systems, power source and conservation, and antenna design.

On-body sensors have to be extremely thin and small, non-invasive, can communicate wirelessly with other devices, and consume as less power as possible. The most suitable power of sensors/antennas is 0 dBm for on-body communication within a distance of 1 meter [35]-[36], which is used to calculate SAR in next sections.

To meet real-time requirements, a specific level of signal processing on sensors is required. Thus, there is a trade-off between processing and communication. Some strategies are studied for power source and conservation like lithium-ion batteries in a small volume, super-capacitors, energy harvesting equipments that gather power from many different sources.

One of the most difficult tasks in WBAN is antenna design which is very important for the reliability of communication as well as power consumption, capacity, coverage, bit error rate (BER) and security of the system. The antenna is influenced by the weight, posture, skin of the human body. To reduce this influence, the antenna with a big ground is propose, but this makes the antenna is less flexible. Another requirement for the antenna design is that the electromagnetic exposure from the antenna is safe for human body or it has to satisfy the specific absorption rate (SAR) which is discussed in next section.

Data transmission is another challenge of WBAN. Sensors need to communicate with each other or with the PD. The communication channels are heavily weakened and shadowed by the human body. There are some solutions for this like adaptive channel coding, QoS-aware MAC, energy-aware routing protocols or smart suits that are integrate sensing and wireless devices into clothing. In our study, we propose a solution to reduce loss of on-body communication for both LOS and NLOS circumstances.

2.2.1.4 SAR Requirement

"Specific absorption rate (SAR) is a measure of the rate at which energy is absorbed by the human body when exposed to a radio frequency (RF) electromagnetic field" [37]. It can also refer to consumption of other forms of power by tissue, comprising of ultrasound. It is characterized as the power absorbed per mass of tissue and has units of watts per kilogram (W/kg). SAR is normally balanced either over the entire body, or over a small sample volume (typically 1 g or 10 g of tissue) [37]. There are two standards for SAR: United States and European Union. In United States, the FCC acquires that commercial phones have a SAR value at or below 1.6 W/kg over the 1-gram volume of tissue absorbing the most signal. Secondly in European Union, CENELEC standards SAR level within the EU,

according to IEC standards. Mobile phones or hand-held devices need to be satisfied the SAR limit of 2 W/kg averaged over the 10 g of tissue absorbing the most signal (IEC 62209-1).

SAR is proportional to the power of the internal electric field ($|E|^2$) and is expressed by

$$SAR = \frac{\sigma \mid E \mid^2}{\rho} \tag{2.12}$$

where σ and ρ are the electric conductivity (S/m) and mass density (kg/m^3) of the medium, respectively.

For simplification, we use the average human body density ρ = 985 Kg/m^3 and σ = 1.8 S/m to calculate SAR in this thesis. The value σ = 1.8 S/m is the electric conductivity of the simplified phantom model (mentioned in 2.2.2.1) which is used in simulation to get the maximum surface electric E_{max}. Thus, the simplified equation to calculate SAR is given by

$$SAR = \frac{1.8 \mid E_{\max} \mid^2}{985} \tag{2.13}$$

2.2.2 Propagation on Body

2.2.2.1 Human Body

This section presents the electromagnetic characteristics of the human body through which the communication in WBAN takes place. The understanding of electromagnetic features of the human body is essential for the study of on-body communication system.

Polarization is the main effect emerging from the interaction between an electromagnetic field and the human body. It takes place when inner charge moves because of outside electromagnetic field. This creates not only displacement but also conduction currents. Thus, the human body works as a lossy dielectric medium. As a rule, dielectric properties of the human body are represented as complex permittivity $\dot{\varepsilon}$ with relative permittivity ε_r and conductivity σ [38]

$$\dot{\varepsilon} = \varepsilon_0 \dot{\varepsilon_r} = \varepsilon_0(\varepsilon_r' - j\varepsilon_r'') = \varepsilon_0(\varepsilon_r - j\frac{\sigma}{\omega\varepsilon_0}) \tag{2.14}$$

where ε_0 represents the permittivity of free space, ω represents the angular frequency, and ε_r'' is a loss factor related to the conductivity σ. The conductivity σ is given as follows

$$\sigma = \sigma_d + \sigma_0 \tag{2.15}$$

where σ_d denotes the displacement conductivity and σ_0 represents the ionic conductivity. This frequency dependence is decided primarily by three interaction mechanisms, each controlled by its individual feature. When the complex permittivity is systematically considered as a function of frequency for human tissue, three main dispersion areas can be seen from the dielectric spectrum as appeared in Fig. 2.6. These dispersions are distinguished tentatively in the hertz, MHz and GHz frequency areas, and are denoted as α, β and γ dispersions, respectively.

The α dispersion at low frequency is related to an ionic diffusion process at the cell membrane. The β dispersion is chiefly because of the polarization of cell membranes which work as obstacles to ionic flow between the internal and external of the cell. Different contributions to the β dispersion originate from the polarization of protein and other organic macromolecules. Regarding to the γ dispersion in the GHz area, the polarization of water particles, which are the fundamental constituent of the human body, is a major contribution. To analyze the human body at tissue level, dielectric properties are normally utilized. The dielectric properties are denoted as ε_r' and ε_r'' values, or ε_r and σ values, as given in Equation 2.14, as a function of frequency. Human body modeling ought to be anatomically exact at the tissue and organ levels in body area communications. Present high resolution computer models of the human body are found on medical imaging data.

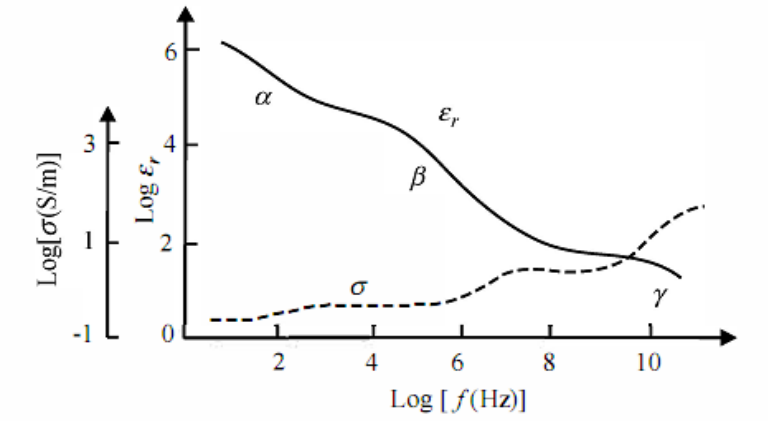

Fig. 2.6. Dispersions in the dielectric spectrum of biological tissue [38].

Table. 2.2. Dielectric characteristics of several main tissues and organs at 2.45 GHz [38].

Tissue	Conductivity (S/m)	Relative permittivity	Loss tangent
Skin dry	1.46	38.01	0.28
Skin wet	1.59	42.85	0.27
Fat	0.10	5.28	0.15
Muscle	1.74	52.73	0.24
Bone cancellous	0.81	18.55	0.32
Bone cortical	0.39	11.38	0.25
Bone marrow	0.10	5.30	0.13
Brain Gray matter	1.81	48.91	0.27
Brain white matter	1.22	36.17	0.25
Vitreous humor	2.48	68.21	0.27
Blood	2.54	58.26	0.32
Heart	2.26	54.81	0.30
Kidney	2.43	52.74	0.34
Liver	1.69	43.04	0.29
Lung deflated	1.68	48.38	0.26
Lung inflated	0.80	20.48	0.29
Esophagus	2.21	62.16	0.26
Stomach	2.21	62.16	0.26
Colon	2.04	53.88	0.28
Duodenum	2.21	62.16	0.26
Small intestine	3.17	54.43	0.43

The level of detail is with the end goal that more than 30 types of tissues are utilized, and the determination is of the request of a few millimeters. The utilization of such models acquires the dielectric characteristics to be designated to a variety of tissues and organs at the target frequencies so that the electromagnetic fields can be determined with Maxwell' equations. A theoretical expression for the dielectric characteristics, that is, the complex permittivity as a function of frequency, is hence exceptionally valuable in body area networks.

The database of dielectric characteristics of biological tissue is chiefly from measurement results on tissue samples which originated from animals and human tissues. Table 2.2 presents dielectric characteristics of some main tissues and organs of the human body at 2.45 GH.

Although the dielectric characteristics of the human body are measured in detail, they are complicated for our estimation. Thus, for simplicity in simulation as well as measurement,

simplified models are used like liquid phantom model (Fig. 2.7 (a)) [20], simplified human body model (Fig. 2.7 (b)) [21] or a perfect conductor plane (PEC) instead of the human body with exact dielectric properties. In this study, PEC is used because human body works as a reflector at some frequency bands [18],[19].

Simplified liquid Phantom
(400 750 50 mm^3)
$e_{r\text{-}Phantom} = 39.2$, $\delta_{Phantom} = 1.8$ S/m

(a) Phantom model

Body model (400 750 41 mm^3)	
Skin (2mm)	$e_{r\text{-}skin} = 38.007$, $\tau_{skin} = 0.28262$
Fat (4 mm)	$e_{r\text{-}fat} = 5.2801$, $\tau_{fat} = 0.14524$
Muscle (17.5 mm)	$e_{r\text{-}muscle} = 38.007$, $\tau_{muscle} = 0.24194$
Bone (17.5 mm)	$e_{r\text{-}bone} = 18.548$, $\tau_{bone} = 0.31849$

(b) Body model

Fig. 2.7. Body human model.

2.2.2.2 Propagation Mechanisms

To characterize the on-body communication, it is necessary to identify the propagation mechanisms that take place in each link. This may be an unfeasible task due to the numerous changes in the geometry and properties of the links, related with the natural and random body kinetics. Figure 2.8 shows probable antenna locations and different communication links.

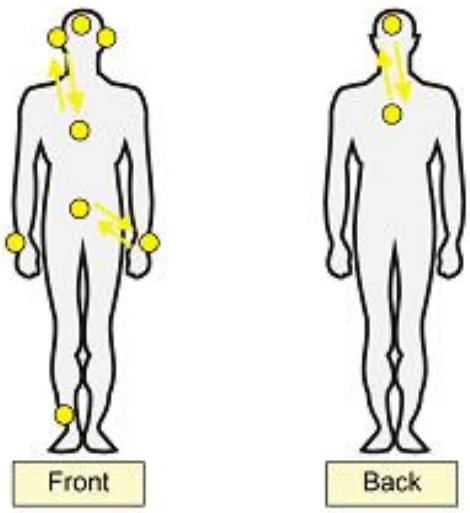

Fig. 2.8. Possible antenna locations on a BAN [2].

Paper [2] suggests a categorization of on-body propagation links depending on the positions of TX and RX antennas (e.g., trunk-to-trunk, trunk-to-head, trunk-to-limb). Characteristics of the propagation links are expected to be different relying upon the link-geometry variability. For instance, a trunk-to-trunk link is expected to be less variable than a trunk-to-limb one. Besides, a path between two places on the body may be built by electromagnetic waves going through the tissue, or propagating around the body surface if the direct LOS path is not available. Most of the work found in literature regarding channel modeling for BANs starts with a simplistic approach, which assumes the inexistence of significant scatterers in the proximity of the human body. Under this approach, the body can be considered as being isolated in space. In theory, the different propagation mechanisms that could take place in this case are:

- Direct transmission from the TX to the RX antennas: In LOS conditions, the transmission will be done in free space, while for NLOS links, waves are transmitted through the body. The wavelength and propagation speed rely on the human tissue parameters.

- Surface waves: The human body comprise of some layers of different tissues, and hence, surface waves can be one possible propagation mechanism. These waves propagate along the boundary between two different tissue and along curvatures.

- Creeping or surface-diffracted waves: If the direct link between the TX and RX antennas is blocked by an obstacle, electromagnetic waves can travel, at the speed of the light, into the shadow zone behind the obstacle. Shadowing is a very often situation in BANs, not only because of the obstruction of the LOS by the distinctive parts of the human body, but also due to mechanisms like antenna misalignment or pattern distortion.

- Reflections and absorption: Reflections may occur, being caused by the different parts of the body or by phenomena like the natural swinging of the arms or the legs. Absorption is another mechanism that can take place in a BAN link, which will be mainly dependent on the tissues involved in the communication.

When the body is put into a multipath environment, it is not easy to isolate the different propagation mechanisms that can occurs. Local scattering can a wellspring of fluctuation of the channel due to the small propagation distances included, as the variations in

the encircling environment can be as important to the channel characteristics as the variations in the channel length. In particular, the reflection of walls (and obstacles in the environment) as well as the density of clutter and environment size can be important. For LOS cases, the major propagation mechanisms are free space propagation and reflections from the different obstacles that comprises the external environment. In [39], it is demonstrated that the received energy due to Multipath Component (MPC) is fundamentally littler than the energy components close the body, thus, it can be neglected. For NLOS cases, reflections from MPCs ought to dominate over creeping waves' paths and "support" to enhance connectivity. For instance, the data obtained in [40] demonstrate that the path loss caused by the nearness of the human body usually achieves 25 dB in the anechoic chamber, while in a hospital room, where there are reflections from the walls and so on, the path loss because of the human body is smaller than 10 dB. Anyway, some MPC coming from walls or similar may be of the same order of magnitude than creeping waves [42].

A popular solution to deal with complex non-stationary wireless channels is to consider them over a little area, where the statistics are roughly stationary (small-scale). Changes in the small-scale statistics over wide areas are then studied independently. For BANs, statistical changes take place not only in aspects of geographical areas, but also over strong variations in body posture, antenna arrangement, and so on. Notwithstanding while standing or sitting, the human body depends on many small movements. In usual activities, movement is important, getting to be extraordinary during the playing of sports or same activities. The motion of the parts of the body on which antennas are mounted is the main source of variability, being particularly serious to the channel when antennas are mounted on the upper bodies (arms and hands). Additionally, dramatic variations in the structure of the local environment are expected to take place. In [2], measured results on propagation losses reveal that the deviations due to different antenna positions and because of posture movements can be 50 dB. Thus, there are some communication links greatly fluctuating with body posture, a combination of channel models is proposed, in view of the grouping of body postures. Consequently, small-scale statistics in WBANs circumstances are because of small variations in positions of the on-body equipments or body postures, in a given brief duration of time, being additionally named as shadowing. Large-scale statistics causes a large motion of the body over a geographical region, and also to major variations in the body posture. But,

it may be not easy to classify between shadowing and multipath fading in a rich multipath environment as presented in [41]. Nonetheless, Paper [43] proposes that independently modeling the small- and large-scale statistics give a quite entire explanation of the channel for many cases of practical concerns and can provide simple, physically motivated modeling forms that are more effective for estimating practical systems.

2.2.2.3 Channel Model

We always want to improve the efficiency/performance of any system, especially, wireless body area network where requires low power for sensors, and there is a high loss between on-body antennas because of human body. Moreover, on-body sensors/antennas really need to save power as well as transmitting power of sensors as small as possible to meet requirements for human safety or satisfy SAR (Specific Absorption Rate) standards). Therefore, any solution is appreciated. This section discusses about the channel model to get an overview of propagation loss of on-body links.

There are two typical on-body links: Line-of-sight (LOS) and Non-line-of-sight (NLOS) where sensors may be located in parts without visibility between themselves. The path losses of these links are influenced by power absorption of human body, reflection, and diffraction mechanisms, and multi-path effects of the surrounding objects. Moreover, much higher losses of the NLOS paths can be seen due to frequent shadowing effects of the body. To show the efficiency of SCPW, we will discuss about the link budget of on-body links or their channel model. The equation below shows the path loss PL(d) of the wideband channel model for on-body links by Dolmans and Fort (IEEE Standard for Local and metropolitan area networks – Part 15.6: Wireless Body Area Networks, 2012).

$$PL(d)_{dB} = P_0[dB] + 10n\log(d/d_0) \tag{2.16}$$

Where

n: path loss exponent

P_0: path loss at the reference distance

d_0: Reference distance

d: Distance between TX and RX.

The authors did measurements on the torso in an anechoic chamber in two cases: NLOS (around torso) and LOS (along torso). The parameters are given as follows:

Table. 2.3. Losses of on-body links.

Surrounding Torso			
Antenna separation from body surface	0	5	10
P_0	56.1	48.4	45.8
d_0	0.1	0.1	0.1
n	5.8	5.9	6.0
Along Torso			
Antenna separation from body surface	0	5	
P_0	56.5	44.6	
d_0	0.1	0.1	
n	3.1	3.1	

It is unmistakably observed that a significantly higher exponent is estimated when the propagation is around the torso ($n \approx 6$) rather than along the front ($n \approx 3$). The channel loss due to the appearance of the human body often obtains 25 dB in the anechoic chamber.

Moreover, measured losses between two antennas on real body and torso in [2], [28] are much lower than these with SCPW. In detail, the average loss is 38.9 dB for the shortest LOS links and at least 45dB for NLOS links while these losses are around 20dB with SCPW as results in Chapter 3-5. Thus, by using the SCPW the effect of the body can be compensated. This is really appreciated.

In this chapter, the basic knowledge of CPW and WBAN was presented. CPW has some advantages compared to microstrip line, for example, low dispersion, small circuit size, high design flexibility. This makes our proposed transmission line is more effective than previously presented transmission lines. Moreover, characteristics of on-body communication are discussed to see that a new and more effective solution is really necessary for on-body links. This solution will be proposed in next chapters.

CHAPTER 3

FREE-ACCESS TRANSMISSION LINE BY A COPLANAR WAVEGUIDE

This chapter provides the idea of the use of the subsidiary waveguides to reduce losses on body. First, sheet-shaped communication surfaces are introduced to see their advantages such as limit coverage to reduce interference between systems or increase the security of the systems in Section 3.1. Sheet-shaped mediums for WBAN are also summarized for an overview on current research on it. The design process of the free access transmission line is presented in detail in Section 3.2. In next sections, basic performances of the transmission line are considered like bent transmission line, coupling to external antennas and discussions about losses of material and small differences between simulation and measurement.

3.1 Sheet-shaped Communication Surface

Too many wireless systems operate at the same time in a coverage region, this causes interference between the systems. Thus, it is crucial to lessen the output power of the transmitter and to constrain interference with other systems or to isolate the coverage area of one wireless system from another. Accordingly, the potential utilization of a auxiliary waveguide is being considered as a new technique of concentrating the transmitted power,

reducing propagation loss, and managing the transmission power of wireless equipments. The coverage area is restricted to a region around the supplementary waveguide, to which the wireless equipment is electromagnetically coupled. Sheet-like waveguides [44]-[51] such as the CarpetLAN, the two-dimensional sheet as shown in Fig. 3.1 and Fig. 3.2 prove to have lower transmission losses than those in free-space and users can utilize their personal waveguides independently so a high security level can be obtained. However, there are some the adversities like sustaining the contact and high cost. Moreover, these waveguides are not suitable for on-body applications because their array configurations of units are not really flexible. Flexibility should be improved for applications in WBAN.

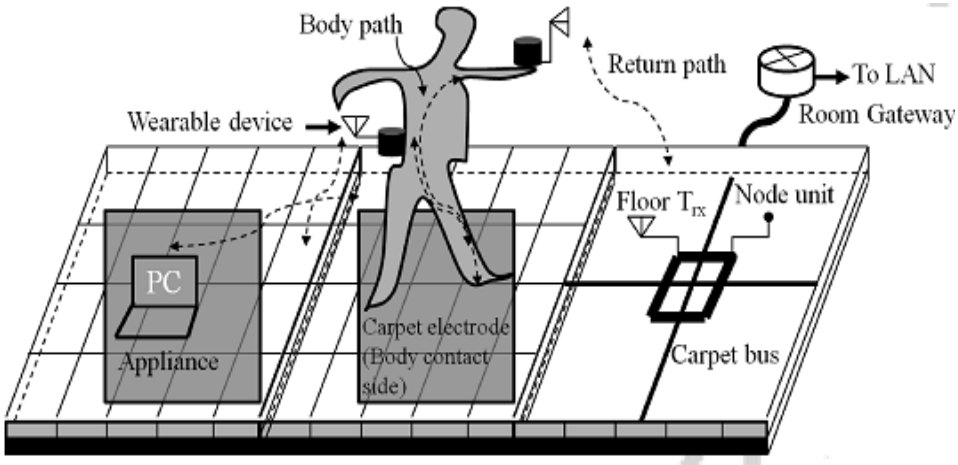

Fig. 3.1. CarpetLAN [51]

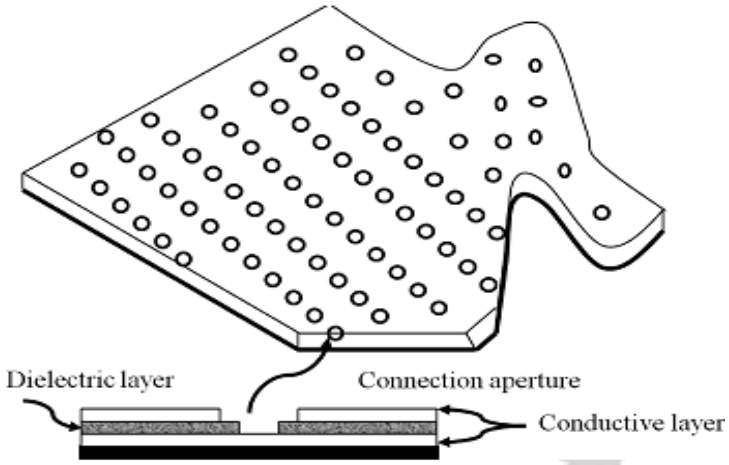

Fig. 3.2. Two-dimensional transmission sheet [48].

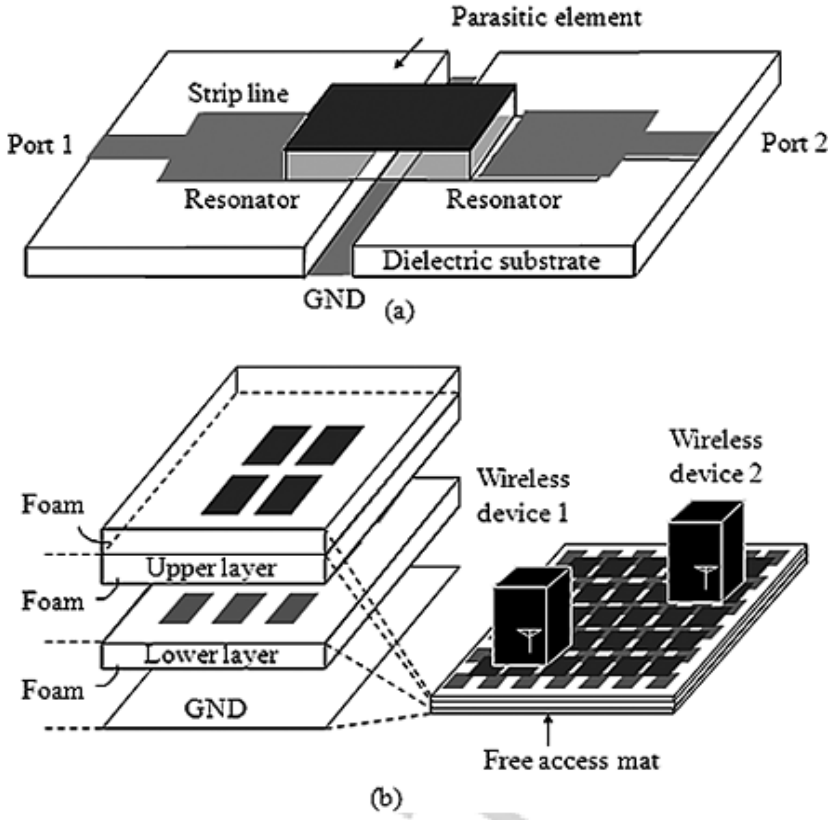

Fig. 3.3. Free access mat: the sheet-like geometry and its basic elements: (a) configuration of the ribbon-wire interconnect and (b) the free access mat [10].

A simpler sheet-shaped medium or "free access mat" has proposed in [10], [52]. The fundamental elements for the 2-D array consists of four patch resonators on the lower layer and one parasitic element centered over them on the upper layer as appeared in Fig. 3.3. The measured results by utilizing this free-access mat in Fig. 3.4 show that transmission loss between two dipoles can be greatly decreased up to more than 40 dB. But, a disadvantage of the free access mat is the utilization of a metallic ground plane which is less convenient and less breathable when it is embedded into a wearable fabric. In addition, the double-layered structure influences the large scale manufacturing to process troublesome and costly. To improve this sheet-shaped waveguide, a periodic bandpass-filter microstrip transmission line is additionally proposed for on-body links as illustrated in Fig. 3.5 [11], [12], [26]. However, its adaptability is still restricted because of the substrate ground plane for the transmission line. Our proposed transmission line is based on the structure of this transmission line. But, by

applying coplanar waveguide structure the flexibility is improved for on-body applications. The design process will present in next section.

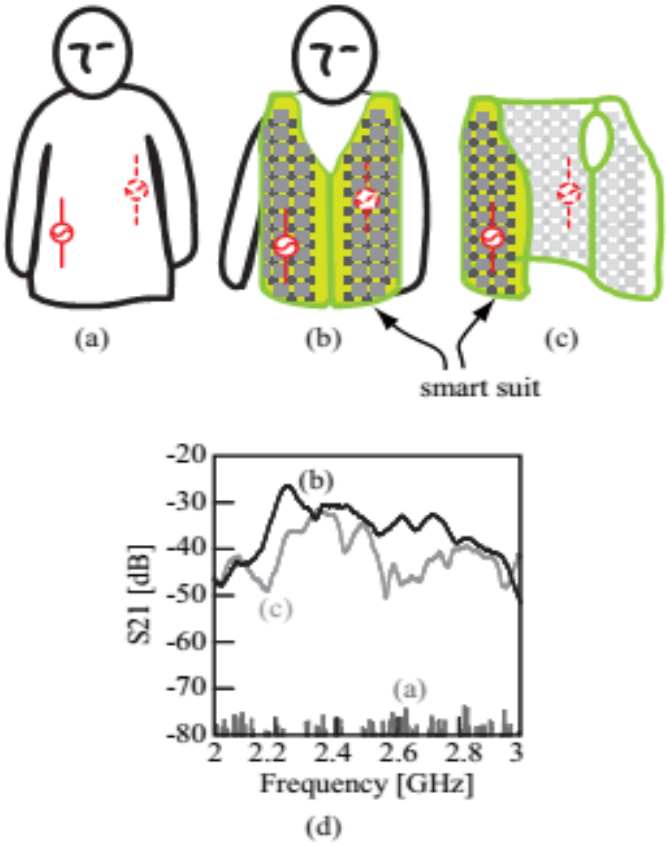

Fig. 3.4. Measured characteristics in S21 with the free access mat with and without a user. One antenna is put on the front of the body and the other on the back. Measured S21 characteristics for two antennas placed (a) on the human body, (b) on the mat with the user wearing it, and (c) on the mat without a human body [52].

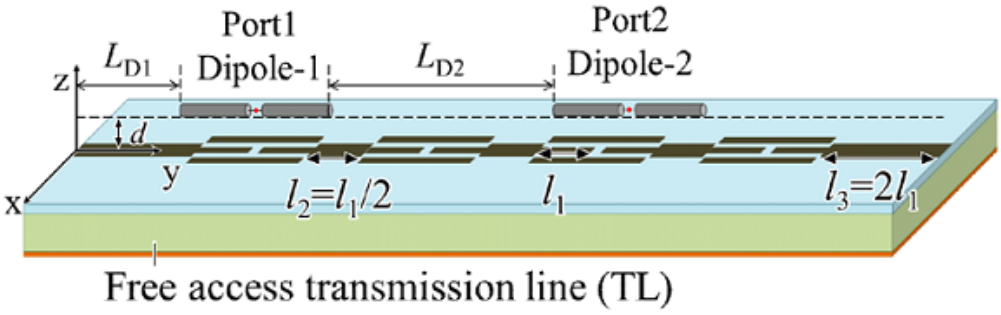

Fig. 3.5. Free access transmission line with dipoles [26].

3.2 Design of Free-Access Transmission Line

Starting from the structure of a free-access transmission line by a microstrip line [14] (A fundamental unit is illustrated in Fig. 3.6 (a)), we change this structure to a coplanar waveguide (CPW) which has execution tantamount to and sometimes even superior than microstrip line regarding guide wavelength, dispersion, and losses [15], [27]. A extraordinary benefit of the CPW is that all conductors are on one plane, comprising of a center strip conductor with two ground planes on both sides. This makes the CPW a great adaptability as well as the manufacture turns out to be substantially less demanding.

The free-access transmission line comprises of some units in arrangement. Every unit is a mix of modified two-side coupled half-wavelength ($\lambda/2$) resonators as demonstrated in Fig. 3.6 (b). Its dimension parameters are upgraded so that the bandwidth is the widest and the coupling between port 1 and port 2 is the most elevated. The length l_2 decides the resonance frequency of the transmission line while the gap s_3 mainly adjusts the input impedance of port 1 to coordinate with 50 Ω input. But, the input impedance cannot be obtained to 50 Ω when the width of s_3 is 0.5 mm, which is the littlest width under our fabrication condition. Thus, gaps g at two ends are applied to adjust the impedance much easier. Additionally, on account of these gaps, potentials of the two ground planes are kept up the same to prevent undesirable propagation modes. The gap s_1 is upgraded so that the coupling between resonators is the biggest. Different parameters are enhanced to make the transmission line small such that it is reasonable for on-body applications.

To lengthen the transmission line, n units are associated in arrangement as illustrated in Fig. 3.6 (c). Upgraded dimension parameters of the fundamental unit are kept unaltered when the number of units increments. This makes the large-scale manufacturing simple and not exorbitant. In addition, together with l_2, the length l_3 adjusts the resonant frequency of n-unit transmission line. At first, the basic characteristics of the transmission line at 5.12 GHz are indicated utilizing the substrate of R4737 by Panasonic with the thickness of t_1 = 0.73 mm, relative permittivity of ε_{r1} = 2.6, tangent loss of τ_1 = 0.007, and 0.035-mm copper conductive layer. For the adaptive transmission line and the fabrication error diminishment at 5.12 GHz, the execution of paper substrate at 2.45 GHz is analyzed, where the thickness of t_2 = 0.18 mm,

$\varepsilon_{r2} = 2.8$, $\tau_2 = 0.15$, and 9 μm silver ink conductive layer with the conductivity of 1.5×10^7 S/m. A fabrication photo of the transmission line at 2.45 GHz is shown in Fig. 3.6 (d).

In our simulation, CST Studio Suite [16] and EMPro [17] are utilized. The impact of dimension parameters on S-parameters of the SCPW at 2.45 GHz and 5.12 GHz has a similar pattern, and thusly, we demonstrate simulation results at one band to minimize the quantity of figures. Figs. 3.7 (a)-(e) demonstrates the S-parameters of the SCPW for the parameters of l_2, s_3, g, s_1 and l_3, respectively. Since these parameters are changed, the others are unchanged as given in Table 3.1. A little change in S_{11} is seen in 1-unit for s_3 whereas the gap g alters the input impedance of port 1 of the SCPW as illustrated in Fig. 3.7 (c).

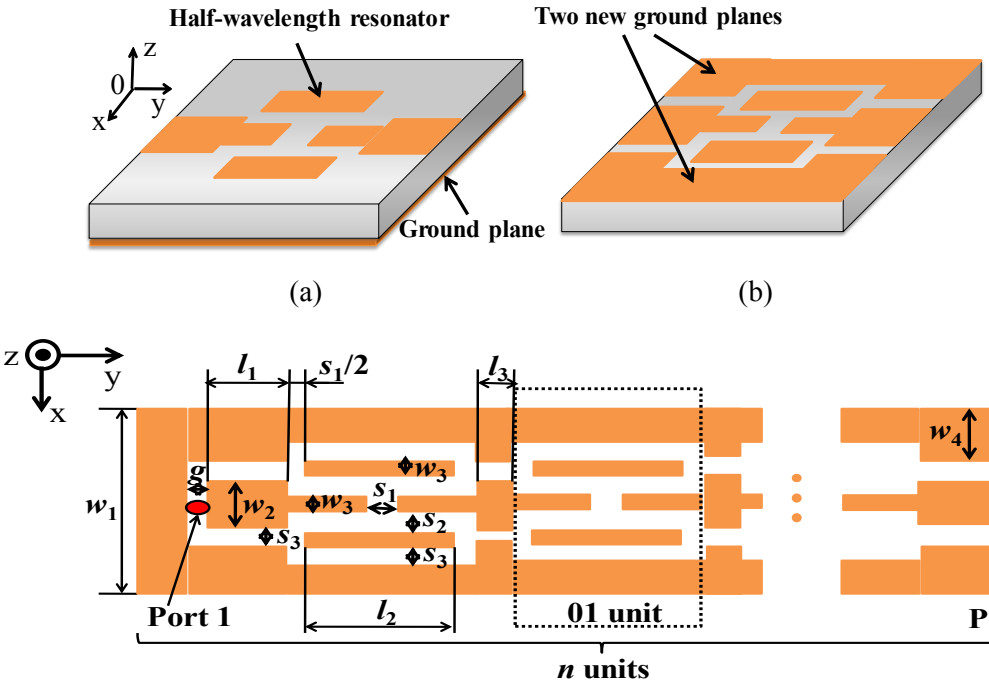

(c) Segmented CPW

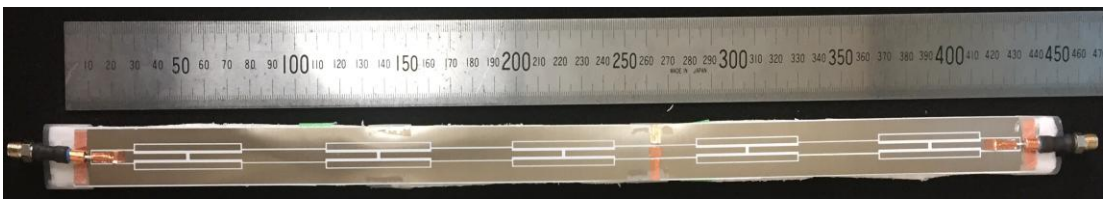

(d) 5-unit transmission line at 2.45 GHz

Fig. 3.6. Geometry of the transmission line.

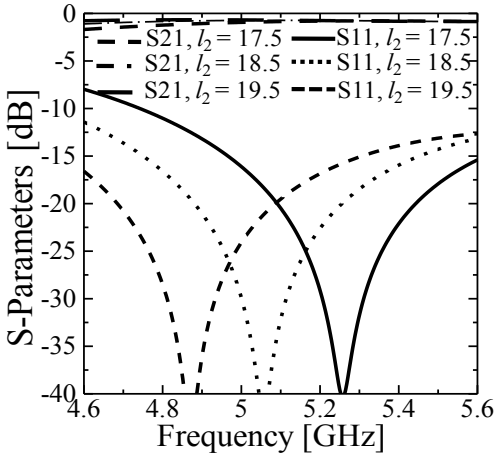

(a) Effect of l_2

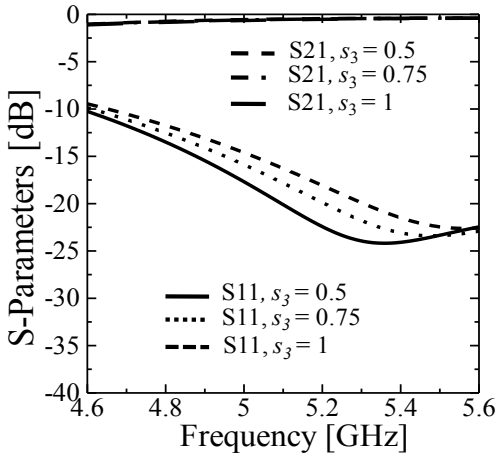

(b) Effect of s_3 (no gap g)

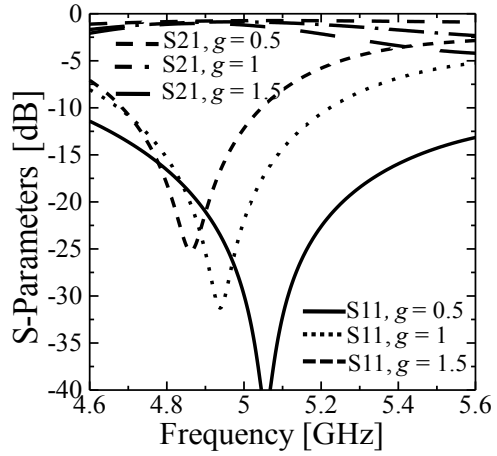

(c) Effect of g

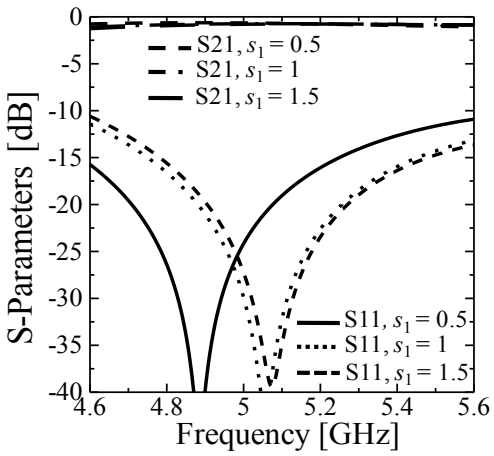

(d) Effect of s_1

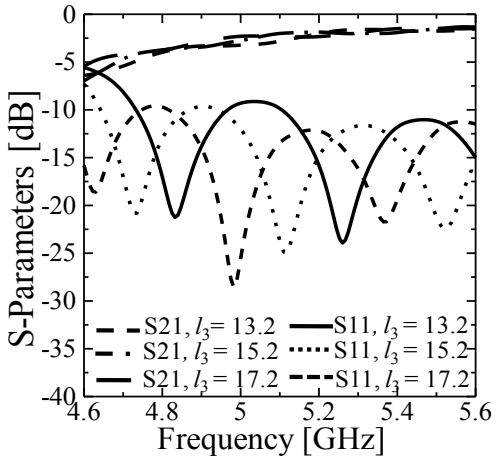

(e) Effect of l_3 at 5.12 GHz

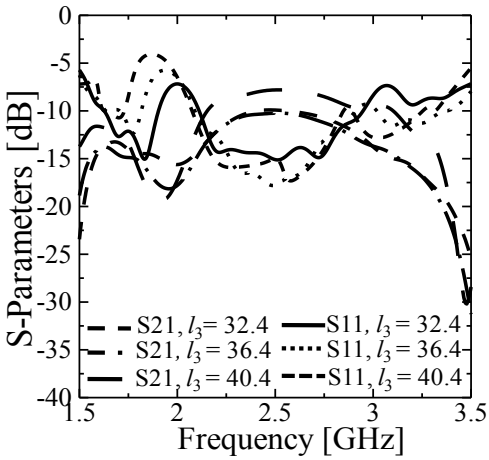

(f) Effect of l_3 at 2.45 GHz

Fig. 3.7. Influence of l_2, s_3, g and s_1 on S-parameter of the 1-unit SCPW at 5.12 GHz, and effect of l_3 on the 5-unit SCPW.

Table 3.1. Fabrication parameters of SCPW.

Parameters[mm]		l_1	l_2	l_3	w_1	w_2
Frequency	**5.12**	9.3	18.5	15.2	16	5
[GHz]	**2.45**	18.2	45.6	36.4	19	4
Parameters[mm]		w_3	s_1	s_2	s_3	g
Frequency	**5.12**	1	1	1	0.5	0.5
[GHz]	**2.45**	2	1.6	1	0.5	0.5

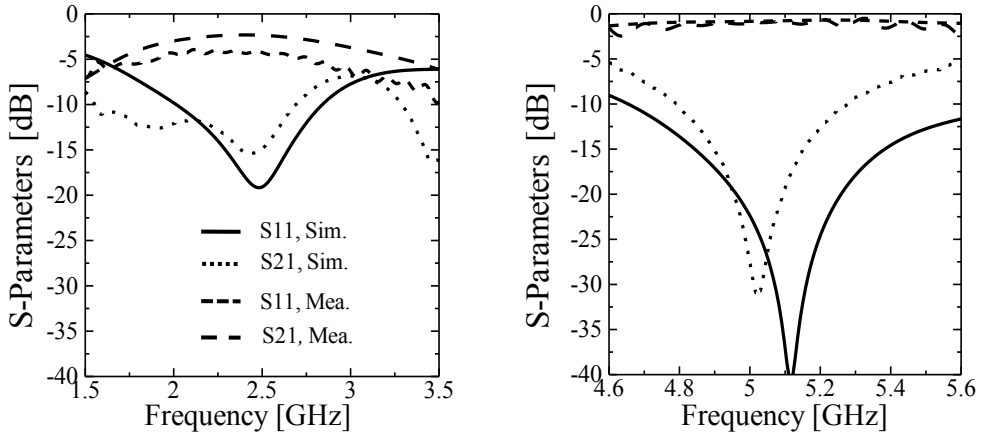

(a) $n = 1$

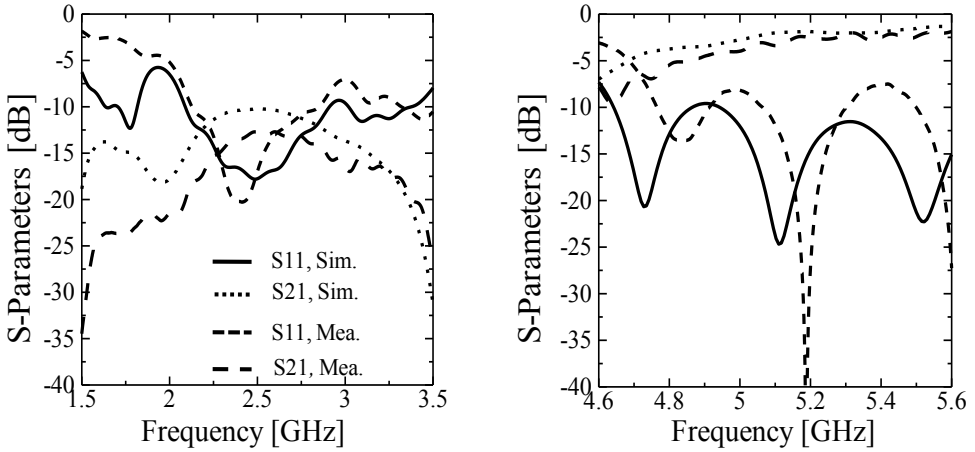

(b) $n = 5$

Fig. 3.8. S-parameter characteristics of n-unit transmission line at 2.45 GHz and 5.12 GHz.

The S-parameter characteristics of the one-unit and five-unit transmission lines at both frequencies of 5.12 GHz and 2.45 GHz are presented in Fig. 3.8. When the quantity of units increments, the bandwidth of S_{11} is slightly widen, and the transmitted power S_{21} reduces due to the dielectric loss of substrate and radiation loss. This will be discussed in detail in Section 3.6.1. The measured results have a good agreement with the simulation results. But, a little difference between simulation and measurement can be observed. The reasons of this difference will be explained in Section 3.6.2.

3.3 Fundamental Performance of the Transmission Line

The free-access microstrip transmission line in [26] is not vigorously influenced by the human body, because it is upheld by the ground plane [14]. The proposed SCPW structure with the ground plane put at both sides of the center line does not have shielding impact to the human body. It is integrated into clothes creating a small distance of *l* from the human body and this smallest distance for the stable operation of the SCPW should be investigated. To evaluate the influence of the human body on the SCPW, a conducting plane (PEC) with the size of 750 × 400 × 1 mm^3 as given in Fig. 3.9 is utilized as a body under the SCPW (as mentioned in 2.2.2.1 [18], [19]). Then, S-parameters of the SCPW are calculated when *l* changes to see this effect.

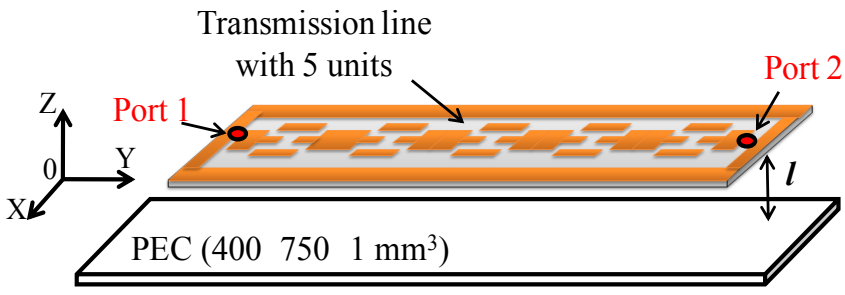

Fig. 3.9 Model used to consider the basic performance of the transmission line.

3.3.1 Fundamental Performance at 5.12 GHz

First, the effect of the human body on the SCPW is considered at 5.12 GHz. By varying the height l from 1 to 7 mm, the S-parameters at 5.12 GHz are presented in Fig. 3.10. The effect of the PEC is reduced for l large, and is ignored for $l \geq 5$ mm. This is also confirmed by the measured results in Fig. 3.10 (c), where the results are identical to those in free space as in Fig. 3.8 (b).

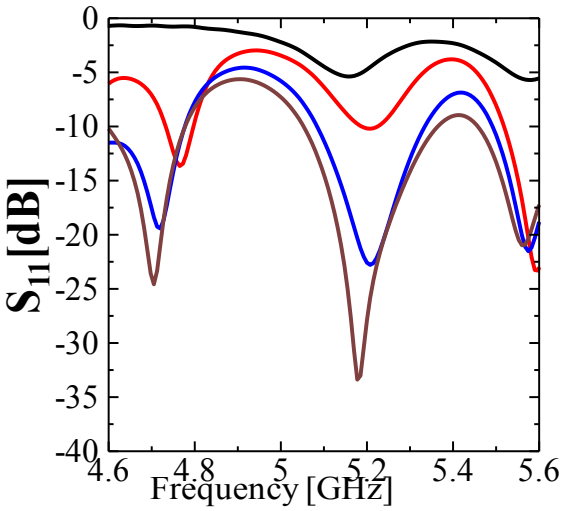

(a) S_{11} for l

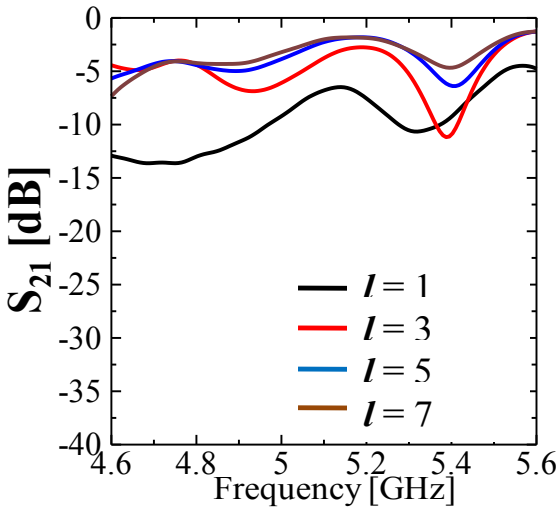

(b) S_{21} for l

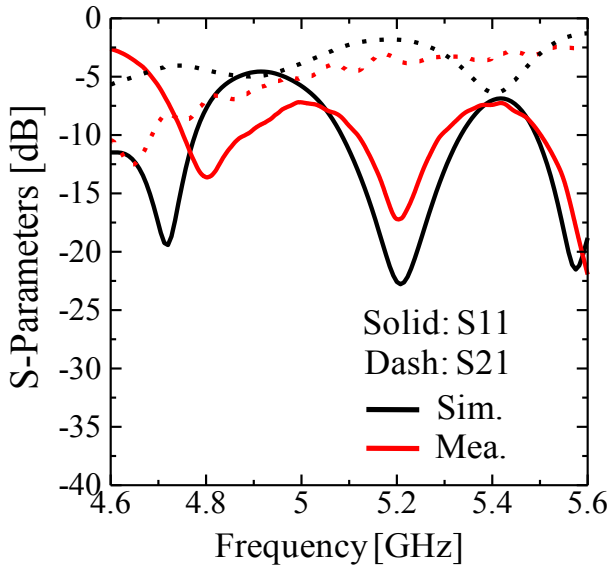

(c) Measurement at l = 5 mm

Fig. 3.10. Fundamental performance of the transmission line at 5.12 GHz.

3.3.2 Fundamental Performance at 2.45 GHz

For 2.45 GHz band, the impact of the PEC plane is not significant when the distance of *l* is equal or greater than 7 mm as demonstrated in Fig. 11, where the results are identical to those in free space as shown in Fig. 3.8 (b). In addition, the minimum distance of *l* is also calculated on the simplified phantom model and the body model (as mentioned in 2.2.2.1) as shown in Fig. 3.12. The results reveal that the fundamental performance of the transmission line on the PEC plane is the worst contrasted to those on the phantom model and the body model, but the PEC plane is utilized for favorable measurements in next sections.

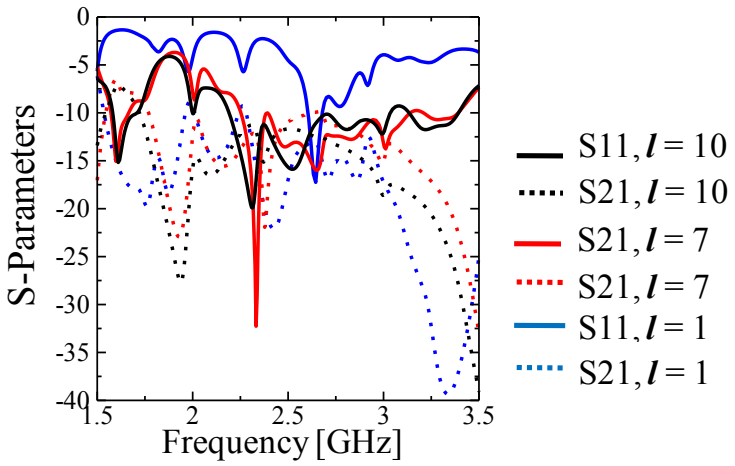

(a) Simulation at l = 1, 7, and 10 mm

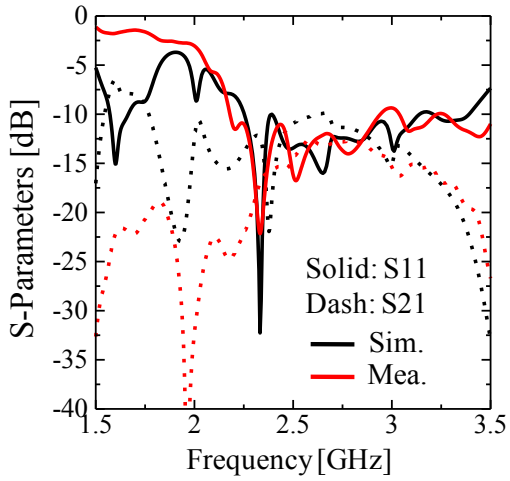

(b) Measurement at 7 mm

Fig.3.11. Fundamental performance of the transmission line at 2.45 GHz on the PEC plane.

Thus, the fundamental performance of the SCPW is not influenced by the human body when it is put above the body with a several millimeters distance. This distance reduces when the operating frequency gets higher because the electrical distance between the body and the transmission line increments. The distance of l = 7 mm will be utilized for investigations in next sections at 2.45 GHz.

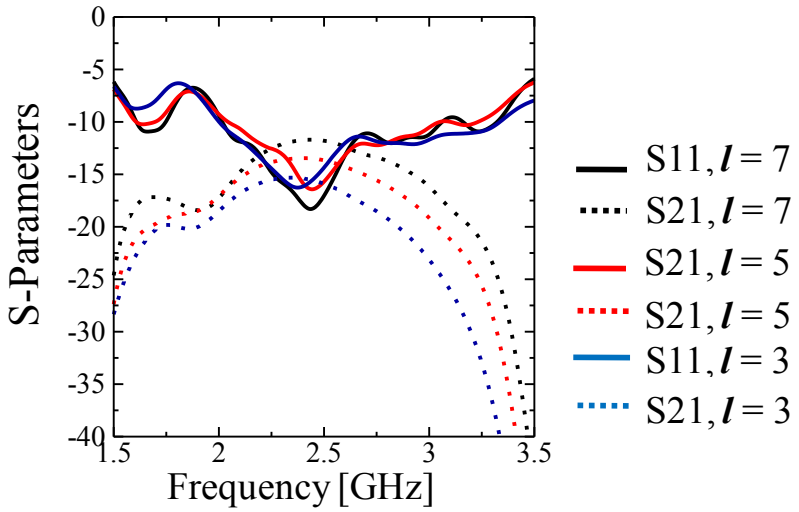

(a) S-parameters on the phantom model at different height of l

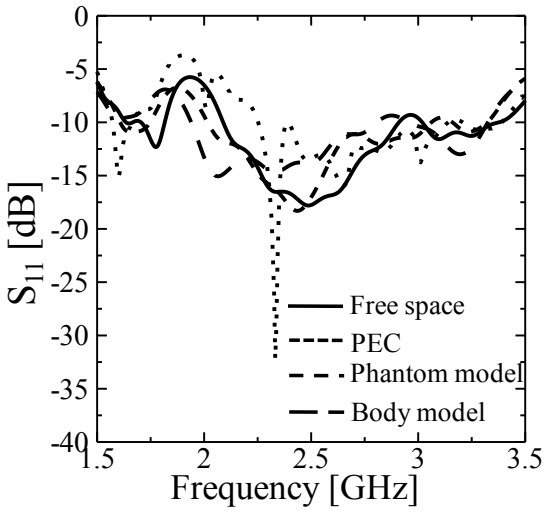

(b) S_{11}

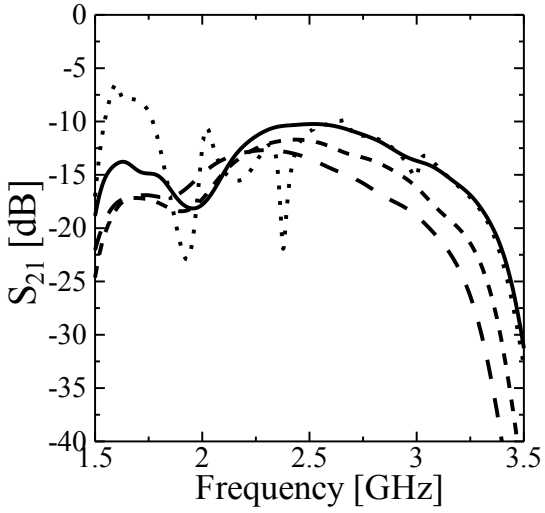

(c) S_{21}

Fig. 3.12. S-parameters of the SCPW on simplified liquid phantom and body model with a distance of 7 mm.

3.4 Bent Transmission Line

The SCPW is supposed to be bent in practical applications. Hence, this section presents the S-parameter characteristics of the SCPW when it is bent. Both the SCPW and the PEC plane or the simplified phantom or the body model are bent as illustrated in Fig. 3.13 (a), where two 90° angles are made. The length of the upper part is equal to the length of two units, and the length of side part is same to the length of 1.5 units. The S-parameters of the bent SCPW are given in Figs. 3.13 (b), (c) and (d). The simulation results are similar to those without bending. In the other words, the performance of SCPW has little influence by bending.

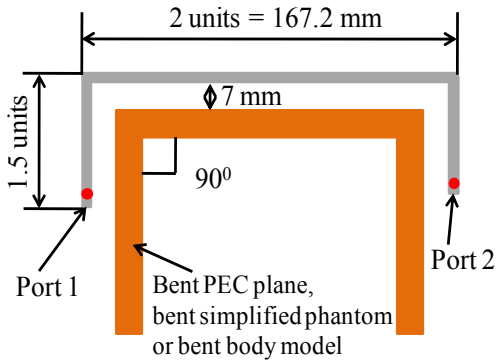

(a) Simulation model

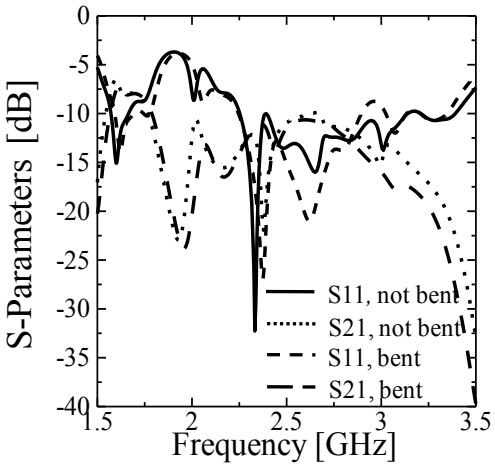

(b) SCPW above PEC

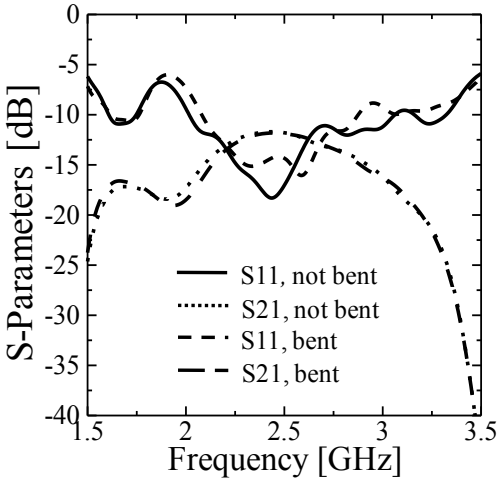

(c) SCPW above simplified phantom

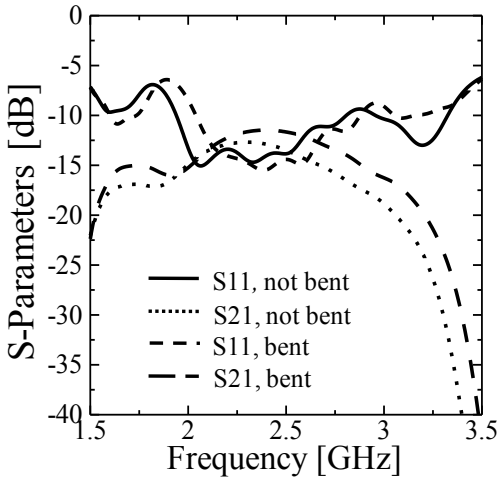

(d) SCPW above body model

Fig. 3.13. S-parameters of the bent SCPW.

3.5 Coupling Power between the SCPW and External Antennas

The coupling between the SCPW and a square patch antenna [22] is discussed in this section at the frequency of 2.45 GHz. The square patch antenna is selected because it is ubiquitus, and is widely-used as printed antennas for on-body communication.

The square patch antenna is fed by a microstrip line with the ground plane size of 50 mm × 50 mm as shown in Fig. 3.14, and its substrate is the same as in Fig. 5 (Fig of TL at 5.12 GHZ). The SCPW height from the PEC plane is l = 7 mm, where the influence of the PEC plane can be neglected as presented in the previous section. The structure and S-parameters of the patch antenna are given in Fig. 3.14. The antennas are put below or above the SCPW to validate the coupling between SCPW and on-body sensors/ antennas. One end of the SCPW works as an input port 1 and other port 2 is terminated to a 50 Ω dummy load. The patch antenna feed is denoted as port 3 as shown in Fig. 3.15 and Fig. 3.17. The radiation direction of the antennas is toward the SCPW.

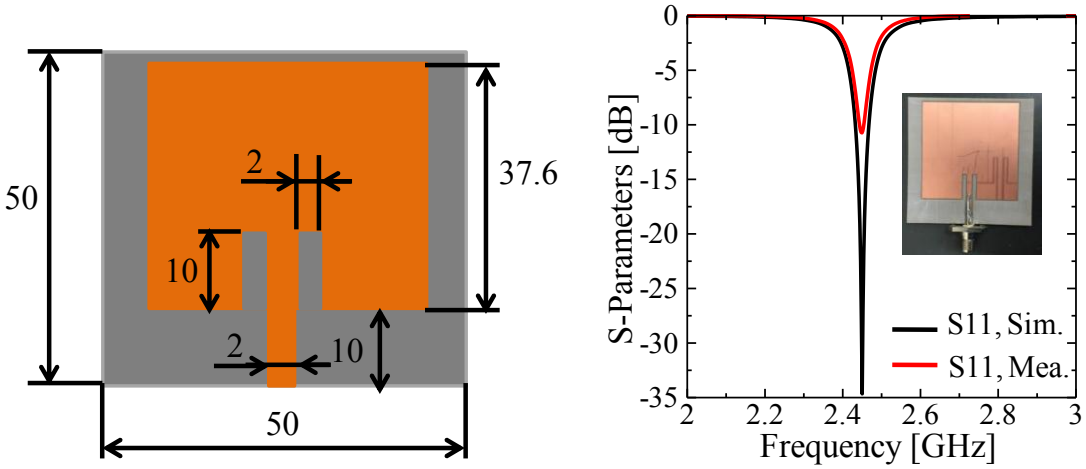

Fig. 3.14. Square patch antenna: (a) geometry in top view and (b) S-parameters.

3.5. 1 Sensors or Antennas below the SCPW

The first case is consideed that the patch antenna is put below the SCPW. By changing the distance of h between the antenna and the SCPW, and moving the antenna cross the SCPW in 30-mm intervals, the coupling in S_{31} between port 1 and 3 is simulated and

measured. The simulation and measurement results for h = 1 and 3 mm are given in Fig. 3.16, where dots are simulated and measured ones at the position y_1 and lines are approximated curves to estimate the coupling factor easily. An exponential function is utilized for the curve as the below,

$$S_{31} = A \times y_1^{b}. \tag{3.1}$$

The values of A and b are constants to approximate data by the function LINEST in the 2007 Microsoft Excel [23], where the least squares method is applied [24].

Data fluctuation in Fig. 3.16 is assumed to be caused by strong coupling between SCPW and the antenna, and its variation range is reduced for large h. Measurement errors of several data are caused by incorrect y_1 by the effect of cable and connector, while approximation curves in Fig. 3.16 are almost the same in simulation and measurement.

Thus, this coupling power between port 1 and port 3 is higher than those of on-body propagation in [2]-[4] in both cases of antennas below or above the transmission line, considering the fluctuation and the loss of paper substrate, which is the advantage of the use of the proposed SCPW.

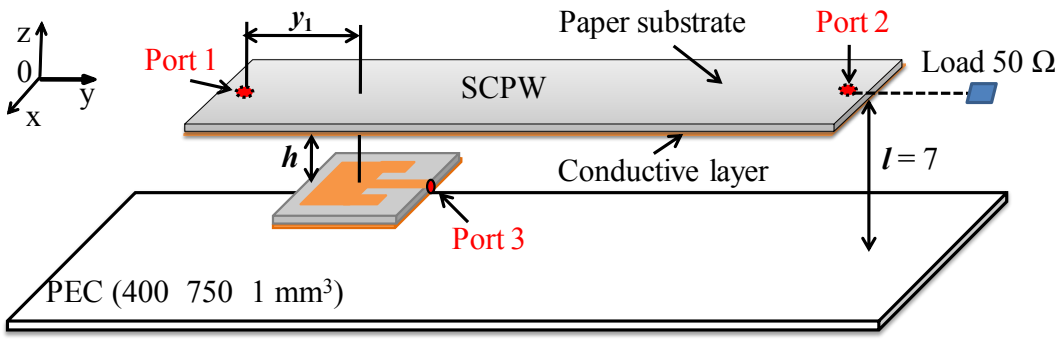

Fig. 3.15. Model used to consider the coupling between the patch antenna and SCPW, the antenna is below the SCPW.

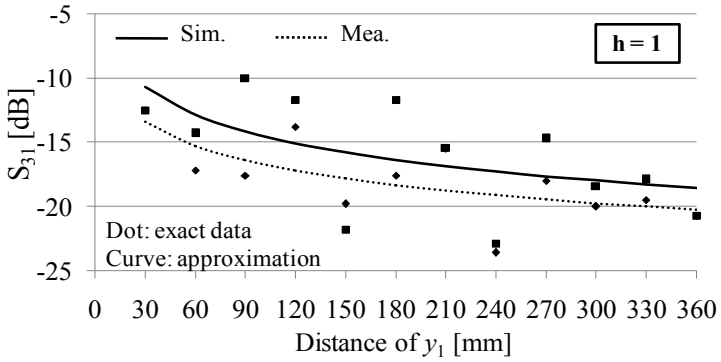

(a) $h = 1$

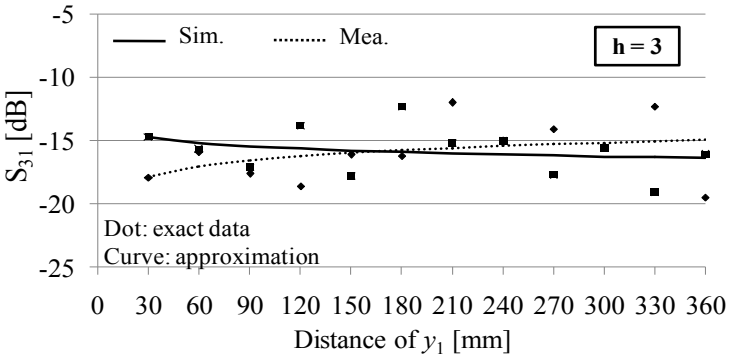

(b) $h = 3$

Fig. 3.16. Coupling power between the patch antenna and the SCPW on the PEC plane at 2.45 GHz, the antenna below the SCPW.

3.5.2 Sensors or Antennas above the SCPW

This section presents the coupling between the square patch antenna and the SCPW when the antenna is put above the transmission line. The model used for both simulation and measurement and the results are given in Fig. 3.17. The results are presented in Fig. 3.18, where the measured results agree well with the simulation results.

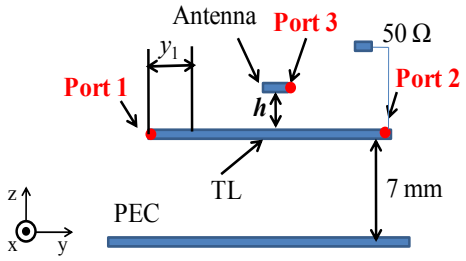

Fig. 3.17. Model used to consider the coupling between the patch antenna and SCPW, the antenna is above the transmission line.

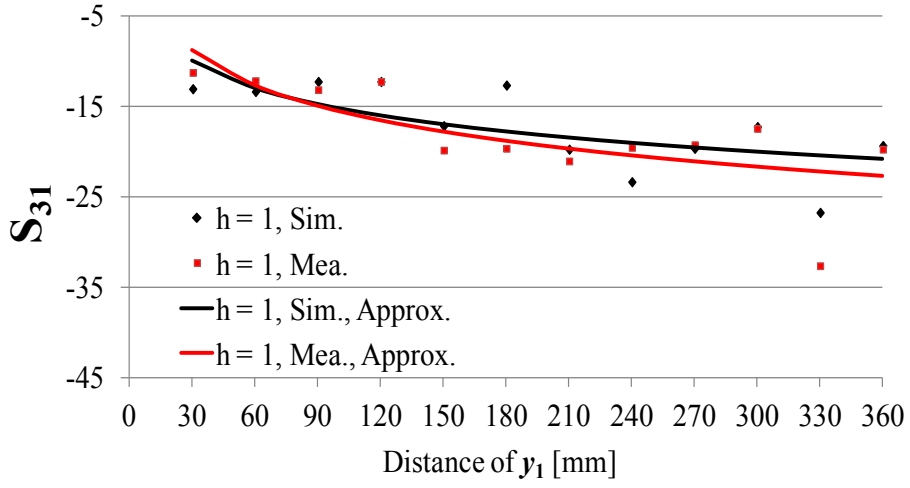

(a)

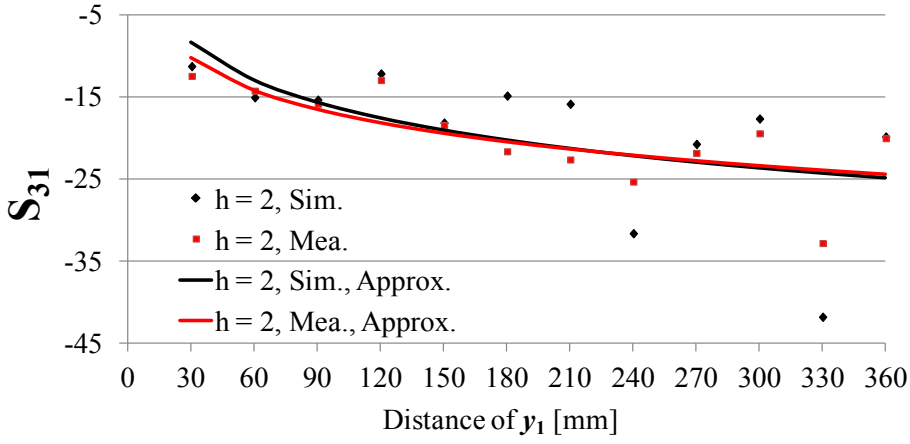

(b)

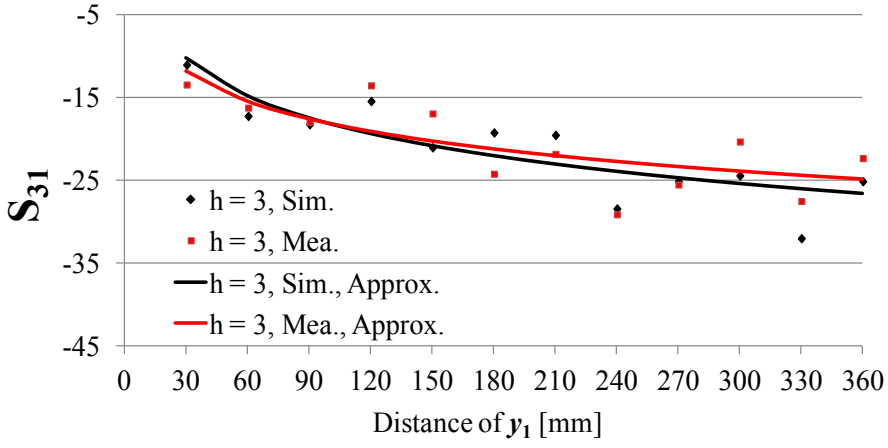

(c)

Fig. 3.18. The coupling power between the patch antenna and the transmission line on the PEC plane at 2.45 GHz, the antenna above the SCPW.

3.6 Other Discussions

3.6.1 Losses of Paper Substrate

To see the effect of the tangent loss of the paper substrate on the transmission coefficients, we simulate how much S_{21} of the SCPW changes when the tangent loss reduces from 0.15 to 0.005 as given in Fig. 3.19. Next, S_{21} of the simple CPW is calculated as illustrated in Fig. 3.20 to compare to the performance of the SCPW. The comparison is given in Fig. 3.21 and Table 3.2. From the results, we can see that main loss of the simple CPW is the dielectric loss because its radiation loss is little while the radiation loss of the SCPW is a little higher, but the radiation is necessary for a high coupling between external antennas and the transmission line, which will be discussed in Section 4.4.2.

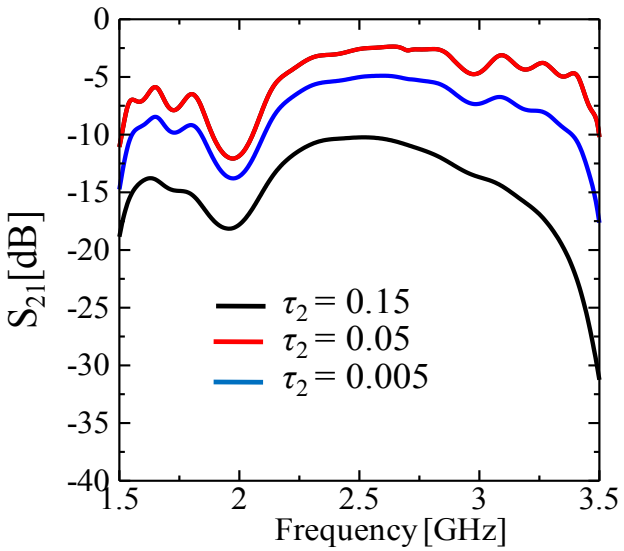

Fig. 3.19. Effect of tangent loss on S-parameters of SCPW at 2.45 GHz.

Fig. 3.20. Geometry of the simple CPW.

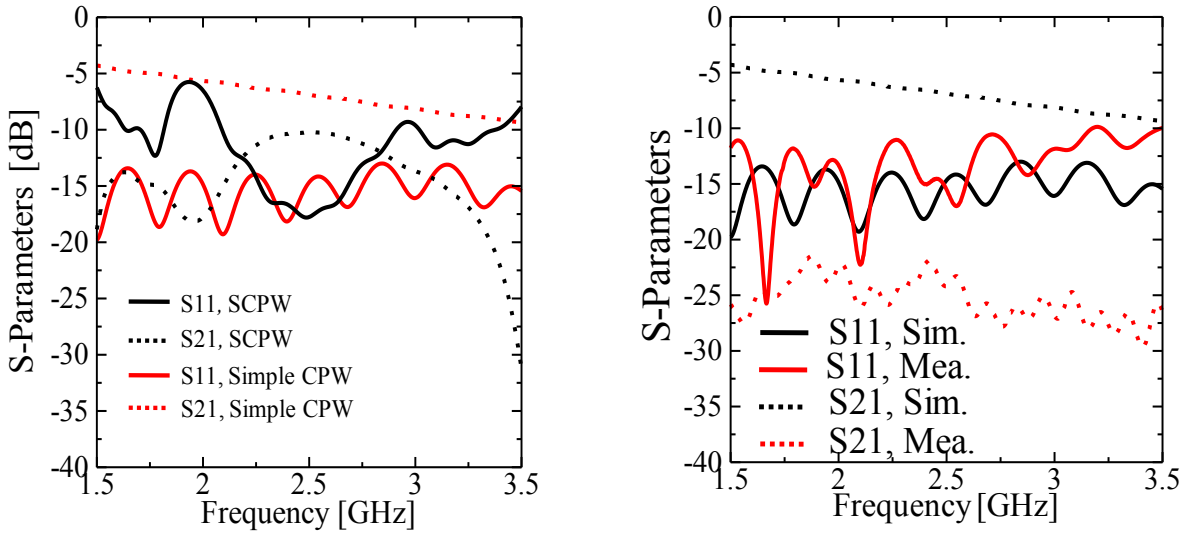

(a) Simulation (b) Measurement

Fig. 3.21. S-Parameters of the simple CPW.

Table 3.2. Comparison between the simple CPW and SCPW.

Frequency [GHz]	Types of CPW	S21 [dB]	Radiation loss [%]
2.45	SCPW	-10.3	21.07
	Simple CPW	-6.95	0.186
5.12	SCPW	-1.97	20.18
	Simple CPW	-0.78	2.18

3.6.2 Differences between Simulation and Measurement

The frequency band in measurement was shifted a little bit to the higher band. This can be because of material errors or fabrication errors. Assumed errors are given in Table 3.3. Fig. 3.22 shows the effect of material errors of dielectric constant e_r on S-parameters of 5-units SCPW at 5.12 GHz. From the results, we can observe that the frequency shifts to higher band when e_r decreases 0.1 (e_r = 2.5), where the simulation results has the better agreement with the measured results. Besides, the connection between the connector and the SCPW at 2.45 GHz

not really good due to the utilization of a copper tape as shown in Fig. 3.23 is another reason. As a result, the coupling in S_{21} in measurement is a little lower than that in simulation.

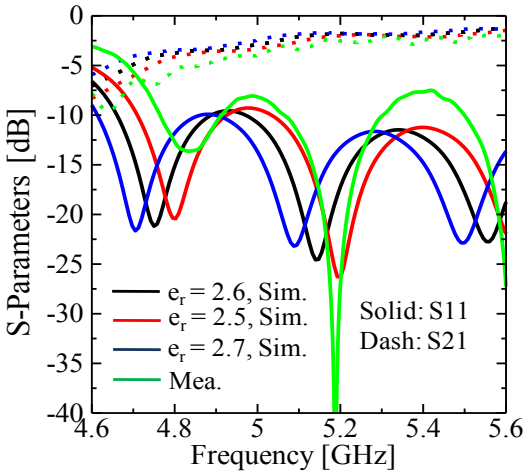

(a)

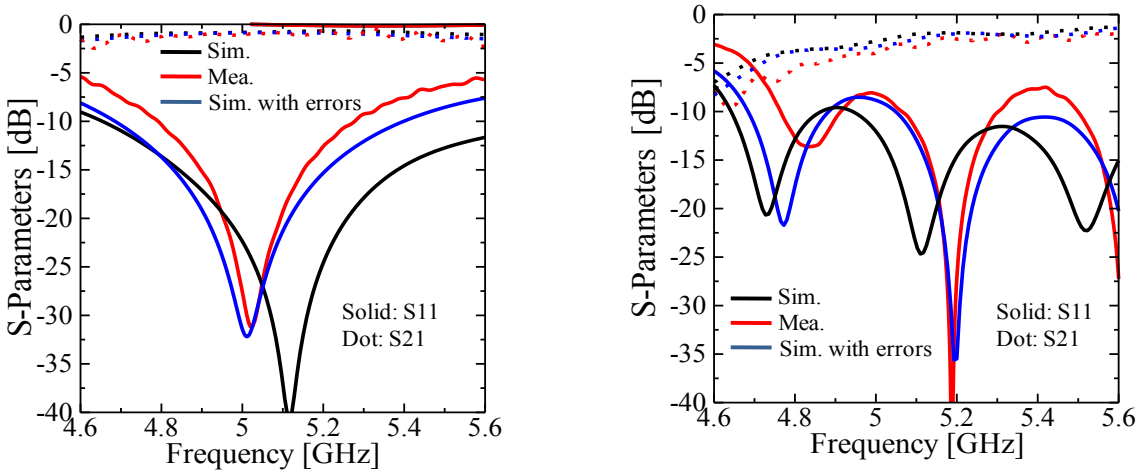

(b)

Fig. 3.22. Effect of errors of material and fabrication.

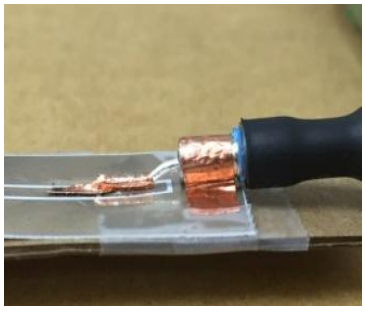

Fig. 3.23. The fabrication picture of the connection between one port of SCPW and a connector by using copper tape.

Table 3.3. Assumed fabrication and material errors at 5.12 GHz.

Parameters [mm]		ε_{r1}	g	s_3	l_2	l_3
No errors		2.6	0.5	0.5	18.5	15.2
Errors	1 unit	2.5	0.7	0.43	18.3	
	5 units	2.5	0.485	0.7	18.5	15.6

In conclusions, the design process of the transmission line or the SCPW and its basic performance were discussed. The transmission line is influenced little by bending and has a good coupling with external antennas. The transmission characteristic improvement of the transmission line will be considered in next chapter.

CHAPTER 4

ON-BODY TRANSMISSION IMPROVEMENT BY THE SCPW

This chapter presents the transmission improvement by the free access transmission line or the SCPW. As presented in Section 1.1, the free access transmission line by using coplanar waveguide has unique advantage that external antennas can communicate with each other at any positions near the transmission line, even at different sides of the transmission line. Thus, in Sections 4.1 we consider the performance of the transmission line on PEC plane in three cases: antennas below the transmission line, antennas above the transmission line and antennas at different sides of the transmission line. Measurement results on phantom and real body in these cases are given in Section 4.2. The specific absorption rate (SAR) is calculated in detail in Section 4.3. Finally, some other discussions about radiation direction of antennas, radiation loss of the transmission line and orientation of antennas are given in Section 4.4.

4.1 Transmission Characteristics between Two Antennas with the SCPW

This section calculates transmission characteristics between external antennas with or without the SCPW on the PEC plane at 2.45 GHz to see the transmission improvement by the SCPW. Three cases are considered depending on the positions of the antennas: antennas below the SCPW, antennas above the SCPW and antennas at different sides of the SCPW. In each case, two square patch antennas (utilized in Chapter 3) and two standard dipoles are used for measurements.

4.1.1 Antennas below the SCPW

The model is utilized for both simulation and measurement as illustrated in Fig. 4.1. In this model, the two patch antennas with port 3 and 4 are set between the transmission line and the PEC plane. The center of port 3 is settled at a distance of y_0 = 30 mm from port 1, and port 4 is shifted along the y-axis in 30 mm intervals keeping the spacing h = 1, 2, 3 and 5 mm. The distance between the centers of two patch antennas is represented as y_2. Port 1 and 2 of the line edges are open, considering practical usage. Fig. 4.2 presents simulation and measurement results. The dots denote exact data whilst curves show approximation. The transmission loss of S_{43} between the two patch antennas through the SCPW is very small and a propagation mode is assumed to be excited on the SCPW. The coupling between two patch antennas with the SCPW is greatly enhanced compared with that without SCPW. The improvement in coupling is more than 10 dB for small y_2 and 20 dB for large y_2 as demonstrated in Fig. 4.2. We prove that measurement results have a good agreement with simulation as shown in Fig. 4.3.

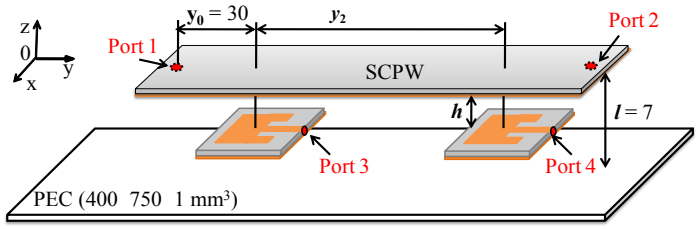

Fig. 4.1. Model utilized to validate the transmission loss between two patch antennas with SCPW on the PEC plane, the antennas below the SCPW.

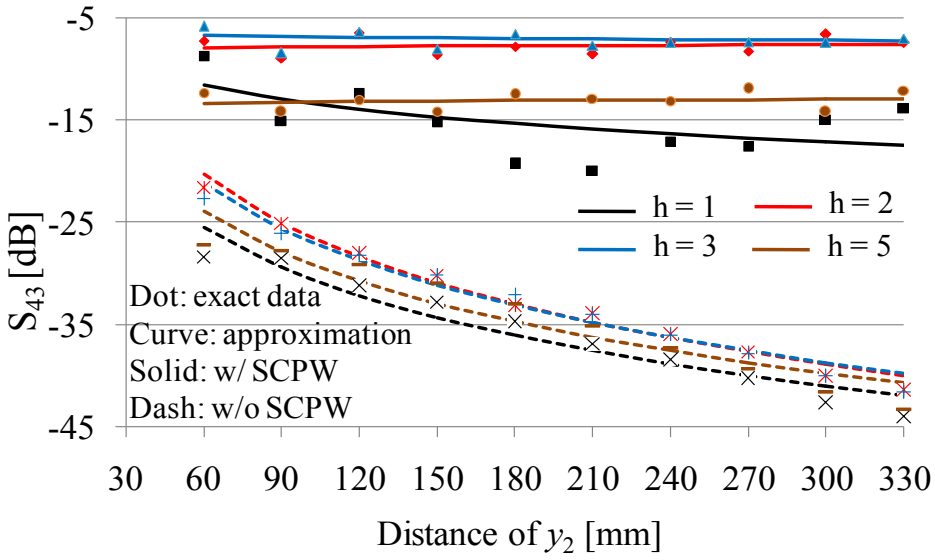

Fig. 4.2. Simulation results of the coupling between two patch antennas with or without SCPW, the antennas below the transmission line.

4.1.2 Antennas above the SCPW

In this section, the transmission loss between two patch antennas with or without the support of the transmission line at 2.45 GHz is presented in the case of the antennas above the SCPW. Fig. 4.4 shows the model utilized in simulation as well as in measurement. In this model, the two patch antennas to Port 3 and Port 4 are put above the SCPW with the PEC plane under the SCPW. Port 3 is fixed. The distance from Port 1 to the center of the patch antenna with Port 3 is y_0 = 30 mm. Port 4 is shifted along the y-axis in 30 mm intervals at the height of h = 1 mm. The distance between the centers of the two patch antennas is y_2. Port 1 and Port 2 of the transmission line are not excited, and left open like the Section 4.1.1. Radiation direction of the antennas is toward the transmission line.

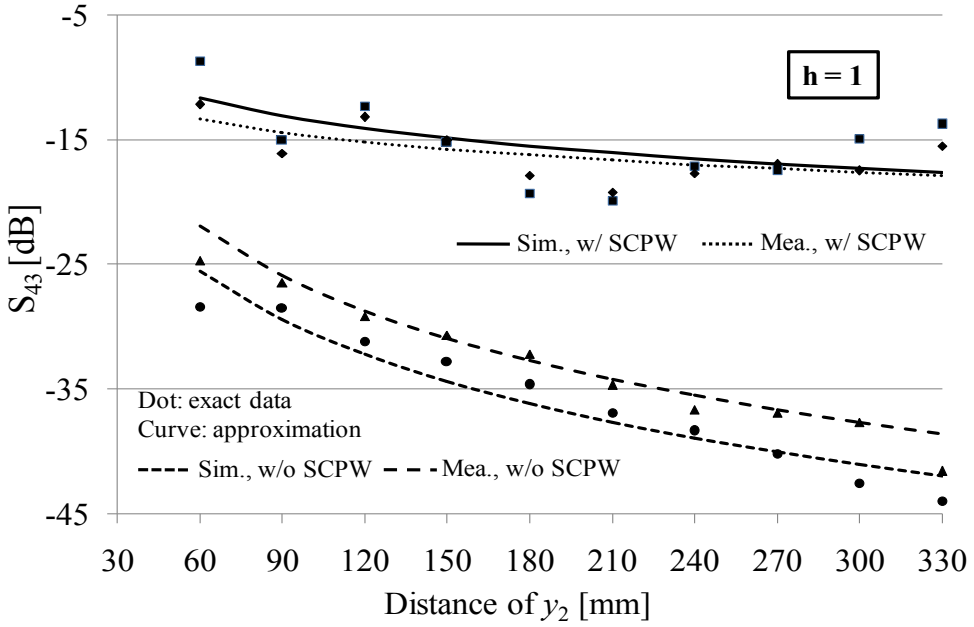

(a) Measurement, h = 1

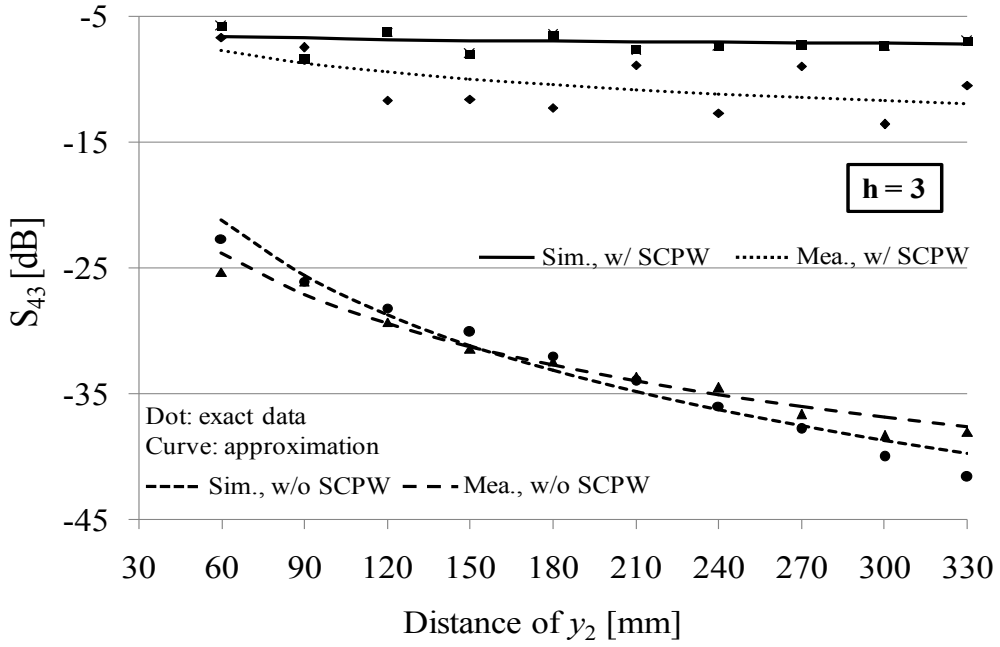

(b) Measurement, h = 3

Fig. 4.3. Measured results of coupling characteristics between two patch antennas with and without SCPW at 2.45 GHz.

Fig. 4.5 shows simulation results in three cases corresponding to h = 1, 2, and 3 mm. The makers denote the exact data whereas the solid lines are the approximated results. The transmission improvement is the difference of the transmission losses between the two patch

antennas in two cases of w/ TL and w/o TL. From the simulation results, when the distance of y_2 is short, the transmission improvement is smaller than 10 dB. However, the improvement is much higher for y_2 large. Thus, the transmission characteristics between two patch antennas on the PEC plane are improved significantly.

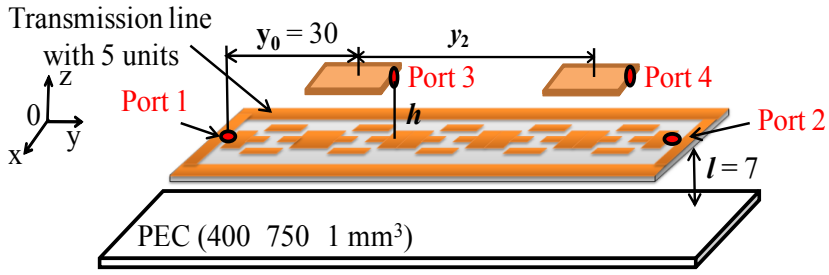

Fig. 4.4. Model utilized to estimate the transmission loss between two patch antennas with the SCPW on the PEC plane, the antennas above the SCPW.

Fig. 4.6 shows measurement results in the case h = 1 mm. In case of w/ SCPW, a good agreement between simulation and measurement can be seen whereas there is a difference in the case of w/ o SCPW. This is because of measurement errors.

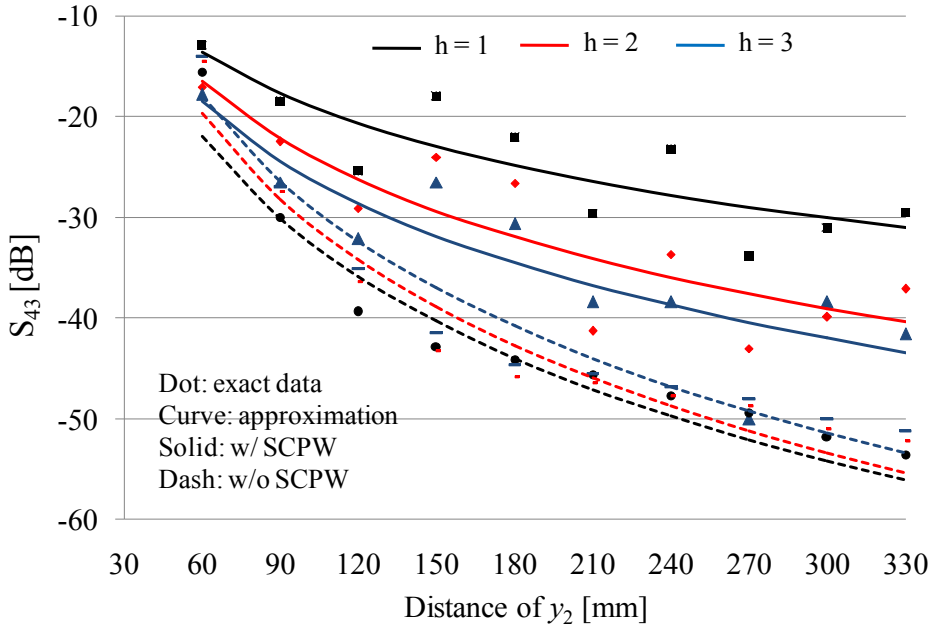

Fig. 4.5. Simulation results with and without the SCPW, the antennas above the SCPW: h = 1, 2 and 3 mm.

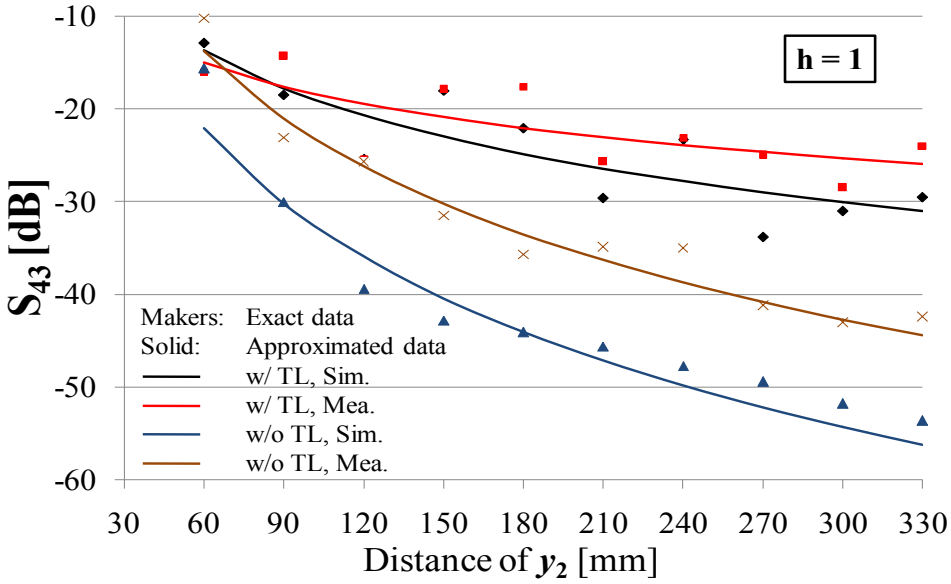

Fig. 4.6. Transmission characteristics between two patch antennas with and without the transmission line on the PEC plane at 2.45 GHz, the antennas above the SCPW h = 1.

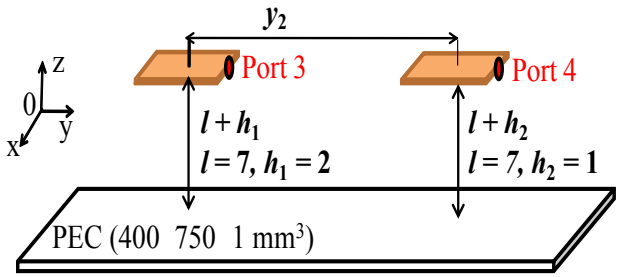

(a) The distances between two patch antennas and the PEC plane are different

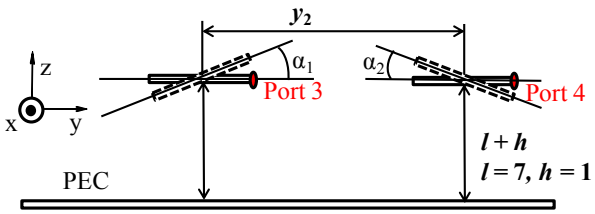

(b) The patch antennas are tilted to the center by small angles of α_1 and α_2.

Fig. 4.7. Model used to evaluate the transmission loss between two patch antennas without the SCPW on the PEC plane, the antennas above the SCPW.

The difference between simulation and measurement results in the case of w/o SCPW is because of unavoidable measurement errors. In detail, the distances between the patch antennas and the PEC plane are different ($h_1 \neq h_2$) in measurement. Another reason is that the

patch antennas in measurement is not parallel with the PEC plane, and they can be tilted by small angles of α_1 and α_2 to the center due to the measurement setting errors as shown in Fig. 4.7. To verify these reasons, we simulate three cases; (a) $h_1 = 2$, $h_2 = 1$ [mm], (b) $\alpha_1 = 2.5$, $\alpha_2 = 0$ [Deg.], and (b) $\alpha_1 = 2.5$, $\alpha_2 = 2.5$ [Deg.]. The simulation results in Fig. 4.8 confirm that the tilted angles are the main reason for the difference between simulation and measurement when the results (blue line and green line) in these cases approach the measured results (red line), and the difference of the distances between the two patch antennas and the PEC plane also contributes to this difference. In this consideration, the MWS software is used to adjust the tilted angles easily compared to the EMPro software.

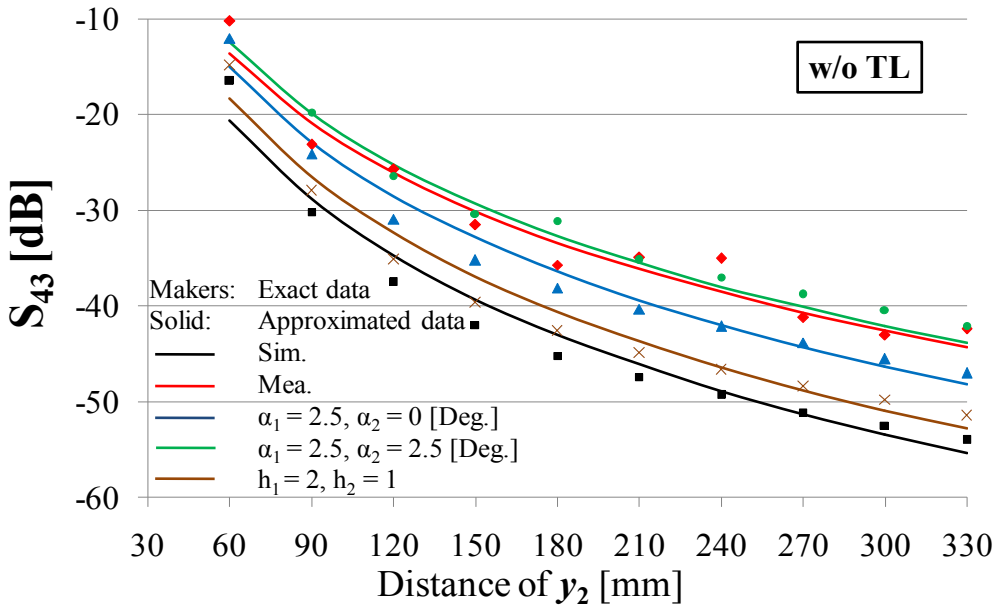

Fig. 4.8. Transmission characteristics between two patch antennas on the PEC plane without the transmission line at 2.45 GHz in three cases: (a) $h_1 = 2$, $h_2 = 1$ [mm], (b) $\alpha_1 = 2.5$, $\alpha_2 = 0$, and (c) $\alpha_1 = 2.5$, $\alpha_2 = 2.5$ [Deg.].

4.1.3 Antennas at Different Sides of the SCPW

This section presents transmission characteristics between two patch antennas when they are placed at different sides of the transmission line. The model utilized for both simulation and measurement is shown in Fig. 4.9. Simulation results with different heights of *h* are given in Fig. 4.10 (a) while measured results are shown in Fig. 4.10 (b). The results

show that the improvement by the transmission line is really significant, 10 dB for y_2 small, and more than 20 dB for y_2 large. The measured results agree well with simulation results.

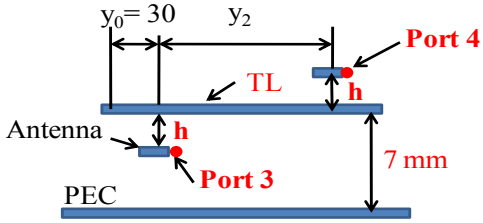

Fig. 4.9. Model used for simulation and measurement when two antennas at different sides of the transmission line.

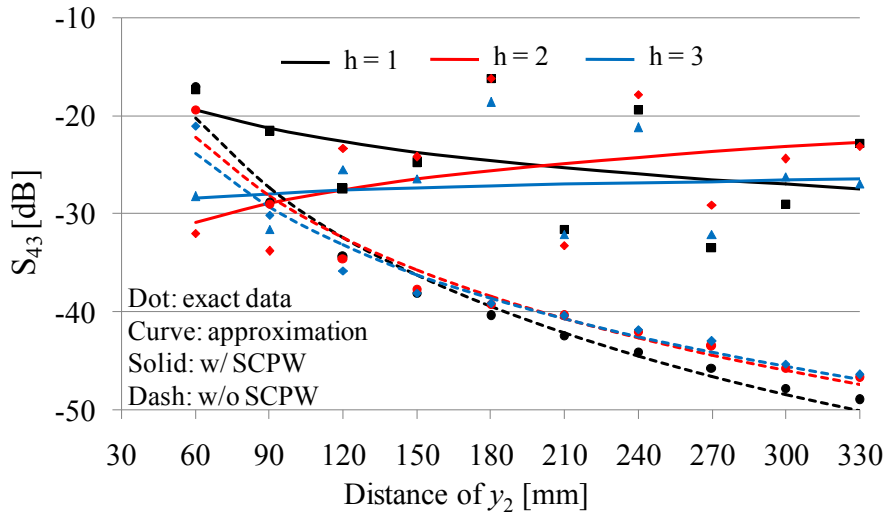

(a) Simulation

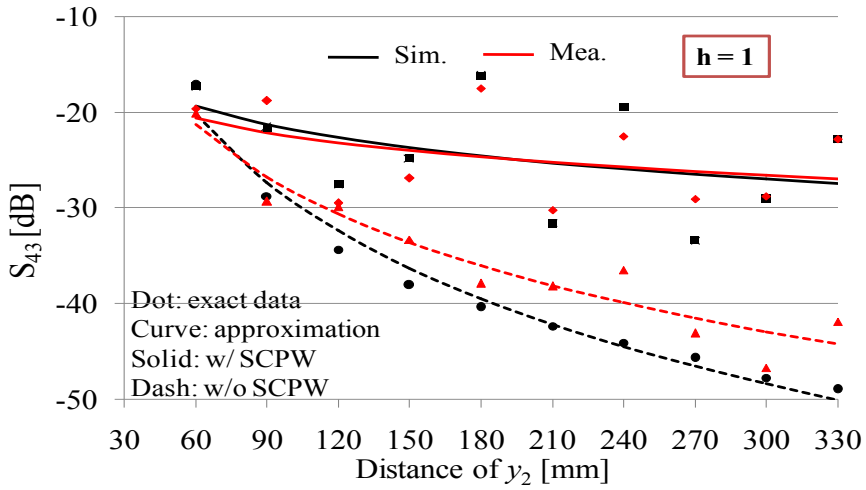

(a) Measurement

Fig. 4.10 Transmission characteristics between two patch antennas with and without the SCPW on the PEC plane at 2.45 GHz, the antennas at different sides of the SCPW.

4.1.4 Discussion about Difference between Simulation and Measurement

The small differences between simulation and measurement originates from the positions of antennas at every points is not really exact as in simulation. Besides, to control the distance between the antennas and SCPW we used small foams which are cut by hand, not really perfect as shown in Fig. 4.11. Thus, these measurement imperfections influence the measured results.

(a) Without SCPW (b) With SCPW

Fig. 4.11. Measurement pictures of the coupling between two patch antennas and the SCPW.

4.2 Measurement on the Phantom and Real Body

The transmission improvement by the transmission line is confirmed on the PEC plane in Section 4.1 in both simulation and measurement. This section will discuss about the improvement measured on the phantom and real bodies at 2.45 GHz. We did measurement with two patch antennas and two standard dipoles in three cases depending on the position of the antennas like Section 4.1.

4.2.1 Antennas below the SCPW

To compete with the measured results on real bodies, the transmission improvement between two patch antennas by the SCPW at 2.45 GHz is demonstrated utilizing ultra-light carbon phantom [25] in this section. This upper body phantom is 280 × 490 × 220 mm^3 in size. The photos of the coupling measurement between the two patch antennas and two standard dipoles with the phantom are shown in Fig. 4.12.

Two cases is measured. The first case is LOS case that two patch antennas are put in front of the phantom and the distance between the two antennas is 210 mm. The second case is NLOS case that one antenna is set on the front side and the other is installed on the back. In both cases, the SCPW is put above the phantom with the distance of 7 mm, and the two antennas are 1 mm below the SCPW. Measured results with the patch antennas and standard dipoles are given in Figs. 4.13. The dipoles are oriented in horizon and the two dipoles are 3 mm below the SCPW due to the size of feeding connector. Coupling characteristics using SCPW are greatly improved and are more than 20 dB compared with those without SCPW. To find these effects clearly, improved values are summarized in Table 4.1. The advantage in use of the SCPW is clear, which is effective for on-body communications.

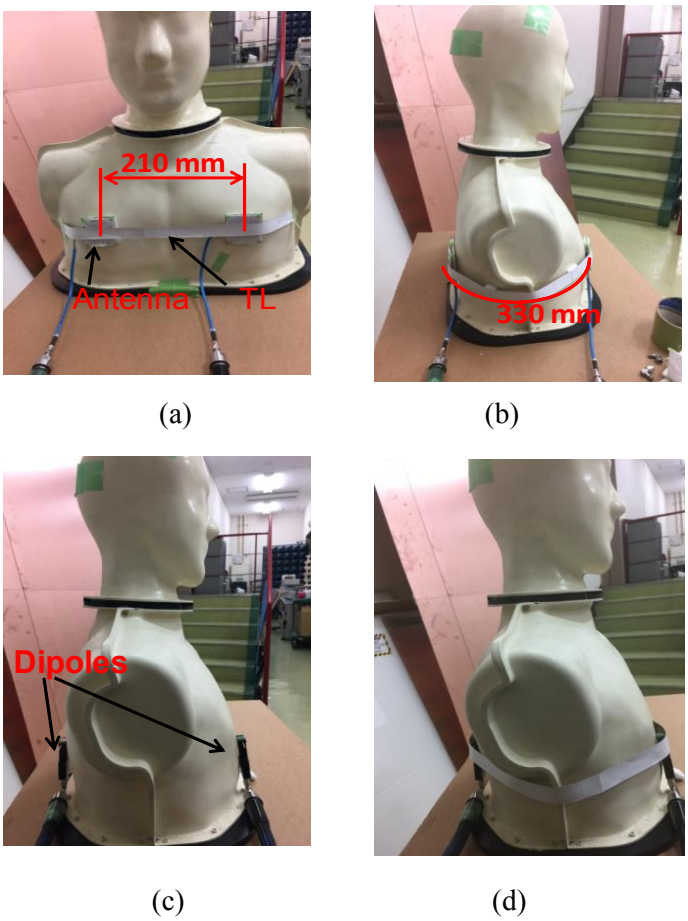

Fig. 4.12. Photos of measurement on the phantom, the antennas below the SCPW: (a) Patch antennas, LOS case;(b) Patch antennas, LOS case; (c) Dipoles, w/o SCPW and (d) Dipoles w/ SCPW.

The coupling power between two patch antennas and two standard dipoles on a real body are measured to confirm the transmission gain by the SCPW. The body is 1.7 m in

height and 55 kg in weight. The measurement installation is similar to that on the phantom in previous section. The measured results are demonstrated in Fig. 4.14. The transmission improvements are also summarized in Table 4.1.

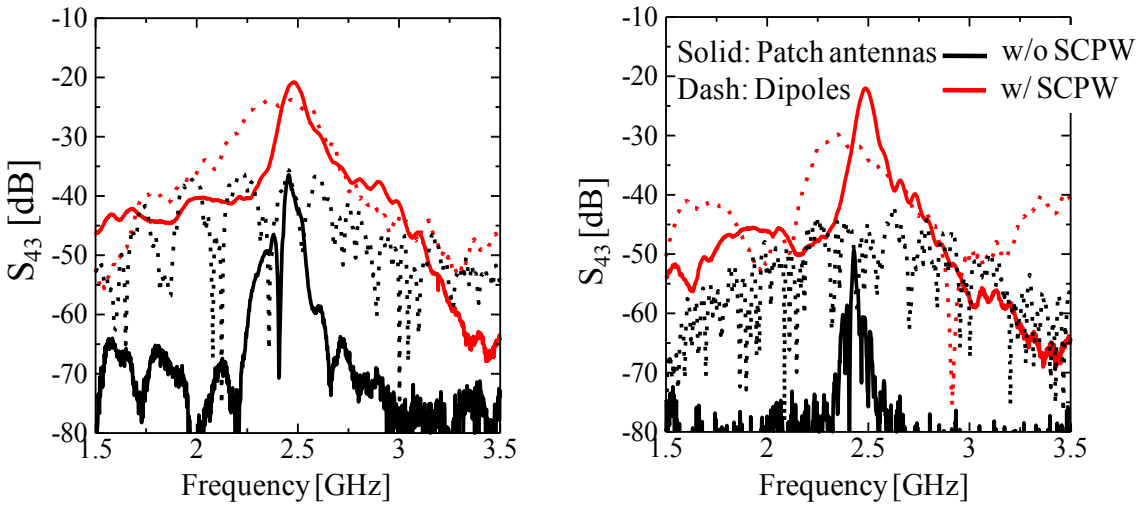

(a) (b)

Fig. 4.13. Transmission losses between two antennas on the phantom w/ SCPW and w/o SCPW, the antennas below the SCPW: (a) LOS case and (b) LOS case.

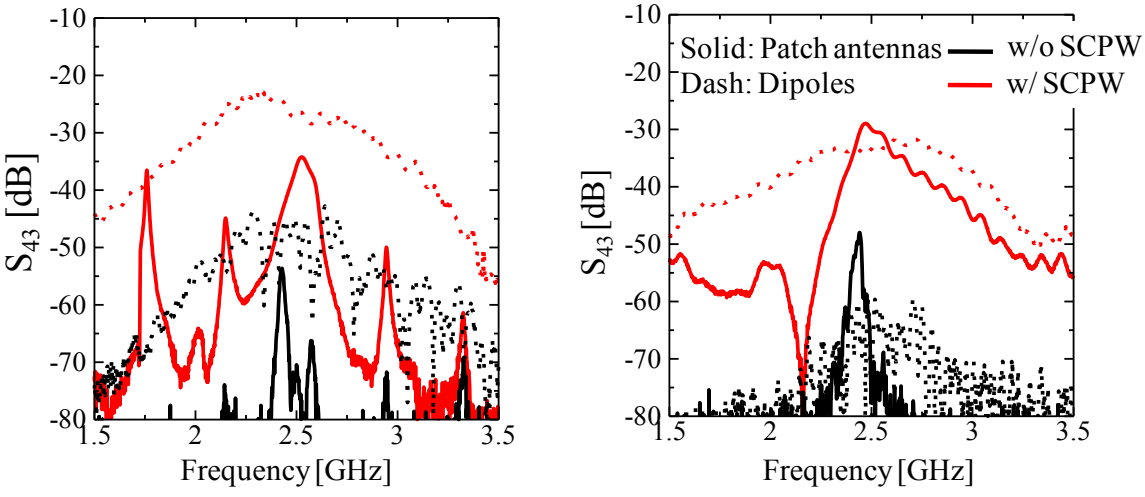

(a) (b)

Fig. 4.14. Transmission losses between two antennas on the real body w/ SCPW and w/o SCPW, the antennas below the SCPW: (a) LOS case and (b) LOS case.

Table 4.1. The transmission gain by SCPW at 2.45 GHz, the antennas below the SCPW.

Two antennas are in front of the phantom/body – LOS case					
Phantom/Body		Phantom		Body	
Type of antennas		Patch	Dipole	Patch	Dipole
S_{43}	w/ SCPW	-22	-24.2	-41.4	-25.5
	w/o SCPW	-37.1	-35.7	-61.7	-45.6
Transmission gain [dB]		15.1	11.3	20.3	20.1
One antenna is in front of the phantom/body, the other is back – NLOS case					
		Phantom		Body	
Type of antennas		Patch	Dipole	Patch	Dipole
S_{43}	w/ SCPW	-25.7	-31.8	-29.8	-33.9
	w/o SCPW	-56.2	-58.8	-49.9	-66.2
Transmission gain [dB]		29.5	27	20.1	32.3

4.2.2 Antennas above the SCPW

The measurement setting is almost similar in Section 4.2.1, except for the position of the antennas. In this case, the antennas are placed above the SCPW as shown in Fig. 4.15. The measured results are shown in Fig. 4.16. Besides, the transmission loss between two antennas without the SCPW is also measured to get the transmission gain or the improvement by the SCPW. In the first case, the transmission gain of 9.8 dB at 2.45 GHz is obtained and 21.1 dB in the second case. We can see that the transmission gain in the second case is larger than that in the first case. This shows that the transmission line is more effective for NLOS paths compared to Line of Sight (LOS) paths.

(a) (b)

Fig. 4.15. Pictures of measurement on the phantom with the SCPW, the antennas above the SCPW: (a) LOS case and (b) NLOS case.

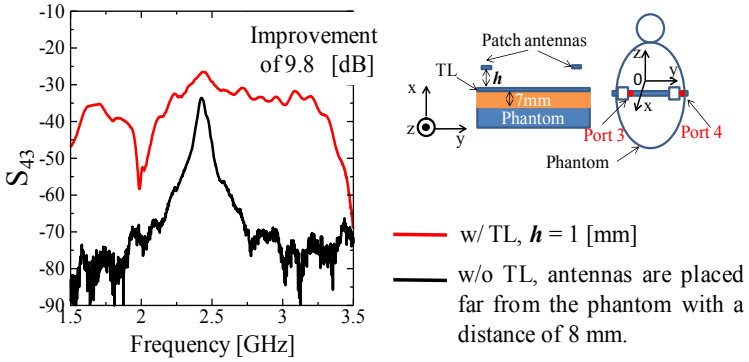

(a) Two patch antennas in front of the phantom

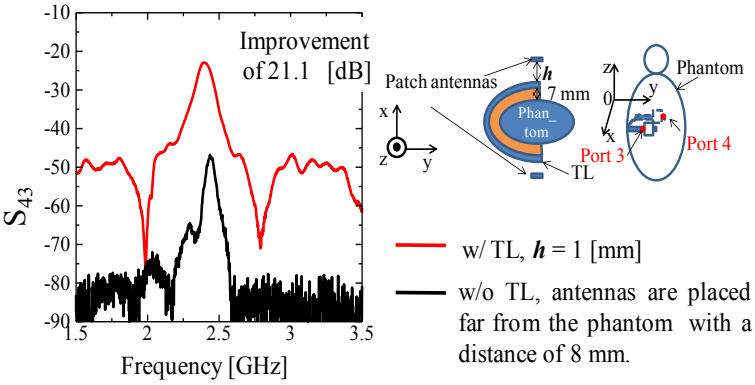

(b) One antenna in front of the phantom, the other one is on the back.

Fig. 4.16. Transmission improvement by the SCPW on the phantom, the antennas above the SCPW.

Next, transmission losses between two antennas on two real bodies (Body 1 and Body 2) are measured to evaluate the performance of the transmission line in improving the transmission characteristics. The first body is 1.7 m in height and 55 kg in weight, and the second body is 1.7 m in height and 70 kg in weight. The reason we measure on two bodies, is to make measured results more objective. The measurement setting on body is the same as that on the phantom in the previous section. The transmission line is placed far from the bodies with the distance of 7 mm, and the antennas are placed above the transmission line at the height of 1 mm. The detailed measured results are shown in Fig. 4.17. The transmission gains are given in Table 4.2.

When both patch antennas are placed in front of the body, the transmission gain is 17.2 dB for Body 1 whereas it is 10.7 dB for Body 2. The transmission gain is much higher when two antennas are not the same side of the bodies. It is 44.7 and 33.8 dB corresponding

to Body 1 and Body 2, respectively. It is observed that the transmission losses with the support of the transmission line on two bodies are quite similar. This shows that the transmission loss does not depend much on body type.

In addition, the improvement of the transmission characteristics by the transmission line is also verified when two standard dipoles at 2.45 GHz are used. The feeding points of dipoles antennas are placed on the center of two end units, far from the transmission line with a distance 3 mm. The distance between the feeding points of two dipoles is the same of the case of two patch antennas. The measured results with two dipoles are shown in Fig. 4.18. The transmission gain is also given in Table 4.2.

From the results in Table 4.2, we can see that the transmission loss is reduced greatly, and the improvement in NLOS paths is much higher than that in LOS paths. This trend is the same as the measured results on the phantom. In addition, the transmission improvement between two standard dipoles can be seen more clearly than that between two patch antennas. This is because the transmission loss between two dipoles on body without the transmission line is higher than that between two patch antennas due to the great reduction of the performance of the dipole when it is placed parallel with the body.

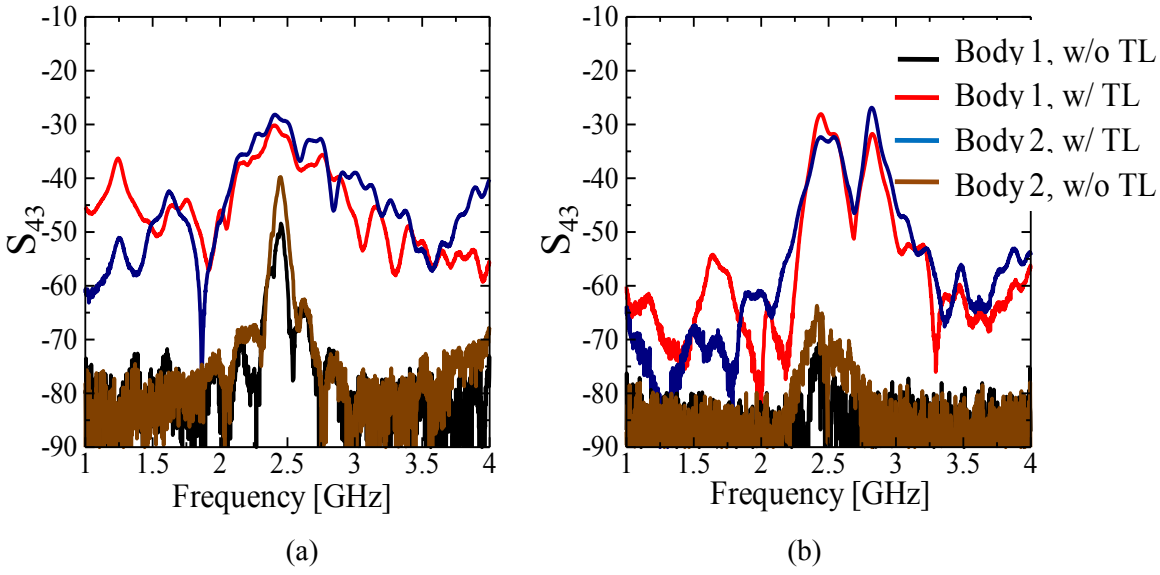

Fig. 4.17. Transmission loss between two patch antennas with and without the SCPW on two real bodies, the antennas above the SCPW: (a) LOS case and (b) LOS case.

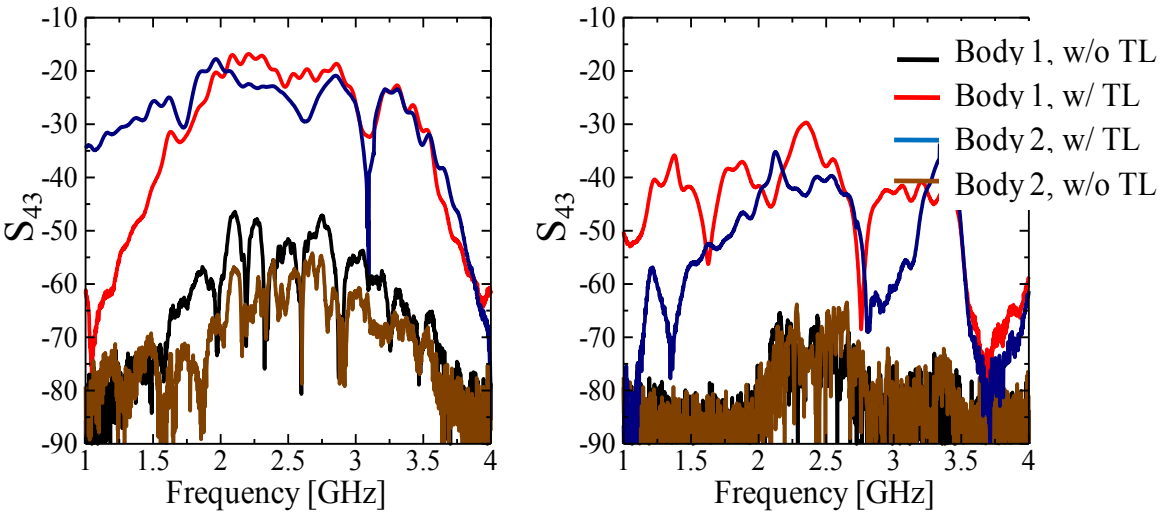

(a) (b)

Fig. 4.18. Transmission loss between two dipoles on two real bodies, the dipoles above the SCPW: (a) LOS case and (b) NLOS case.

Table 4.2. The transmission gain by the SCPW at 2.45 GHz, the antennas above the SCPW.

Two antennas are in front of the body – LOS case					
Type of antennas		Patch antenna		Standard dipole	
Type of bodies		Body 1	Body 2	Body 1	Body 2
S_{43}	w/ TL	-31.5	-29.1	-22	-24
	w/o TL	-48.7	-39.8	-55.8	-60.2
Transmission gain [dB]		17.2	10.7	33.8	36.2
One antenna is in front of the body, the other is on the back – NLOS case					
Type of antennas		Patch antenna		Standard dipole	
Type of bodies		Body 1	Body 2	Body 1	Body 2
S_{43}	w/ TL	-28.2	-32.4	-31.3	-40.1
	w/o TL	-72.9	-66.2	-74.1	-92.8
Transmission gain [dB]		44.7	33.8	42.8	52.7

4.2.3 Antennas at Different Sides of the SCPW

The performance of the transmission line is verified on phantom in this section when two patch antennas are placed at different sides of the transmission line as shown in Fig. 4.19.

Measurement setting is the same as previous sections. Measured results are shown in Fig. 4.20. The improvement performance is as good as those of previous cases.

Thus, in Section 4.2 we considered fully the performance of the transmission line on phantom and real bodies by measurements. The results confirm that the improvement by the transmission line is significant, especially for NLOS case.

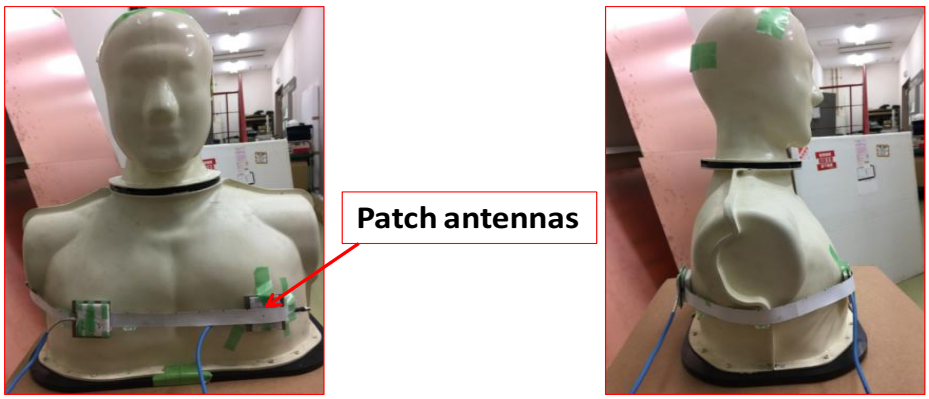

(a) LOS (b) NLOS

Fig. 4.19. Measurement pictures on phantom when two patch antennas at different sides of the transmission line.

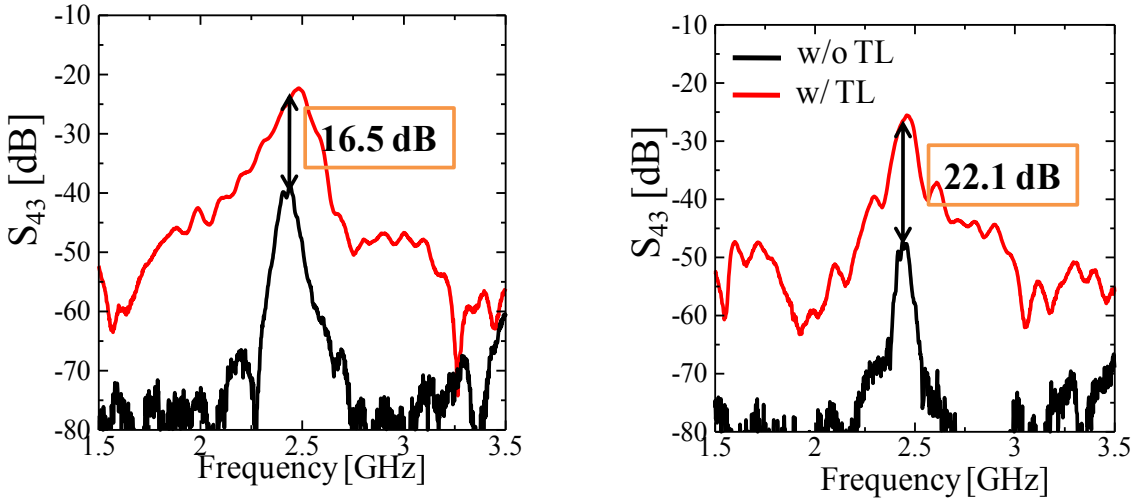

(a) (b)

Fig. 4.20 Measurements on the phantom, the antennas at different sides of the SCPW (a) two antennas in front of phantom (b) one antenna is in front, the other is on the back.

4.3 Calculation of SAR

As mentioned in Section 2.2.1.4, SAR has to satisfy standards for human safety. It is strongly required by on-body devices. Thus, SAR is checked when the transmission line is placed near body. To calculate SAR, we do simulation to get the maximum amplitude of E-field on the surface of the simplified phantom (mentioned in Section 2.22). Model is used for calculation as follows:

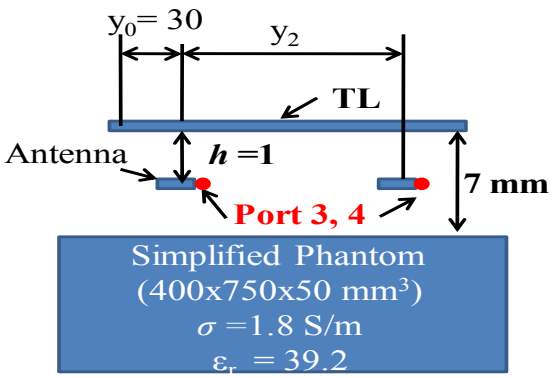

Fig. 4.21. Model used for SAR calculation.

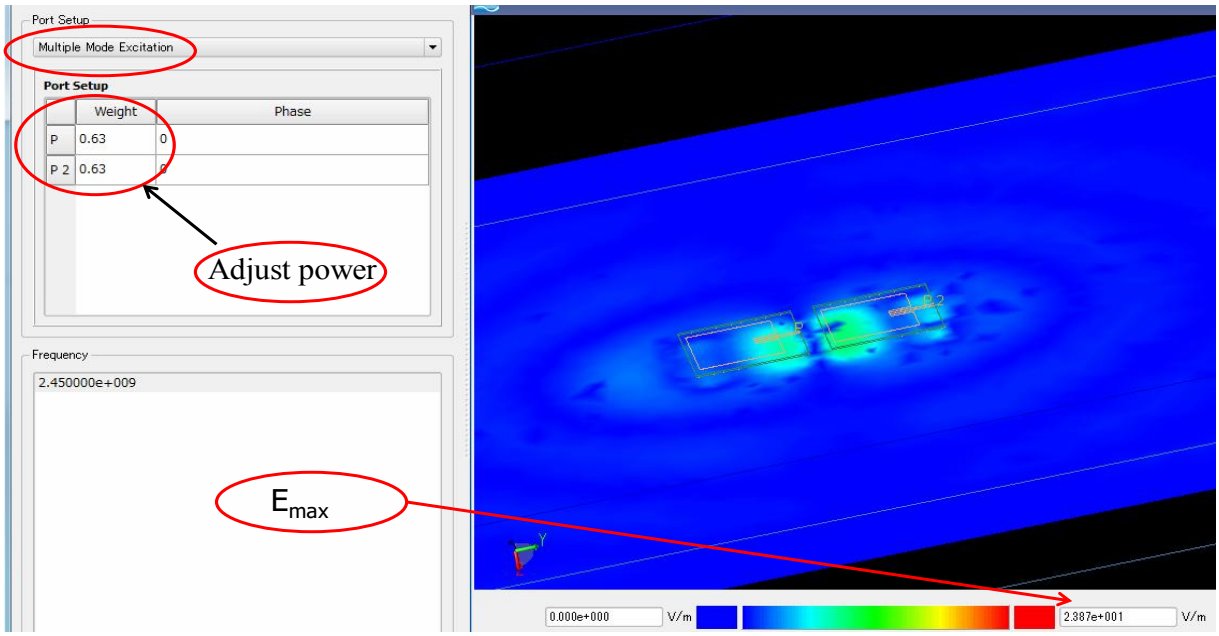

Fig. 4.22. Advanced result window to get the amplitude of E-field in EMPro software.

Fig. 4.21 is for calculation in the case of when two antennas are below the transmission line. The amplitude of E-filed is determined at every reference points of y_2. The way of calculating for two other cases (antennas above the transmission line and antennas at different sides) is the same. The distance of *h* between antenna and the transmission line is 1 mm Fig. 4.22 shows window results where we can get the maximum amplitude of E-field. To change the input power of the antennas, we can adjust value of "weight" in Fig. 4.22, and to get the total E-field from both antennas, we choose "Multiple Mode Excitation" in "Port Setup".

The power of 0 dBm which is expected for on-body devices is chosen for calculation. In detail, calculated results are given in Tables 4.3-4.5.

4.3.1 Antennas below the SCPW

This section discusses about SAR when antennas are placed below the transmission line. The results in Table 4.3 show that when the input power is $P_1 = 0$ dBm, SAR some points is not satisfied. When the input powers are -8.6, -9.8 dBm, SAR satisfies standards EU and US, respectively.

Table. 4.3. SAR values when antennas are placed below the transmission line.

y_2 [mm]	E_{max} [V/m			**SAR** [W/kg]		
	$P_1 = 0$ dBm	$P_2 = -8.6$ dBm	$P_3 = -9.8$ dBm	$P_1 = 0$ dBm	$P_2 = -8.6$ dBm	$P_3 = -9.8$ dBm
60	88.9	33.2	29	**14.5**	**2.02**	**1.54**
90	40	14.9	13	**2.92**	**0.41**	**0.31**
120	28.1	10.5	9.1	**1.45**	**0.21**	**0.16**
150	38.9	14.5	12.7	**2.78**	**0.39**	**0.3**
180	37.9	14.2	12.3	**2.63**	**0.37**	**0.28**
210	31.7	11.8	10.3	**1.84**	**0.26**	**0.2**
240	33	12.3	10.7	**2**	**0.28**	**0.22**
270	35	13.1	11.4	**2.24**	**0.32**	**0.24**
300	33.8	12.6	11	**2.09**	**0.3**	**0.23**
330	27.9	10.4	9.1	**1.43**	**0.2**	**0.16**

4.3.2 Antennas above the SCPW

This section presents the SAR calculation when the antennas are placed above the transmission line. The results in Table 4.4 show that when the input power is P_1 = 0 dBm, SAR values are satisfied.

Table. 4.4. SAR when antennas above the transmission line.

y_2 [mm]	E_{max} [V/m]	**SAR [W/Kg]**
60	25.3	**1.18**
90	11.5	**0.25**
120	12.4	**0.29**
150	20.7	**0.79**
180	24.2	**1.08**
210	12.9	**0.31**
240	12.5	**0.29**
270	20.3	**0.76**
300	10.7	**0.21**
330	14.3	**0.38**

4.3.3 Antennas at Different Sides of the SCPW

The SAR values are calculated in this section when the antennas are placed at different sides of the transmission line. The results in Table 4.5 show that when the input power is P_1 = 0 dBm, SAR some points is not satisfied. When the input powers are -18.5, -19.6 dBm, SAR values satisfies standards EU and US, respectively.

In brief, when the input power of antennas ranges from 0 dBm to -20 dBm, SAR requirement is satisfied.

Table. 4.5. SAR when antennas are at different sides of the transmission line.

y_2 [mm]	E_{max} [V/m]			SAR [W/kg]		
	P_1 = 0 dBm	P_2 = -18.54 dBm	P_3 = -19.63 dBm	**P_1 = 0 dBm**	**P_2 = -18.5 dBm**	**P_3 = -19.6 dBm**
60	25.8	3.1	2.7	**1.22**	**0.02**	**0.02**
90	175.1	20.8	18.3	**56**	**0.8**	**0.62**
120	49.1	5.8	5.1	**4.4**	**0.07**	**0.05**
150	227.6	27.1	23.8	**94.7**	**1.35**	**1.04**
180	78.1	9.3	8.2	**11.16**	**0.16**	**0.13**
210	66.6	7.9	7	**8.1**	**0.12**	**0.09**
240	3.24	0.39	0.34	**0.02**	**0.01**	**0.01**
270	34.7	4.13	3.64	**2.21**	**0.04**	**0.03**
300	43.6	5.19	4.57	**3.48**	**0.05**	**0.04**
330	278.4	33.15	29.2	**141.6**	**2.01**	**1.6**

4.4 Other Discussions

4.4.1 Radiation Direction of Antennas

In previous sections, we present the cases that antennas radiate toward the SCPW. The cases of that the antennas do not radiate toward the SCPW are discussed here. The first case is when two antennas above the SCPW and the second case is when two antennas are placed at different sides of the SCPW.

4.4.1.1 Antennas above the SCPW

The radiation direction of antennas is changed as shown in Fig. 4.23. The distance between antennas and SCPW is h = 1 mm. Antennas radiate out of body and the transmission line or SCPW. Simulation results are shown in Fig. 4.24. From the results, we can see that the improvement by SCPW is more than 10 dB for y2 large, but not as good as that in case of when antennas radiate toward SCPW.

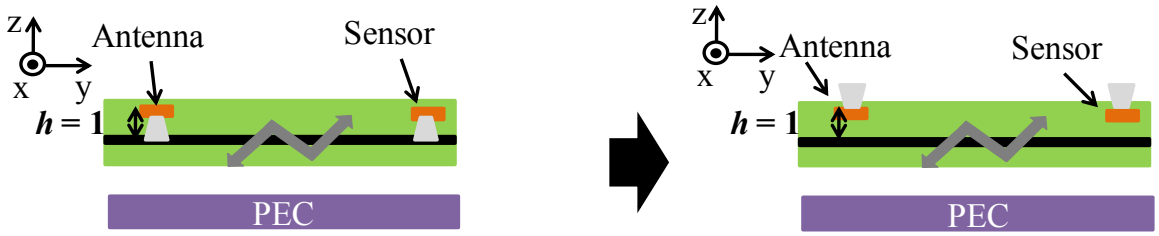

(a) Old model (b) New model

Fig. 4.23. Radiation direction of antennas is toward outside: (a) toward SCPW (b) toward outside.

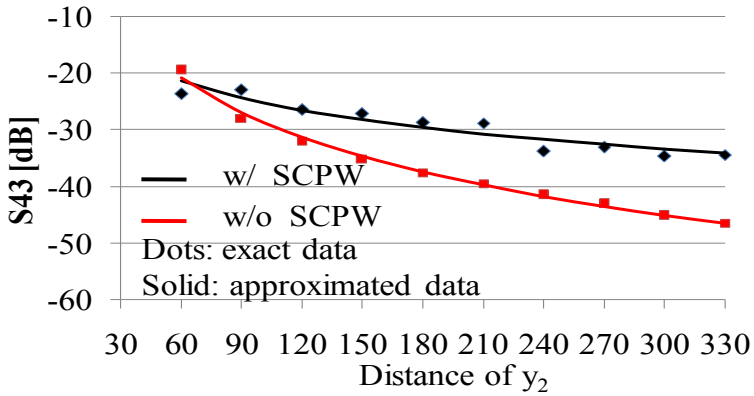

Fig. 4.24. Transmission characteristics between two antennas radiate out of body with/ without SCPW, antennas above the SCPW.

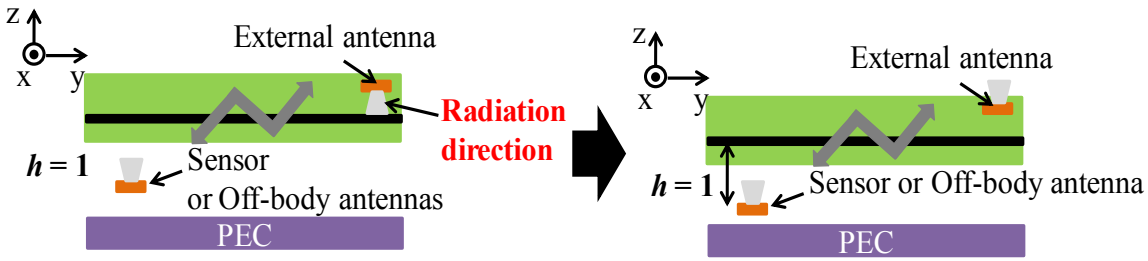

(a) Old model (b) New model

Fig. 4.25. Antenna radiates out of the SCPW, the antennas at different sides of the SCPW.

4.4.1.2 Antennas at Different Sides of the SCPW

Radiation direction of one antenna is changed as shown in Fig. 4.25. Simulation results are given in Fig. 4.26. We can see that the improvement by SCPW increases when the

distance of y_2 increases, but is not as good as that in the case of when the antenna radiates toward SCPW. Thus, higher coupling can be achieved when radiation direction of antennas is toward SCPW. As a result, we propose that antennas on body should radiate toward SCPW, this gives a higher performance.

4.4.2 Radiation Loss

In Section 3.6.1, we discussed about the radiation loss of the transmission line by comparing its S-parameters to those of the simple coplanar waveguide. This work will be discussed more in this section by comparing the transmission characteristics between two antennas below the transmission line to those with the simple coplanar waveguide.

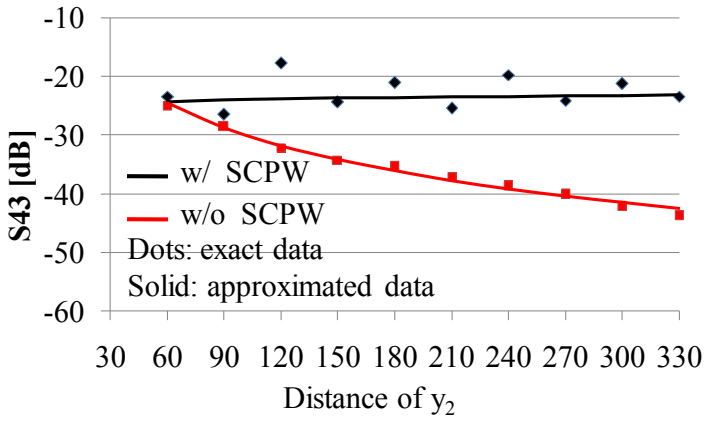

Fig. 4.26. Transmission characteristics between two antennas radiate out of SCPW with/ without SCPW.

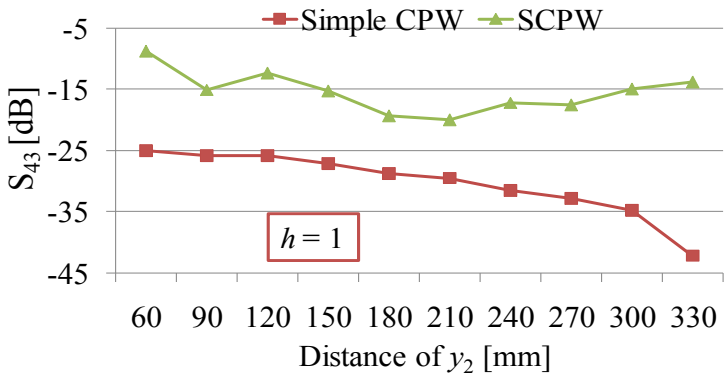

Fig. 4.27. Transmission characteristics between two patch antennas with the simple CPW.

The simulation results in case of h = 1 mm in Fig. 4.27 show that the radiation from the transmission line is necessary to get higher coupling between two antennas. Thus, radiation loss from unwanted modes of the transmission line is insignificant.

4.4.3 Orientation of Antennas

This part presents the effect of the orientation of the microstrip patch antennas on the coupling between SCPW and the antennas. We change the orientation of the microstrip antennas from "parallel to SCPW" (the orientation is proposed in the manuscript) to "orthogonal to SCPW" as shown in Fig. 4.28 (a) below. The results in Fig. 4.28 (b) show that the performance of the new orientation is not as good as that of the proposed orientation. Thus, the proposed orientation is the best choice.

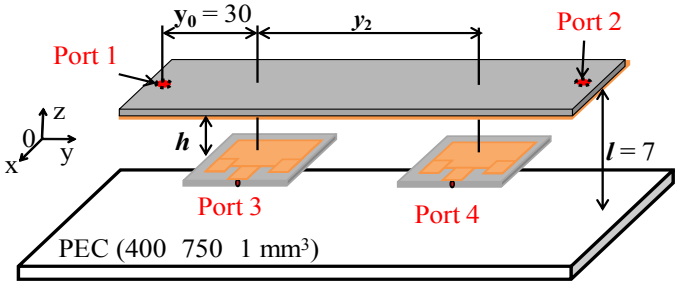

(a) Antennas are orthogonal to SCPW

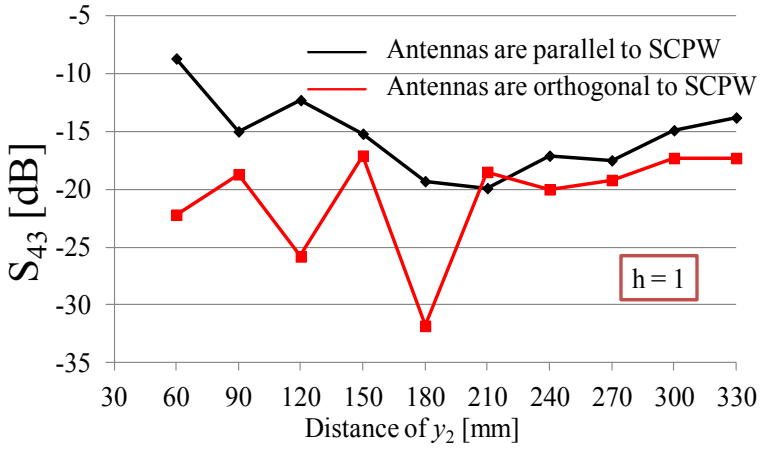

(b) Simulation results

Fig. 4.28. Simulation results when the orientation of the microstrip antennas are changed.

Besides, the effect of the orientation of dipoles is considers as shown in Fig. 4.29. The dipoles is changed from horizontal (H) to vertical (V), are placed below the transmission line. Measured results are given in Fig. 4.30 and Table. 4.6. It can be seen that when the dipoles are in vertical, the results is not as good as that when they are put in horizontal.

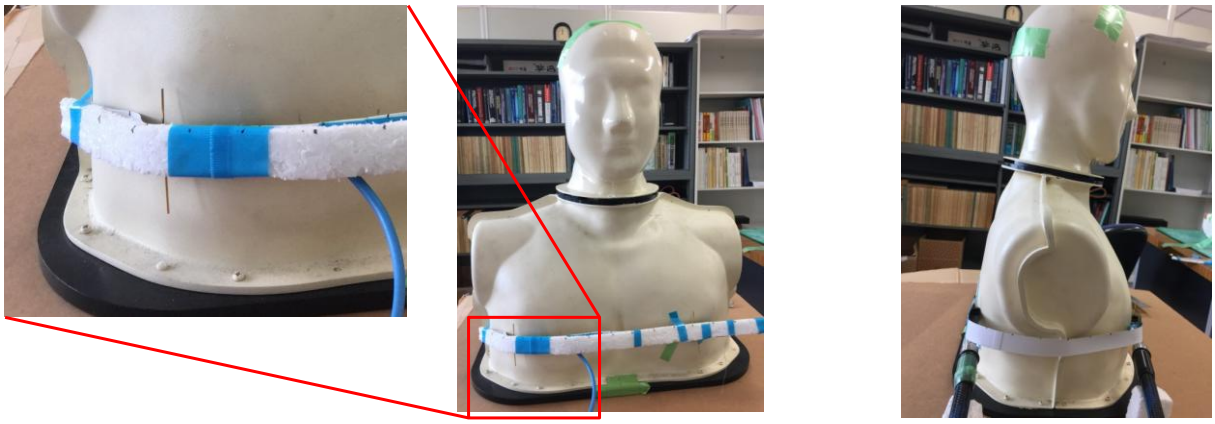

(a) (b)

Fig. 4.29. Measurement pictures on phantom with dipoles in vertical, the dipoles below the SCPW: (a) two dipoles are in front of phantom; (b) one dipole is in front, the other is back.

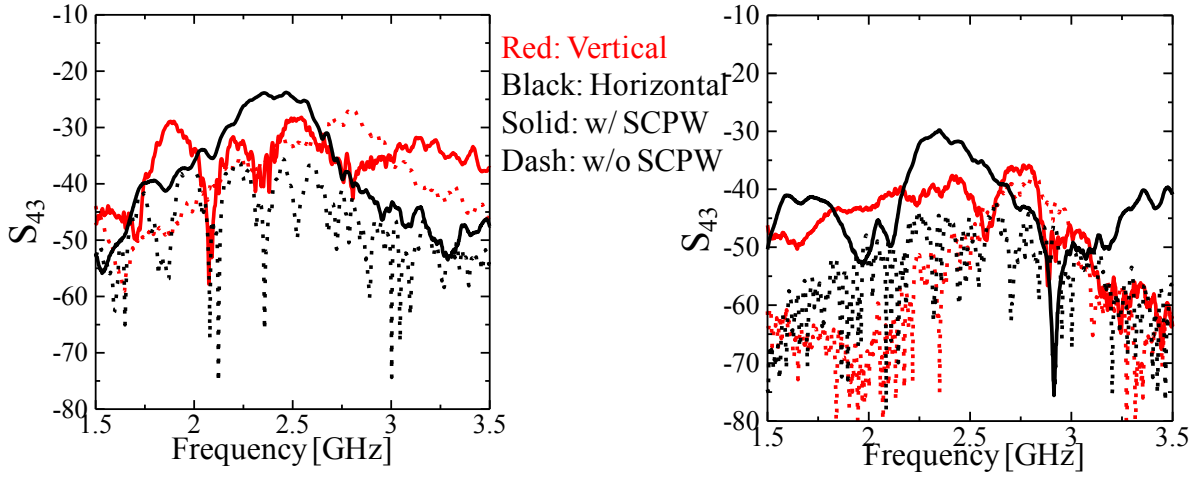

(a) (b)

Fig. 4.30. Measured results on phantom with dipoles in vertical, the dipoles below the SCPW: (a) LOS case; (b) NLOS case.

Table. 4.6. Transmission gain by the SCPW with dipoles in vertical.

Two dipoles are in front of phantom – LOS case			
Orientation		H	V
S43	w/ SCPW	-24.2	-31.2
	w/o SCPW	-35.7	-30.8
Transmission gain		11.3	**0.4**
One dipole is in front, the other is back – NLOS case			
Orientation		H	V
S43	w/ SCPW	-31.8	-38.2
	w/o SCPW	-58.8	-52.8
Transmission gain		27	**15.4**

Thus, this chapter verified the performance of the transmission line on the PEC plane, a phantom and on real bodies. The transmission improvement by the transmission line is more than 20 dB in NLOS case. Besides, other problems like the difference between simulation and measurement, the tangent loss of the paper substrate, the effect of the orientation of the antennas were discussed in detail.

CHAPTER 5

ON-BODY TRANSMISSION IMPROVEMENT BY A CONDUCTIVE STRIP LINE

A simple solution for on-body communication is proposed in this chapter by using a conductive strip line (CSL). To communicate with each other, on-body antennas are placed below the CSL. First, the performance of the CSL is compared to that of SCPW on both PEC plane and simplified phantom in Section 5.1. Next, optimal dimension parameters of the conductive strip line are discussed in Section 5.2. The performance of the CSL is confirmed by measured results on phantom in Section 5.3. Section 5.4 presents the calculation of SAR.

5.1 Comparison with the SCPW

In Section 4.1.1, when considering the coupling between the two patch antennas below the transmission line, we found that the coupling performance does not follow the same pattern when the distance of *h* changes. This may be because of the effect of the reflection from the transmission line. Thus, we will discuss about this reflection in this section by replacing the transmission line by a conductive strip line with the same dimension in width and in length.

5.1.1 Comparison on the PEC Plane

We compare the performance of the CSL with the SCPW in two cases corresponding to h = 1 and 3 mm when the antennas are placed below the SCPW. From the simulation results in Fig. 5.1, we can see that they have the same pattern when *h* increases.

Fig. 5.2 shows simulation results when two antennas are placed above the SCPW or the CSL. The simulation results when the two antennas are put at different sides of the SCPW and the CSL are shown in Fig. 5.3. In both these cases, the distance of *h* is 1 mm.

It can be seen that the CSL has a good performance as good as that of the SCPW when antennas are placed below it. The other cases, the CSL does not have a good performance. Thus, in specific cases the CSL can be a candidate for on-body communication when antennas are placed near body.

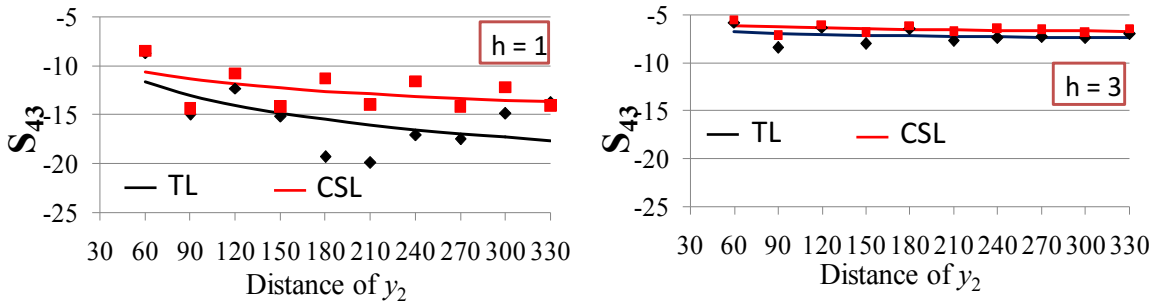

(a) *h* = 1 (b) *h* = 3

Fig. 5.1. Performance comparison between the SCPW and the CSL on the PEC plane, the antennas below the TL or CSL.

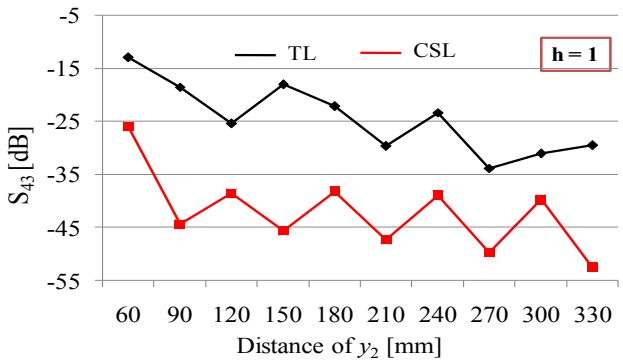

Fig. 5.2. Performance comparison between the TL and CSL on the PEC plane, the antennas above the TL or CSL.

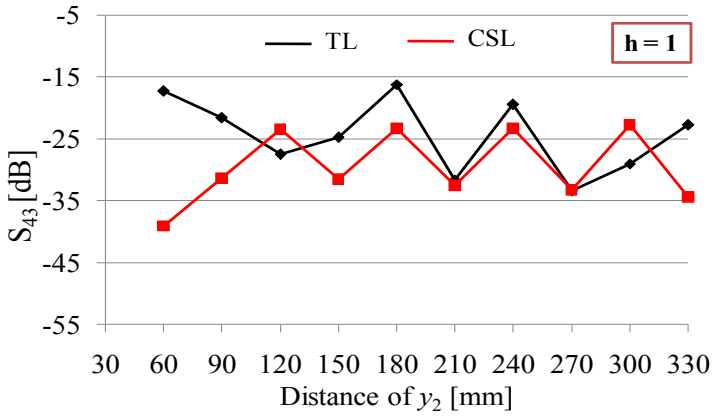

Fig. 5.3. Performance comparison between the TL and the CSL on PEC, the antennas at different sides of the TL or CSL.

5.1.2 Comparison on the Phantom Model

Another comparison on the simplified phantom model is presented in this section. We just consider the case of two antennas below the conductive strip line. This is the case that the conductive strip line has a good performance on PEC plane as mentioned in the previous section.

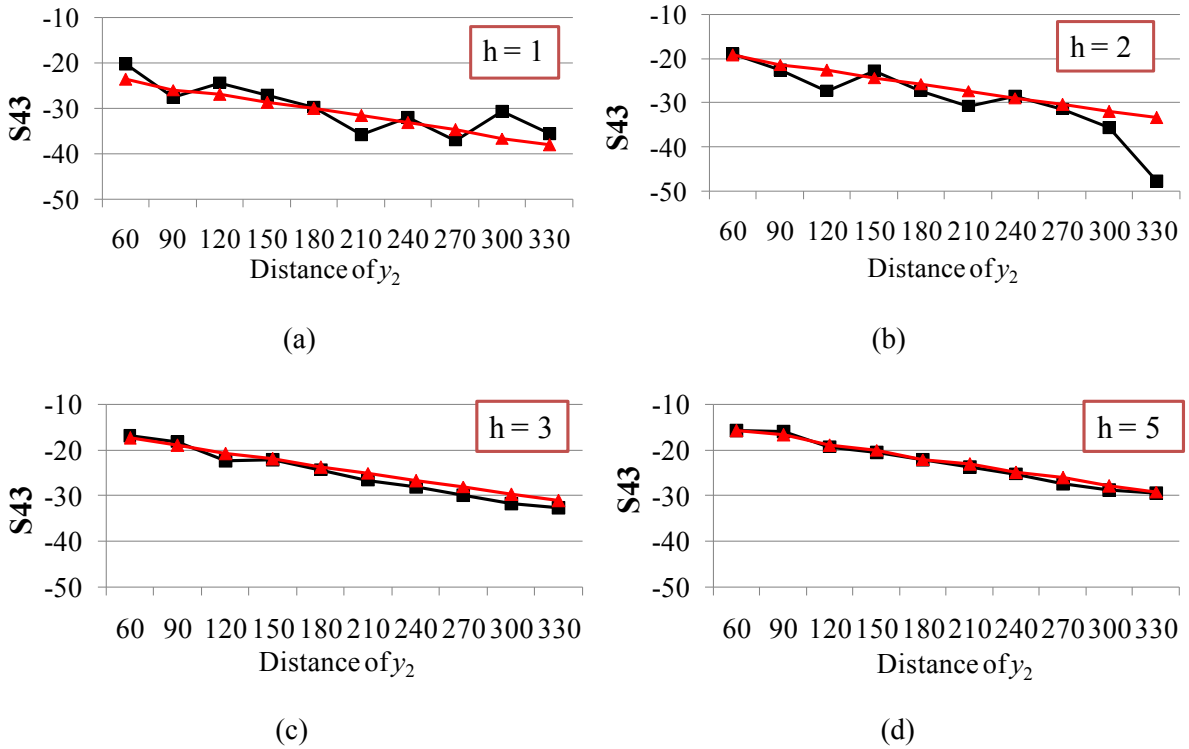

Fig. 5.4. Comparison between the TL and CSL on the simplified phantom.

Simulation results in Fig. 5.4 show that the performance of the CSL is similar to those of the transmission line when *h* increases. This agrees with the results on PEC plane. Thus, the CSL can be a simpler solution for on-body communication in specific cases when antennas are placed between the body and the CSL. In next sections of this chapter, we find the optimal dimension for the CSL, and then, check its performance on the real phantom.

5.1.3 Current Distribution Comparison on the PEC Plane

To understand the principle of the CSL, its current distribution is shown in this part. The current surface on the PEC plane, on the conductive layer of the CSL and the E-field are shown in Figs. 5.5-5.7, respectively. From the current distributions, we can observe that the CSL works as a microstrip line, fed by antennas when it is placed near body.

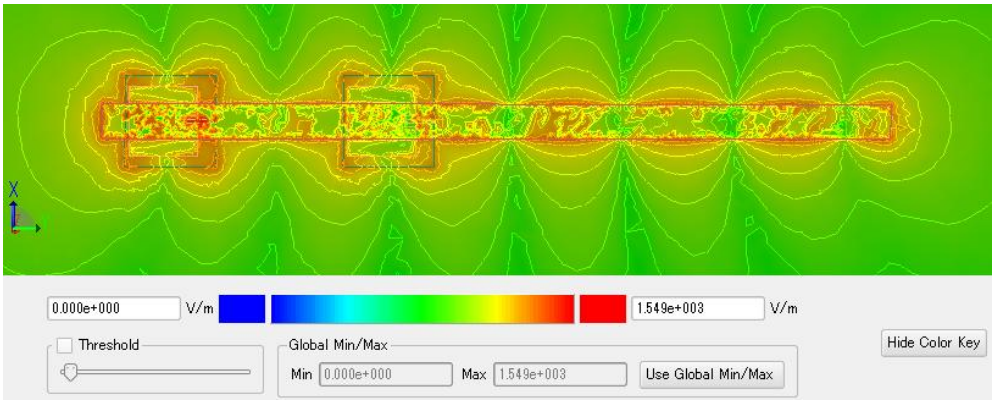

(a) On CSL

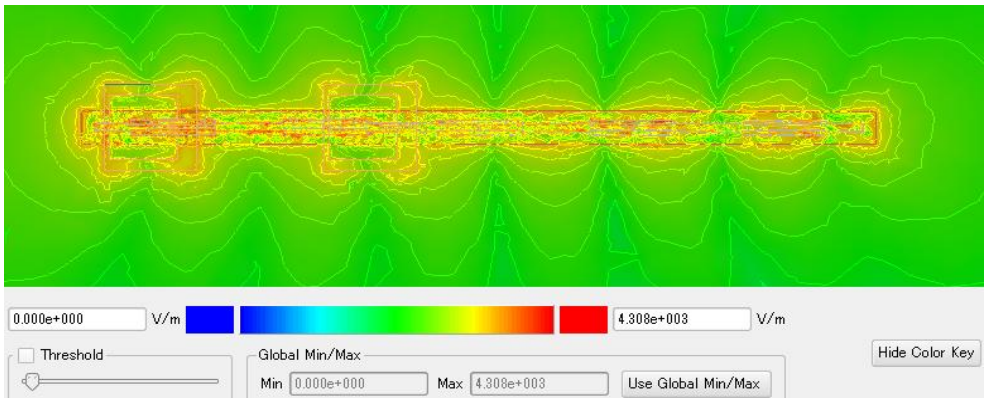

(b) On Transmission line

Fig. 5.5. Current surface on the conductive layer of CSL and the TL.

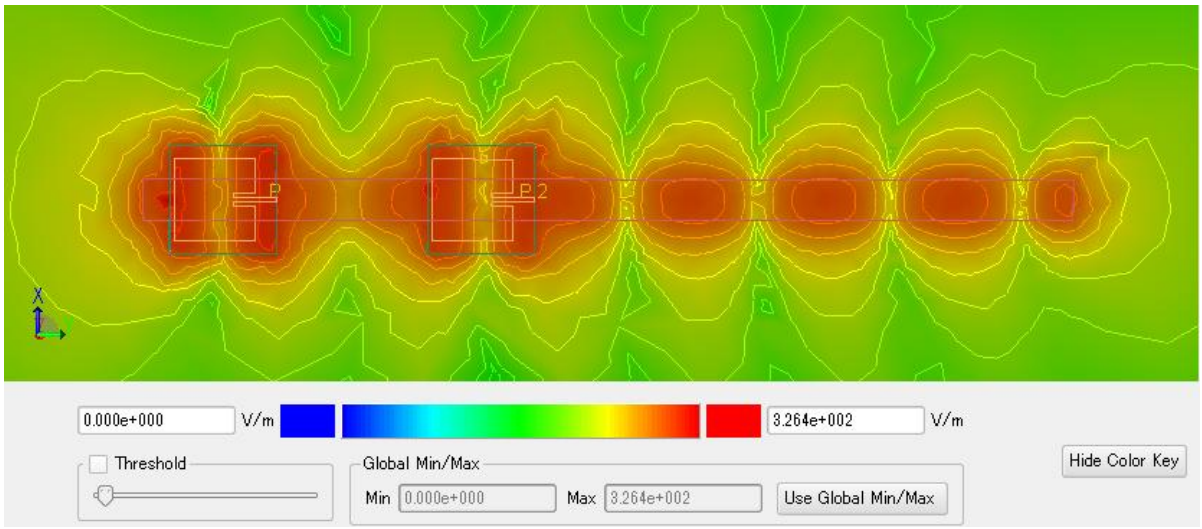

(a) On PEC with CSL

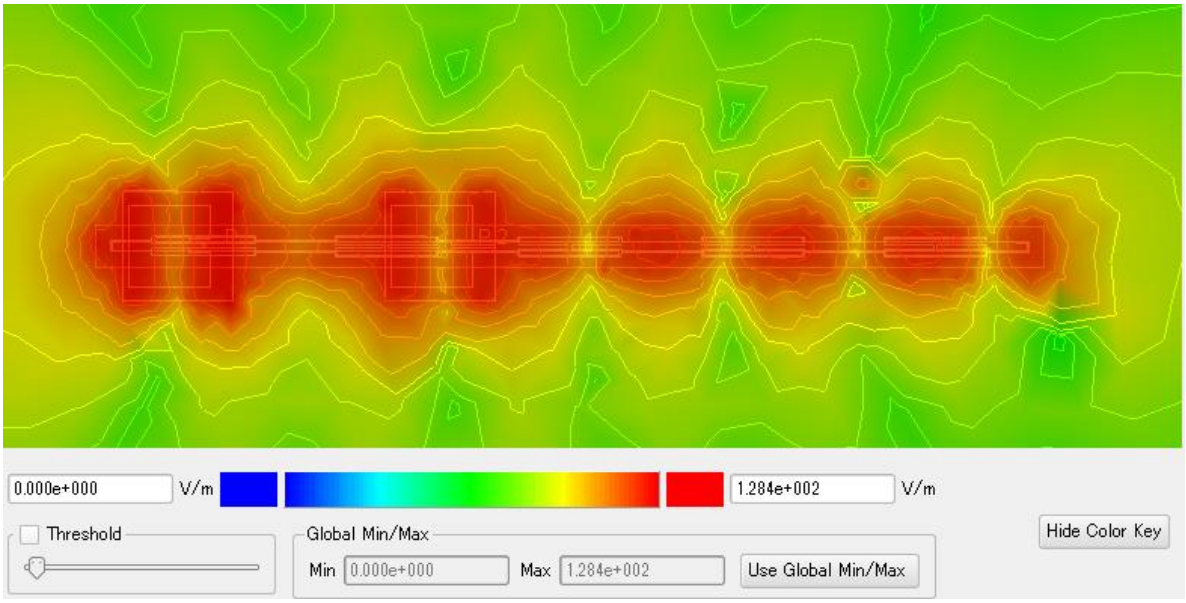

(b) On PEC with the transmission line

Fig. 5.6 Current surface on PEC plane with the conductive layer of CSL and the transmission line.

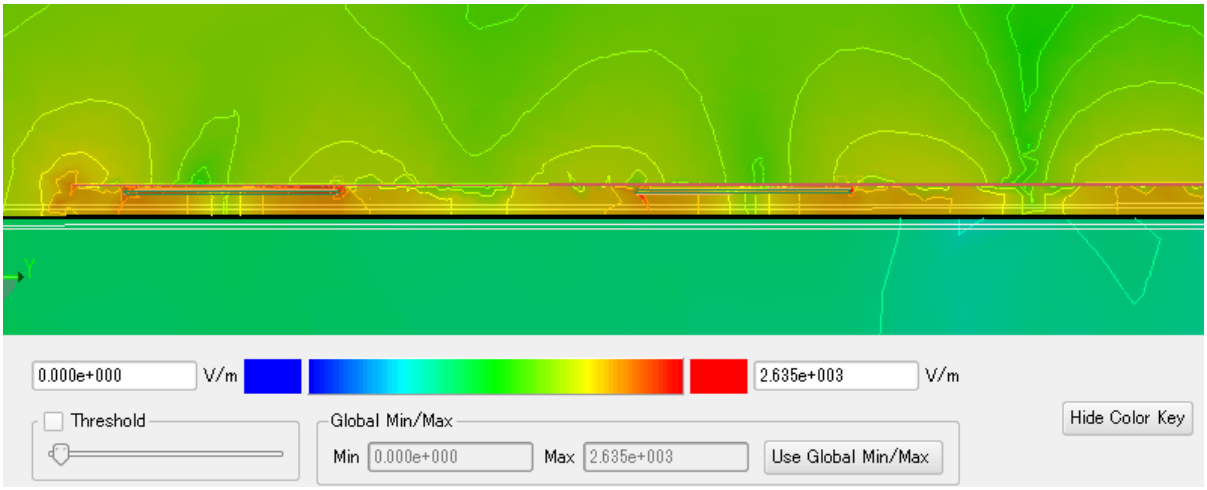

(a) With CSL

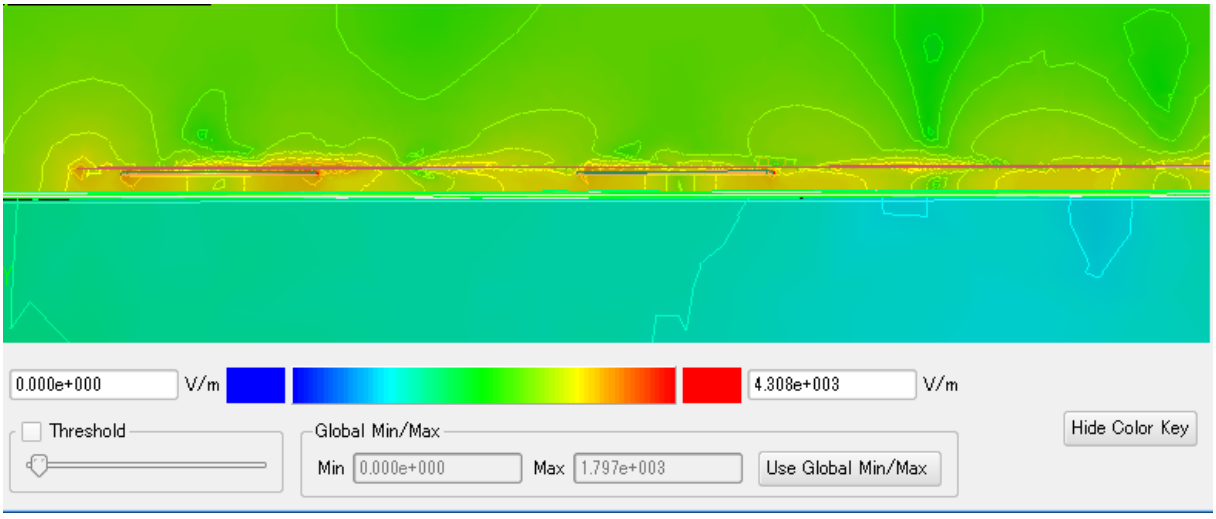

(b) With transmission line

Fig.5.7 E-field on ZY plane with the CSL and TL.

5.2 Optimal Parameters of the CSL

In this section, we present the process of finding optimal parameters of the CSL by considering transmission characteristics between the two patch antennas with the CSL. The process is shown in Fig. 5.8. First, the length and the width of CSL are fixed as those of the transmission line to find the optimal height of *h*. In detail, width (W) = 19 mm ($0.15\lambda_0$), length (L) = 430 mm ($3.5\lambda_0$). We set the target that the coupling in S_{43} between two antennas with the CSL should be equal or greater than -20 dB. The distance between the antennas and the PEC plane is 1.2 mm. Next, the optimal of the width is calculated by using the optimal height in the first step. In this step, only the width is changed. The optimal height may change with the optimal width. Thus, after finding the optimal width, the optimal height is recalculated. Finally, the length of CSL is increased to check its performance. The process is carried out on both the PEC plane and the simplified phantom model.

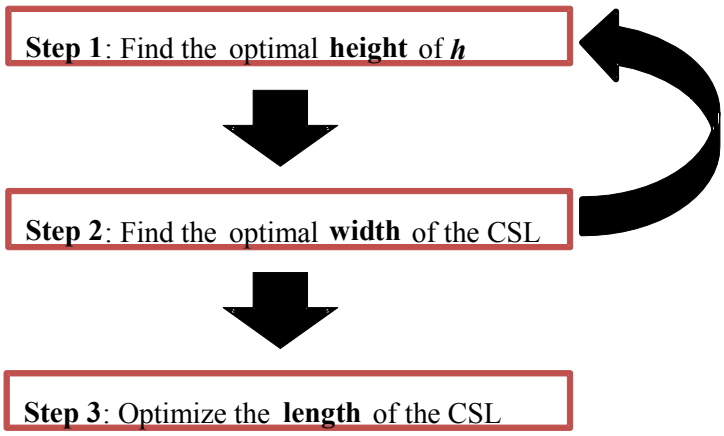

Fig. 5.8. The process of finding optimal parameters for the CSL.

5.2.1 Optimal Parameters on the PEC

5.2.1.1 Optimal Height on the PEC Plane

To find the optimal height of CSL from PEC plane, the model as shown in Fig. 5.9 (a) is used. In this model, the patch antennas are placed far from PEC plane with a fixed distance of 1.2 mm, below the CSL. The coupling between the two antennas is calculated at different height of h = 1, 3, 5 and 10 mm. The simulation results are shown in Fig. 5.9 (b). We can see that when *h* increases, S_{43} decreases. The distance of *h* should be smaller 20 mm to get S43 ≥ -20 dB, and *h* = 1 mm is the best distance. However, considering the practical application, *h* should be equal to 5 mm.

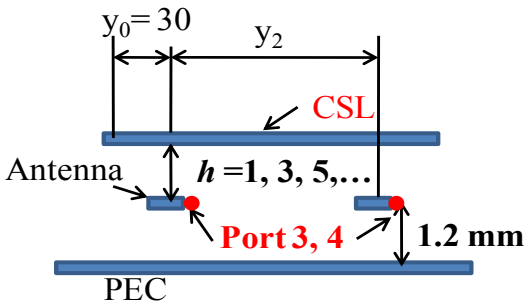

(a) Model used for simulation

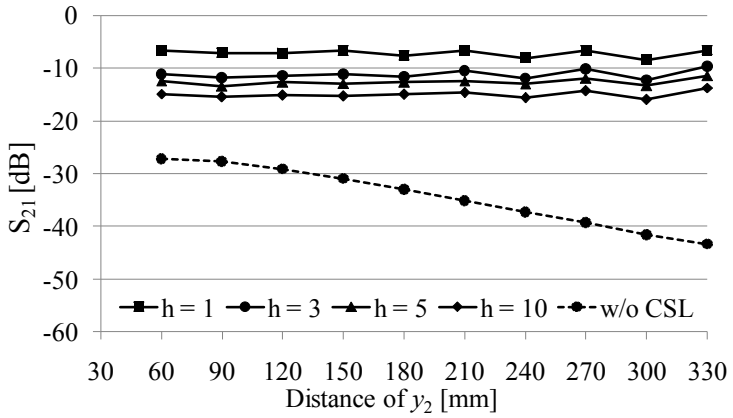

(a) Simulation results

Fig. 5.9. Coupling characteristics between two patch antennas with CSL on PEC plane when the height of CSL is changed.

5.2.1.2 Optimal Width on the PEC Plane

Next, we fix the length of the CSL, L = 430 mm (3.5λ_0) and the height h = 1mm, only change the width of W from 0.02 to 0.5 λ_0. The used model and simulation results as shown in Fig. 5.10 (a). The simulation results is shown in Fig. 5.10 (b), S43 is around -10 dB. Depending on the deviation of S43 as shown in Fig. 5.10 (c), we devide the results into three groups: Group 1, Gorup 2 and Group 3.

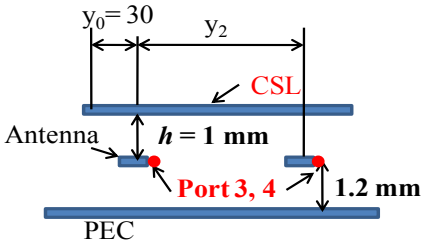

(a) Model used for simulation

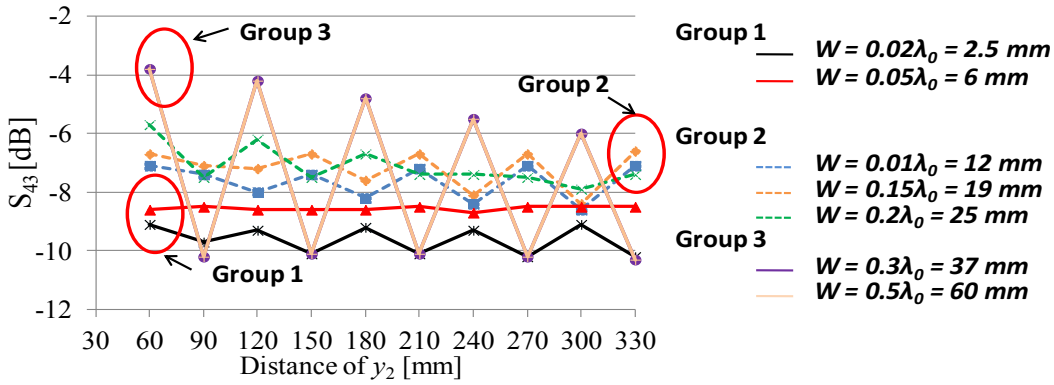

(b) Coupling characteristics with CSL

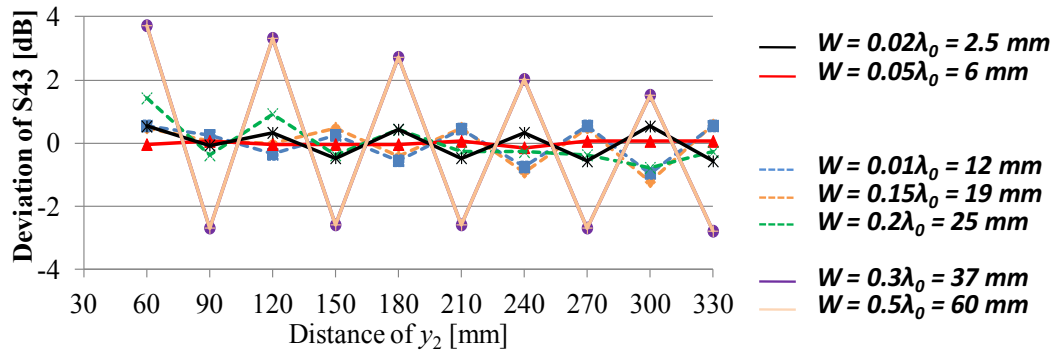

(c) Deviation of S43

Fig. 5.10. Coupling characteristics between two antennas with CSL on PEC plane when the width of CSL is changed.

In Group 1, W is smaller than $0.05\lambda_0$ (6 mm), the deviation is approximately zero. The devivation in Group 2 with the width from $0.01\lambda_0$ (12 mm) to $0.2\lambda_0$ (25 mm) is around 0.5 dB while the higher deviation can be seen in Group 3, where the width from $0.3\lambda_0$ (37 mm) to $0.5\lambda_0$ (60 mm). The deviation is given in Table 5.1 in detail. The smaller deviation is expected, and therefore, the width smaller than 6 mm should be chosen. Thus, we choose w = 6 mm for the next calculation.

Besides, the optimal width is calculated when the optimal height of h = 5 mm. The simulation results are shown in Fig. 5.12. The simulation results in Fig. 5.11 reveal that the best results can be obtained when W = 6mm. This agrees with the results when h = 1 mm. Thus, W = 6 mm, h = 5 mm are chosen for next considerations.

Table. 5.1 Deviation of S43.

Group	**Group 1**		**Group 2**			**Group 3**	
Width (W)	$0.02\lambda_0$	$0.05\lambda_0$	$0.1\lambda_0$	$0.15\lambda_0$	$0.2\lambda_0$	$0.3\lambda_0$	$0.5\lambda_0$
Average S43 [dB]	-9.63	-8.56	-7.65	-7.18	-7.12	-7.52	-7.52
Average deviation (|S43|- |Aver.|)	0.43	0.06	0.516	0.52	0.552	2.66	2.66

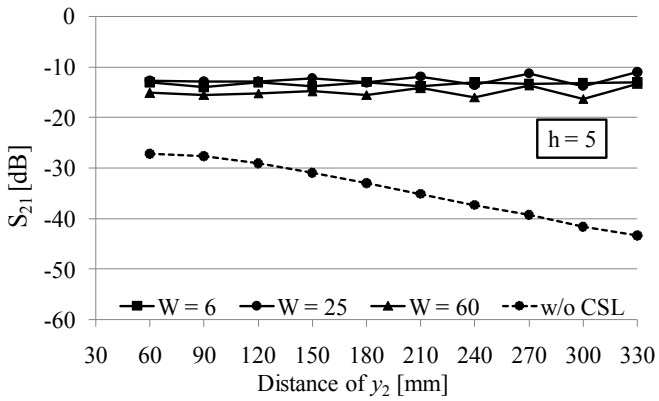

Fig. 5. 11. Coupling characteristics between two antennas with CSL on PEC plane when the width of CSL is changed, h = 5 mm.

5.2.1.3 Optimal Length on the PEC Plane

Considering applications in practice, the length of the CSL, $L = 4.5\lambda_0$ is long enough. Thus, we increase the length of the CSL to $4.5\lambda_0$. Then, the simulation results of the coupling between two antennas are calculated as shown in Fig. 5.12. The coupling in S_{43} is around 10 dB and reduces little when y_2 increases.

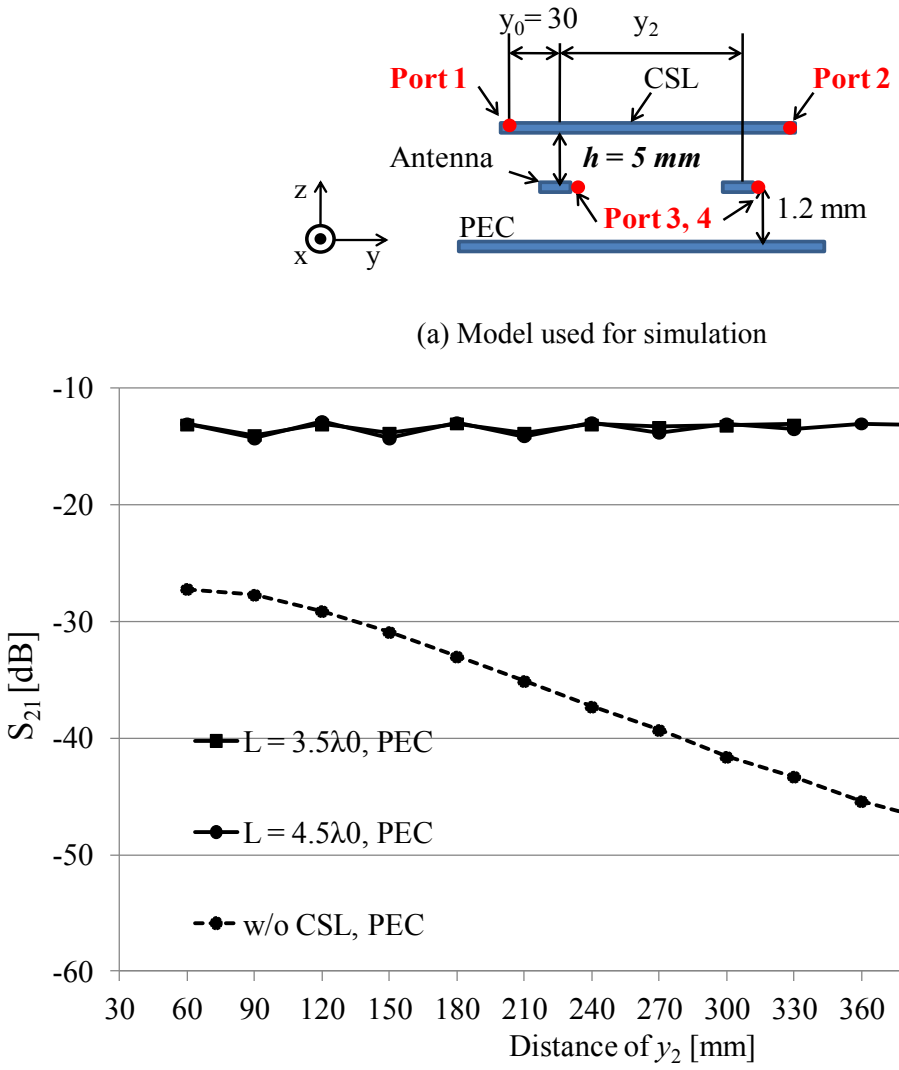

(a) Model used for simulation

(b) Coupling characteristics

Fig. 5.12. Coupling characteristics between two antennas with CSL on PEC plane when the length of CSL is changed from 430 mm ($3.5\lambda_0$) to 550 mm ($4.5\lambda_0$).

5.2.2 Optimal Parameters on the Phantom Model

The process to find optimal parameters of CSL on phantom is the same as that on PEC plane.

5.2.2.1 Optimal Height on the Phantom Model

To find the optimal height of CSL from PEC plane, the model as shown in Fig. 5.13 (a) is used. In this model, the antennas are placed far from PEC plane a fixed distance of 1.2 mm, below CSL. The coupling between two antennas is calculated at different height of h = 1,2,.., and 20 mm. The simulation results are shown in Fig. 5.13 (b). We can see that when *h* increases, S43 increases. This trend is opposite results on PEC. The distance of *h* should be bigger than 5 mm to get S43 ≥ -30 dB. Thus, we choose *h* = 5 mm for next steps. However, this optimal distance may change when the width changes.

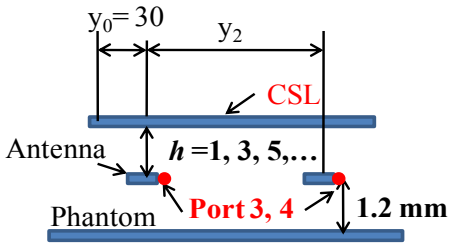

(a) Model used for simulation

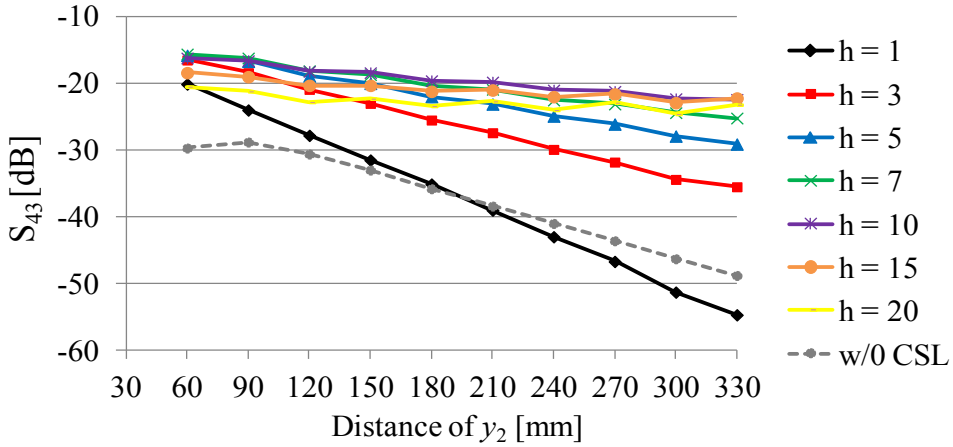

(b)Simulation results

Fig. 5.13. Transmission characteristics between two antennas on phantom model with CSL when the height is changed.

5.2.2.2 Optimal Width on the Phantom Model

We fix the length of the CSL, L = 430 mm ($3.5\lambda_0$) and the height h = 5 mm, only change the width W from 0.02 to 0.5 λ_0. The used model and simulation results as shown in Fig. 5.14 (a). The simulation results is shown in Fig. 5.14 (b). From the simulation results, we can see that the smaller width is, the higher perfomance is. Thus, we choose the optimal width W = 6 mm.

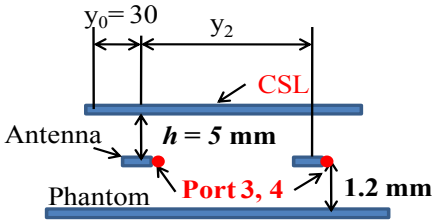

(a) Model used for simulation

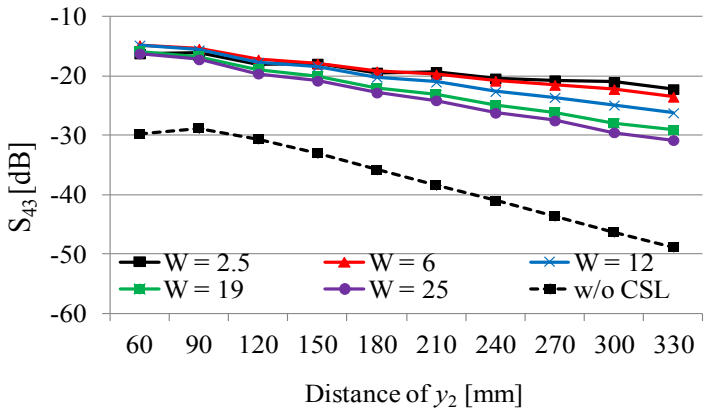

(b) Simulation results

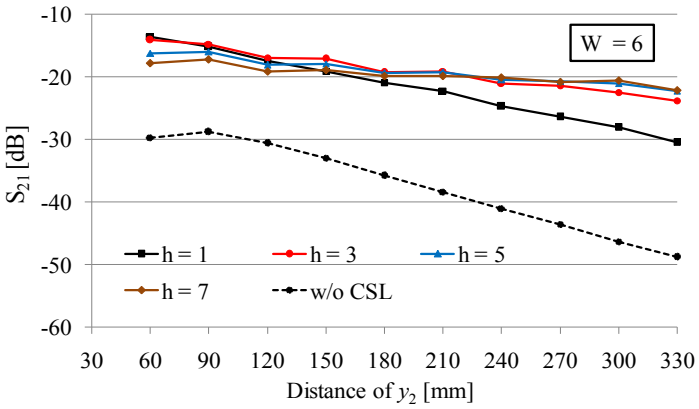

(c) Check the optimal height of h again with the optimal width.

Fig. 5.14. Transmission characteristics between two antennas on phantom model with CSL when the width is changed.

Then, we find the optimal height again with the optimal width of W = 6 mm. Results are shown in Fig. 5.14 (c), where the height should be higher than 1 mm, which is smaller than that when W = 19 mm (Fig. 5.13). As a results, when W = 6 mm, the height of the CSL can works well at any values. However, we choose h = 5 for parctical deployments, where the CSL is integrated into clothes and a spacing may exists between the body and the CSL.

5.2.2.3 Optimal Length on the Phantom Model

We increase the length of the CSL to $4.5\lambda_0$ which is long enough for practical applications. Then, the simulation results of the coupling between two antennas is calculated as shown in Fig. 5.15, where W = 6 mm, h = 5. The coupling in S_{43} is around 10 dB and reduces little when y_2 increases.

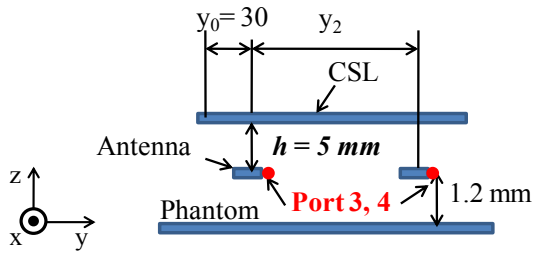

(a) Model used for simulation

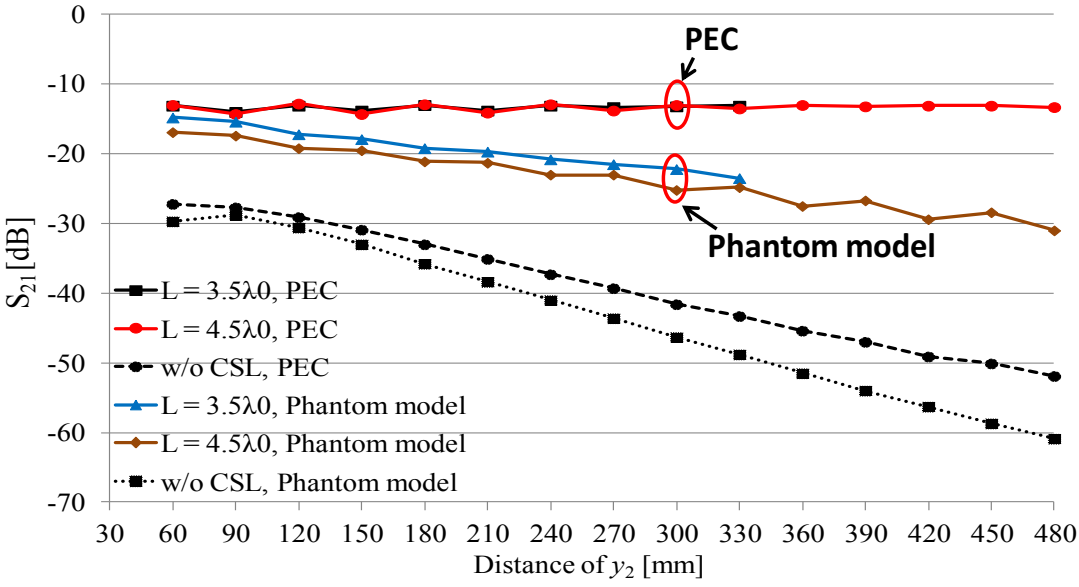

(b) Simulation results

Fig. 5.15. Coupling characteristics between two antennas with CSL on phantom model when the length of CSL is changed from 430 mm (3.5λ0) to 550 mm (4.5λ0).

In conclusion, the height of *h* from external antennas to the CSL should be higher than 5 mm while the width of the CSL should be smaller than 12 mm. The length of CSL can be extended to 4.5 λ_0 which is long enough for practical applications. The performance of the CSL with the optimal parameters will be confirmed in next section.

5.3 Measurement on the PEC plane

This section presents the measured results on the PEC plane with the CSL. The measured results on the PEC plane are shown in Fig. 5.16. The simulation results agree well with measurement results.

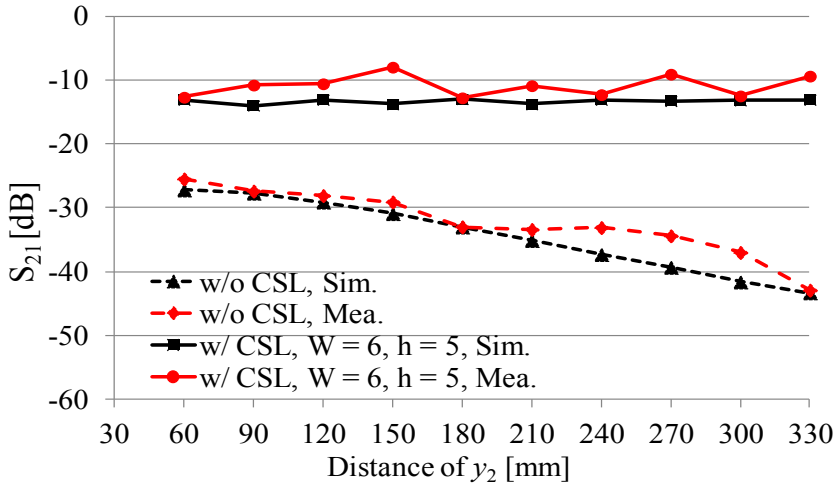

Fig. 5.16. Measured results of the transmission characteristics between two antennas with the CSL on the PEC plane.

5.4 Measurement on the Phantom

We measure the coupling between two antennas with the CSL on the phantom in this section. To the patch antennas, the distance from the antennas to the phantom is 1.2 mm, and distance between the antennas and the CSL is 5 mm. To the standard dipoles, the distance from the antennas to the phantom and the distance between the antennas and the CSL is the same as 3.5 mm. We do measurement in three cases corresponding to the width of CSL W = 2.5, 6 and 19 mm.

5.4.1 Measurement with the Patch Antennas

Measurement setting with the patch antennas is shown in Fig. 5.17. In the case, the two antennas are placed at different sides of the phantom. The distance between the two antennas is 330 mm in the NLOS case whereas this distance is 270 mm in the LOS case.

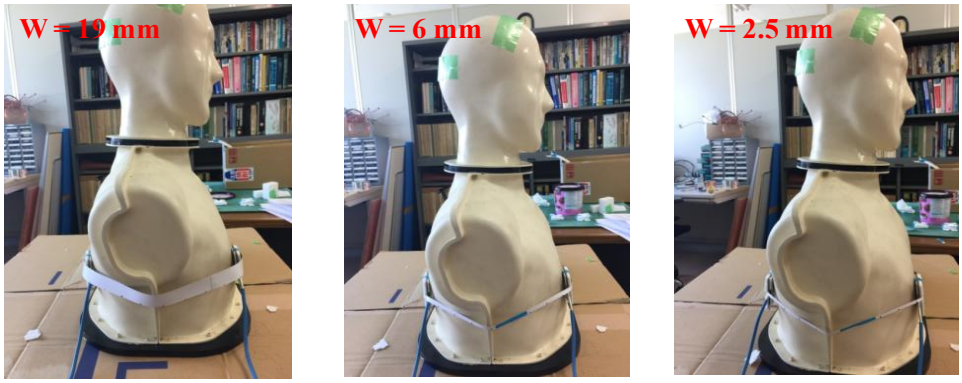

Fig. 5.17. Measurement pictures with the CSL and the patch antennas.

Measured results are shown in Fig. 5.18 and Table 5.2. From the results, we can see that couplings between two antennas when W = 2.5, 6 and 19 mm don't have much difference. This may be because of measurement errors. The transmission gain is more than 10 dB for the LOS case and 20 dB for the NLOS case. For practical employments, the width of the CSL should be 6 mm for flexibility and avoiding misalignment between the antennas and the CSL.

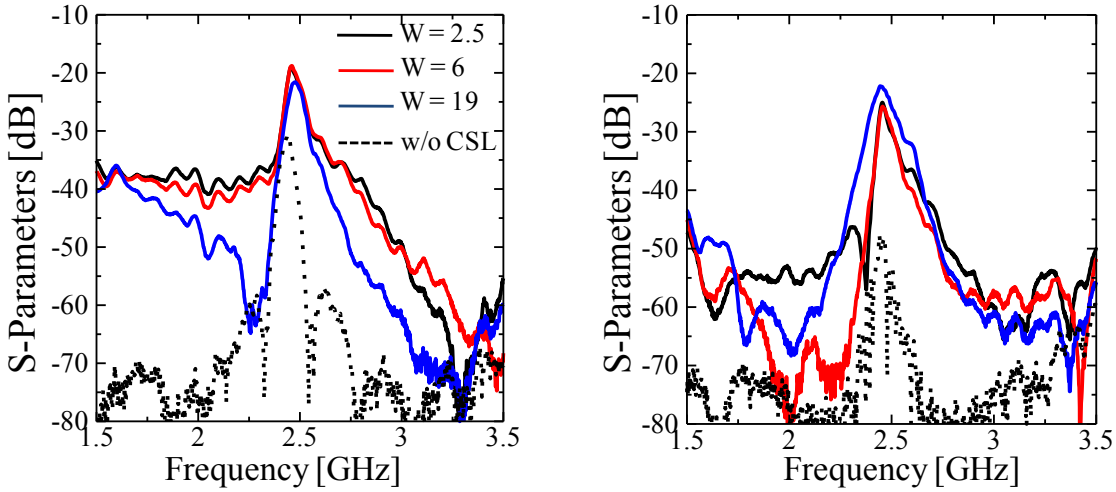

(a) (b)

Fig. 5.18. Transmission characteristics between two patch antennas with CSL on the phantom.

5.4.2 Measurement with the Standard Dipoles

Some measurement pictures with dipoles are shown in Fig. 5.19, where two dipoles are placed in front of the phantom. The distance between two dipoles is the same as the case of the patch antennas. In these measurements, the dipoles are put in horizontal. Measured results are given in Fig. 5.20 and Table 5.1. Transmission gain is more than 20 dB for NLOS, but there is no transmission gain for LOS case. This may be because the dipoles are affected by the CSL, which works as a reflector.

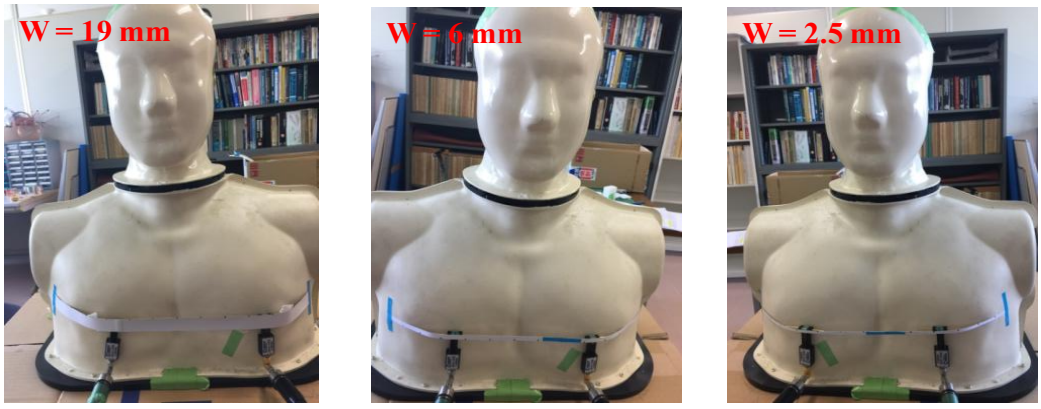

Fig. 5.19. Measurement pictures with two dipoles and the CSL.

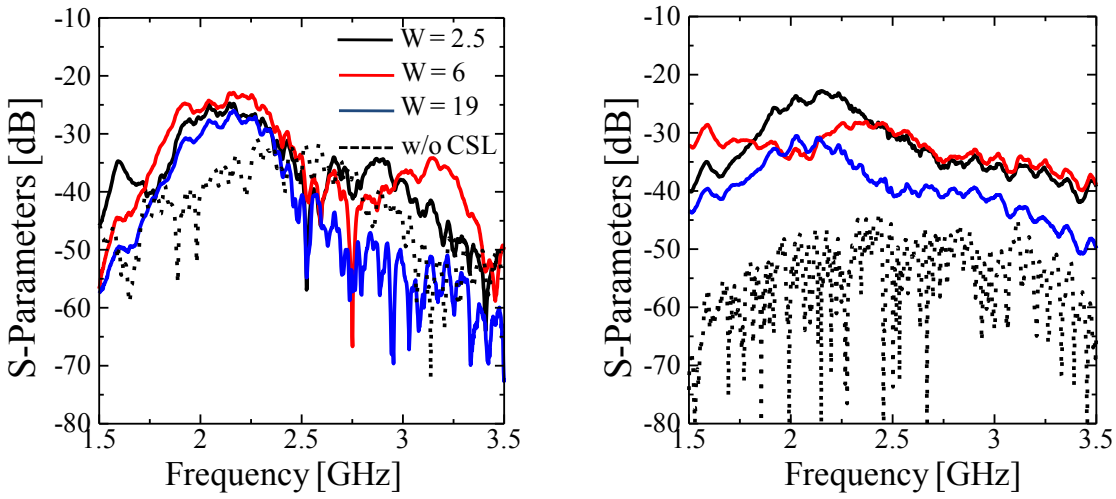

(a) LOS (b) NLOS

Fig. 5.20. Transmission characteristics between two standard dipoles with the CSL.

Table 5.2. Transmission gain by the CSL on the phantom.

Two antennas are in front of phantom – LOS case							
Types of antennas		Patch antennas			Dipoles		
w [mm]		2.5	6	19	2.5	6	19
S43	w/ CSL	-19.6	-19.5	-23.8	-33.7	-32.4	-31.7
	w/o CSL	-31.3	-31.3	-31.3	-32.6	-32.6	-32.6
Transmission gain		11.7	11.8	7.5	-1.1	0.2	0.9
One antenna is in front of phantom, the other is back – NLOS case							
Types of antennas		Patch antennas			Dipoles		
w [mm]		2.5	6	19	2.5	6	19
S43	w/ CSL	-25.4	-26.3	-22.3	-28.6	-28.3	-38.3
	w/o CSL	-49.2	-49.2	-49.2	-51.7	-51.7	-51.7
Transmission gain		24.4	22.9	26.9	23.1	23.4	13.4

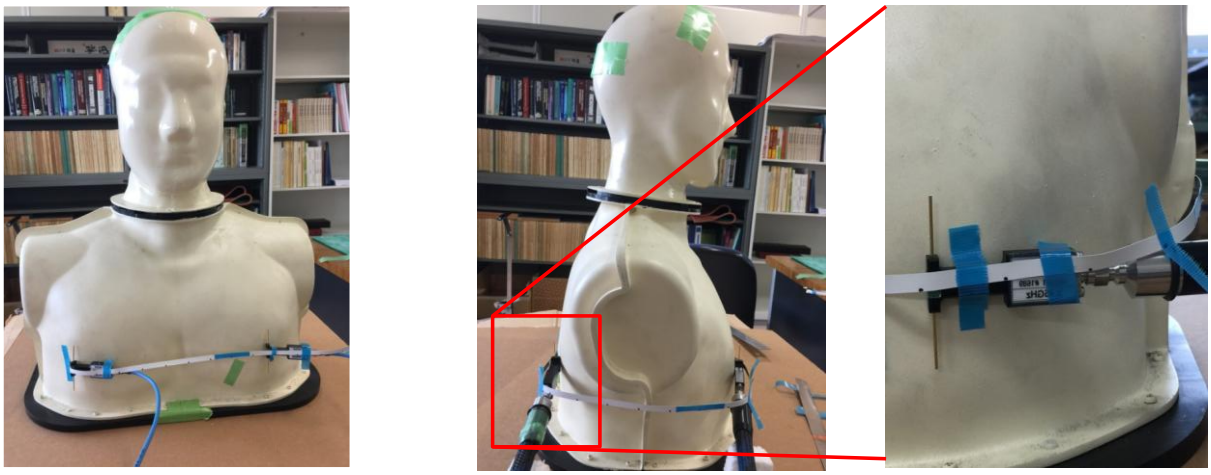

Fig. 5. 21. Measurement pictures with the two dipoles in vertical and the CSL.

Besides, measurements with dipoles in vertical are done to check the effect of the orientation of dipoles on the performance of CSL. Measurement pictures, results are shown in

Fig. 5.20, Fig. 5.21 and Table. 5.3. The results show that when dipoles are put in vertical, the performance of CSL is not as good as those when they are in horizontal.

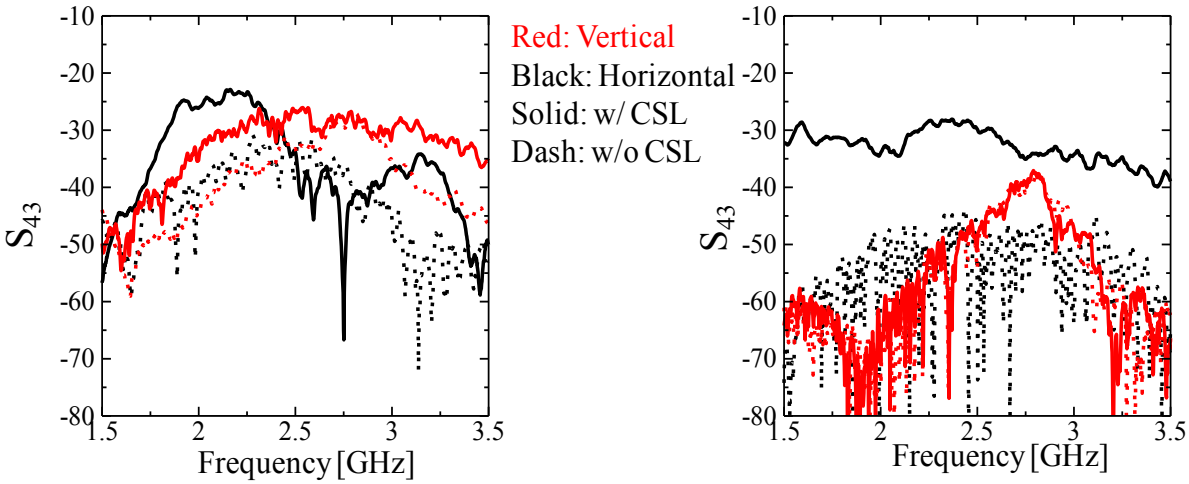

Fig. 5. 22. Measured results with the two dipoles in vertical and the CSL.

Table 5.3. Transmission gain by the CSL with the dipoles in vertical.

Dipoles are in front of phantom			
Orientation		H	V
S43	w/ CSL	-32.4	-26.8
	w/o CSL	-32.6	-30.8
Transmission gain		**0.2**	**4**
One dipole is front, the other is back			
Orientation		H	V
S43	w/ CSL	-28.3	-47.8
	w/o CSL	-51.7	-52.8
Transmission gain		**23.4**	**5**

5.5 Calculation of SAR

This section calculates SAR when the CSL is employed near the body. The way of calculation is the same as that of the SCPW. The width of the CSL is 6 mm. The results are given in Table 5.4 and 5.5 in two cases of h = 1 and 5 mm.

Table. 5.4. SAR with CSL, h = 1 mm.

y_2 [mm]	E_{max} [V/m]			**SAR** [W/kg]		
	P_1 = 0 dBm	P_2 = -6.5 dBm	P_3 = -7.55 dBm	**P_1 = 0 dBm**	**P_2 = -6.5 dBm**	**P_3 = -7.55 dBm**
60	47.82	22.8	20.1	**4.18**	**0.95**	**0.74**
90	69.4	33.1	29.2	**8.81**	**2**	**1.56**
120	46.2	22	19.4	**3.9**	**0.89**	**0.69**
150	50.4	24	21.2	**4.65**	**1.06**	**0.83**
180	43	20.5	18.1	**3.39**	**0.77**	**0.6**
210	60.8	28.9	25.6	**6.75**	**1.53**	**1.2**
240	50.7	24.1	21.3	**4.69**	**1.07**	**0.83**
270	42.2	20.1	17.8	**3.26**	**0.74**	**0.58**
300	39.1	18.6	16.4	**2.8**	**0.64**	**0.5**
330	55.2	26.3	23.2	**5.58**	**1.27**	**0.99**

We use the simplified phantom model to get maximum amplitude of E-field, and then use the equation in Section 2.2.1.4 to calculate. The width of CSL is 6 mm. Detailed results are given in Table 5.3 and 5.4, corresponding to h = 1 mm and h = 5 mm. From the results, we observe that SAR is satisfied when input power of antennas is around – 10 dBm, which is acceptable for on-body application.

In conclusion, this chapter presented a performance comparison between the SCPW and the CSL. The results show that the CSL can be replaced the SCPW in the case of the antennas placed between the body and the SCPW. Moreover, the optimal dimension parameters of the CSL were found. The width of the CSL is 6 mm while the height from the

antennas to the CSL should be greater than 5 mm. Finally, the performance of the CSL was confirmed by measurements on the PEC plane and on the phantom.

Table. 5.5. SAR with CSL, h = 5 mm.

y_2 [mm]	E_{max} [V/m]			**SAR** [W/kg]		
	P_1 = 0 dBm	P_2 = -9.5 dBm	P_3 = - 8.4 dBm	P_1 = 0 dBm	P_2 = -9.5 dBm	P_3 = -8.4 dBm
60	48.4	18.5	16.4	4.3	0.6	0.5
90	60.9	23.3	20.6	6.8	1	0.8
120	53.3	20.4	18	5.2	0.8	0.6
150	49.3	18.9	16.6	4.4	0.7	0.5
180	41.2	15.8	13.9	3.1	0.5	0.4
210	64.7	24.8	21.9	7.7	1.1	0.9
240	86.4	33.1	29.2	13.6	2	1.6
270	61.1	23.4	20.6	6.8	1	0.8
300	43.6	16.7	20.6	3.5	0.5	0.8
330	47.6	18.2	20.6	4.1	0.6	0.8

CHAPTER 6

CONCLUSION

This chapter concludes the Thesis, providing summary of the problems addressed, highlighting the major results, and proposing topics for future investigation.

6.1 Summary

Body Area Networks (BANs) plays an important role in the next generation of wireless systems, connecting personalization and convergence, through a wearable sensor network. A key challenge for on-body communications is the influence of human body on the wireless channel. Our study is motivated by this challenge. The main objective of the work is to analyze the effect of human body on the loss between on-body antennas/ sensors and find solutions to reduce these losses to improve the reliability of on-body communication. Our idea is by using low loss channels for on-body sensors. These channels are supplementary waveguides concentrating energy around them. The thesis is organized as follows.

Chapter 1 introduces a general overview of the thesis, presenting motivations and then pointing out the purpose of this study or novelties of the proposed transmission line for on-boy communication. Next, two strong 3D software tools are also introduced, which are CST software and EMPro software. The outline of the thesis is also given in this chapter.

Chapter 2 prompts important theories for dimension parameters of the proposed transmission line. The characteristics of coplanar waveguide which is applied to the proposed transmission line are discussed in detail such as the impedance, the losses, the effect of dielectric substrate thickness, the thickness of conductive layer. A comparison between CPW and microstrip line is also done. Another important content of this chapter is related to on-body communication. Characteristics of tissues at 2.45 GHz are discussed, but some simplified models are used for easy simulation and measurement like PEC, simplified liquid phantom and human body model. Mechanisms of on-body propagation and body channel are mentioned, which are very useful to design the transmission line in term of improvement target. The standards of SAR are discussed to compare to SAR values when the proposed transmission line is employed near body. Besides, a simplified equation to calculate SAR is given.

Chapter 3 describes the design of the proposed transmission line. The transmission line has a periodic structure, consists of some basic units connected in series. Each unit is a combination of modified two-side coupled half-wavelength ($\lambda/2$) resonators. Its dimension parameters are optimized so that the bandwidth is the biggest and the coupling between port 1 and port 2 is the highest. First, one basic unit is simulated to find dimension parameters, which are kept unchanged when the number of units increases. This makes the mass production process simple and not costly. The effect of body on the transmission line is considered at two frequencies 2.45 GHz and 5.12 GHz. The transmission line has been fabricated at both frequencies and the measured results agree well with the simulation results. Next, the minimum distance where the effect of body can be neglected from the transmission line to body is 5 mm and 7 mm corresponding to 5.12 GHz and 2.45 GHz, respectively. This distance decreases when the operating frequency increases because the electrical distance between the body and the transmission line increases. Then, the performance of the bent transmission line is discussed. The simulation results show that the proposed transmission line is influenced little by bending, which is useful for on-body communication. Moreover, the coupling power between the transmission line or the SCPW with the square patch antennas is presented in both simulation and measurement. The coupling power is higher than that on body without the transmission line. Some other discussions are also described like losses of paper substrate, mismatch between simulation and measurement.

Chapter 4 presents the improvement of transmission characteristics between on-body antennas/ sensors by the SCPW. Three cases corresponding to relative positions of antennas to SCPW are considered respectively: the first case is that antennas are below the SCPW; the second is that antennas above SCPW and the third is antennas are at different sides of the SCPW. We simulated and measured with PEC plane which is assumed to work as a body. The results show that the coupling improvement is more than 10 dB for small y_2 and 20 dB for large y_2. This is verified by measurement on real phantom and real bodies. Especially, the improvement by the SCPW is much higher for NLOS cases. Furthermore, SAR is calculated for each case, and the results show that SAR values are satisfied when input power of antennas is in the range from -20 to 0 dBm, which is accepted power for on-body sensors. Finally, radiation direction of antennas, radiation loss of the SCPW and orientation of antennas are discussed by simulation results. The results show that the direction of antennas should be toward the SCPW while the radiation of the SCPW is necessary for high coupling between the SCPW with external antennas. Orientations of antennas affect the performance of SCPW. But, the proposed orientation is the best choice.

Chapter 5 proposes a simpler solution for on-body communication by using a conductive strip line (CSL). The performance of SCPW is compared to that of the CSL. The results show that CSL has a good performance when antennas are placed below the CSL. Next, optimal dimension parameters of the CSL are calculated. The width of CSL should be 6 mm, considering the flexibility for practical applications. Then, the performance of the CSL is confirmed on phantom.

This chapter concludes the thesis and gives some suggestions for future research.

6.2 Future work

In future work, the solution to employ the SCPW in practice will be validated by covering it by thin plastic film to avoid moisture and sweat, and integrating it in clothes. Moreover, the effect of moving users on the performance of the transmission line will be considered.

ACKNOWLEDGEMENT

My parents are poor farmers, who didn't receive any education from school but they used to say to their children that studying is the best way to get out of poverty and become a useful person for the society. I believed them, and I nurtured my dream of entering university, and then, studying abroad. Today, I can say that my dream becomes true, and I would like to express my sincere gratitude to all of people I met on my way.

My main acknowledgement goes to my supervisor, Prof. Hiroyuki Arai, who guided me with his leadership excellence. Thank you very much for your absolute support.

I would like to express my appreciation to the committee members, Prof. Takehiko Adachi, Prof. Toshihiko Baba, Assoc. Prof. Nobuhiro Kuga and Assoc. Prof. Koichi Ichige for giving me value comments and advices during my doctoral course.

I would also like to give many thanks to the University of Transport and Communication, Vietnamese, Ministry of Education and Training – Vietnam International Education Cooperation Department government for giving the opportunity to study in Japan.

I would also like to express my profound gratitude to my lab-mates Shinozaki Chan, Okura San, Riho San– my tutor, Hiro San, Sugimoto san, Yamamoto Kun, Kane Yan, Kanata, Sei, Yone and Yuya kun for their unconditional support.

Special thanks to Thomas and Roha who are like my family members in Japan always stand by me in the most difficult time and give me continuous encouragements.

Whatever I make or I feel, they always stay there to help me overcome difficulties - my dear family. Thanks to my beloved family, my husband and my daughter, you make me smile to move on every day.

TRAN THI LAN

15th August 2018

Yokohama, Japan

REFERENCES

[1] Bogdan Antonescu, Stefano Basagni, "Wireless body area networks: Challenges, trends and emerging technologies," [Online]. Avilable: http://www.ece.neu.edu/fac-ece/basagni/papers/AntonescuB13.pdf

[2] P. S. Hall, Y. I. Nechayev, C. C. Constantinou, Y. Hao, A. Alomaainy, R. Dubrovka, and C. G. Parini, "Antennas and Propagation for on-body communication system," *I*EEE Antennas and Propagation Magazine, Vol. 49, No. 3, pp. 41-58, 2007.

[3] V. Pleskachev, I. Vendik, O. Vendik, V. Kirillov, P. Turalchuk, and M. Odit, "On-body surface electromagnetic wave propagation: Modeling and Measurements", 10th EuCAP, 2016.

[4] A. Pellegrini, A. Brizzi, L. Zhang, K. Ali, Y. Hao, X. Wu, C. C. Constantinou, and et al., "Antennas and Propagation for Body-Centric Wireless Communications at Millimeter-Wave Frequencies: A Review," *IEEE Antennas and Propagation Magazine*, vol. 55, no. 4, pp. 262-287, Aug. 2013.

[5] M.Koohestani, J.F.Zürcher, A. A. Moreira, and A. K. Skrivervik, "Anovel, low-profile, vertically-polarized UWB antenna for WBAN,"*IEEE Trans. Antennas Propag.*, vol. 62, no. 4, pp. 1888-1894, Apr. 2014.

[6] Purna B. Samal*,* Ping Jack Soh, and Guy A. E. Vandenbosch*, "*UWB All-Textile Antenna With Full Ground Plane for Off-Body WBAN Communications," IEEE Trans. Antennas Propag., vol. 62, no. 4, pp. 102-108, Jan. 2014.

[7] A.Michalopoulou, A. A. Alexandridis, K.Peppas, T.Zervos, F.Lazarakis, K.Dangakis, andD. I. Kaklamani, "Statistical Analysis for On-Body Spatial Diversity Communications at 2.45 GHz," *IEEE Trans. Antennas Propag.*, vol. 60, no. 8, pp. 4014-4019, Aug. 2012.

[8] Q. H. Abbasi, E.Serpedin, K.Qaraqe, A.Alomainyand Y. Hao, "Multiband-OFDM based Ultra Wideband System Modelling of On/Off-Body Antenna Diversity," IEEE International Symposiumon *Antennas* and Propagation & USNC/URSI National Radio Science Meeting, 2015, pp. 2363-2364.

[9] Y. Yao, J. Zheng,and Z. Feng, "Diversity Measurements for On-Body Channels Using a

Tri-Polarization Antenna at 2.45GHz," *IEEE antennas and wireless propagation letters*, vol. 11, pp. 1285-1288, 2012.

[10] C.Mikeka and H. Arai, "Novel wearable sensors for body area network applications," in *Microwave and Millimeter Wave Circuits and Systems: Emerging Design, Technologies, and Applications*, 1st ed., John Wile& Sons, 2012.

[11] H. Arai, "Free access transmission line for body centric communication (Invited)," *2015 IEEE MTT-S 2015 International Microwave Workshop Series on RF and Wireless Technologies for Biomedical and Healthcare Applications (IMWS-BIO)*, Taipei, 2015, pp. 136-137.

[12] Y. Shinozaki, T. Okura and H. Arai, "Coupling characteristics between two dipole antennas over free access transmission line using paper substrate," *2016 International Symposium on Antennas and Propagation (ISAP)*, Okinawa, 2016, pp. 310-311.

[13] T. L. Tran, Y. Shinozaki, and H. Arai, "A Flexible Transmission Line Using Coplannar Waveguide for On-body Links," *2017 ISAP*, Phuket, Thailand.

[14] T. Okura, and H. Arai, "One-dimensional free access transmission line for RFID reader," *IEICE comex*, vol.2, no.1, 7-11, 2013.

[15] Rainee N. Simons, "Conventional Coplanar waveguide," in *Coplanar waveguide circuits, Components, and systems*, John Wiley&Sons, 2001.

[16] CST software. [Online]. Available: https://www.cst.com/products/cstmws

[17] EMPro software. [Online]. Available: http://www.keysight.com/en/pc-1297143/empro-3d-em-simulation-software?cc=GB&lc=eng

[18] N. P. B. Kammersgaard, S. H. Kvist, J.Thaysenand K. B. Jakobsen, "Validity of PEC Approximation for On-Body Propagation," 10th EuCAP, Apr. 2016.

[19] Z. Ma, J.Sarrazin, L. Petrillo and T.Mavridis, "Antenna Radiation Characterization for On-Body Communication Channel Using Creeping WaveTheory," 9thEuCAP,Apr. 2015.

[20] K. Fukunaga, S. Watanabe and Y. Yamanaka, H. Asou, Y. Ishii and K. Sato, "Dielectric properties of liquid phantoms for evaluations of mobile phones," *IEICE EMC'04*, Sendai, Japan.

[21] M. Rizwan, M. W. A. Khan, L. Sydanheimo and L. Ukkonen, "Performance evaluation of circularly polarized patch antenna on flexible EPDM substrate near human body," 2015 LAPC.

[22] C. A. Balanis, “Microstrip antennas,” in *Antenna Theory*, John Wiley & Sons, 3rded., pp. 816-843, 2005.

[23] FINEST function. [Online]. Available: https://support.office.com/en-us/article/LINEST-function-84D7D0D9-6E50-4101-977A-FA7ABF772B6D

[24] J. Wolberg, “The method of least squares,” in *Data Analysis using the method of least squares*, Springer, 2006.

[25] Phantom [Online]. Avilable: http://www.mwf.co.jp

[26] Y. Shinozaki and H. Arai, “Free access transmission line using paper substrate in body area network,” 2017 International Workshop on Electromagnetics: Applications and Student Innovation Competition, IEEE, 2017.

[27] K. C. Gupta, Ramesh Garg, InderBahl, and Prakash Bhartia, “Microstrip lines and Slotlines,” Chapter 7, 2nd ed., Artech House, 1996.

[28] R. Chandra and A. J. Johansson, “An elliptical link loss model for wireless propagation around the human torso,” 6th EUCAP, 2012.

[29] Phatak, D.S., et al., “Dispersion characteristics of optically excited coplanar striplines: Comprehensive full-wave analysis,” IEEE Trans., Vol. MTT-38, 1990, pp. 1719-1730.

[30] Riaziat, M., et al., “Propagation modes and dispersion characteristics of coplanar waveguide,” IEEE Trans., Vol. MTT-38, 1990, pp. 245-251.

[31] Jackson, R. W., “Considerations on the use of coplanar waveguide for millimeter-wave integrated circuits,” IEEE Trans, Vol. MTT-34, 1986, pp. 1450-1456.

[32]http://www.rfwireless-world.com/Terminology/Microstrip-line-vs-Coplanar-Waveguide.html

[33]http://www.qsl.net/va3iul/Microstrip_Stripline_CPW_Design/Microstrip_Stripline_and_CPW_Design.pdf

[34] Kyung Sup Kwak, Sana Ullah, and Niamat Ullah, “An Overview of IEEE 802.15.6 Standard,” 978-1-4244-8132-3/10/$26.00 ©2010 IEEE.

[35] Dhafer Ben Arbia, Muhammad Mahtab Alam, Yannick Le Moullec,and Elyes Ben Hamida, “Communication Challenges in On-Body and Body-to-Body Wearable Wireless Networks—A Connectivity Perspective,” Technologies, 2017.

[36] Ian F.Akyildiz and Mehmet Can Vura, “Wireless sensor network,” WILEY, 2010.

[37] https://en.wikipedia.org/wiki/Specific_absorption_rate

[38] Jianqing Wang and Qiong Wang, “Body Area Communications: Channel Modeling, Communication Systems, and EMC,” Chapter 2, 1st edition, John Wiley & Sons Singapore Pte. Ltd. 2013.

[39] Fort,A., Ryckaert,J., Desset,C., Doncker,P. and Wambacq,P., “Ultra-Wideband Channel Model for Communication Around the Body”, IEEE Journal on Selected Areas in Communications, Vol. 24, No. 4, Apr. 2006, pp. 927-933.

[40] IEEE, Channel Models for WBANs - NICT, IEEE P802.15 Working Group for Wireless Personal Area Networks, IEEE P802.15-08-0416-04-0006, USA, Nov. 2008.

[41] Takada,J., “Static Propagation and Channel Models in Body Area”, TD(08)639, in Proc. of COST 2100 - 6th Management Meeting, Lille, France, Oct. 2008.

[42] Ryckaert,J., Doncker,P., Meys,R., Hoye,A. and Donnay,S., “Channel model for wireless communication around human body”, Electronic Letters, Vol. 40, No. 9, Apr. 2004, pp. 543-544.

[43] Fort,A., Desset,C., Wambacq,P. and Biesen,L., “Indoor body-area channel model for narrowband communications”, IET Microwaves, Antennas & Propagation, Vol.1, No. 6, Dec. 2007, pp. 1197-1203.

[44] Scott, J., Hoffmann, F., Addleseet, M. et al. (2002) Networked surfaces: a new concept in mobile networking. ACM Mobile Networks and Applications, 7 (5), 353–364.

[45] Minami, M., Nishizawa, Y., Hirasawa, K. et al. (2005) MAGIC surfaces: magnetically interfaced surfaces for smart space applications, 3rd International Conference on Pervasive Computing, Munich, Germany, pp. 59–64.

[46] Minami, M., Nishizawa, Y., Hirasawa, K. and Aoyama, T. (May 2007) Deployment Scalable Sensor Networks,ISSN 0913-5685.

[47] Fukumoto, M. and Shinagawa, M. (2005) CarpetLAN: a novel indoor wireless(-like) networking and positioning system. 7th International Ubiquitous Computing, pp. 1–18.

[48] Sekitani, T., Takamiya, M., Noguchi, Y. et al. (2007) A large-area wireless power-transmission sheet using printed organic transistors and plastic MEMS switches. Nature Materials, 6, 413–417.

[49] Makino, Y. and Shinoda, H. (2005) Selective stimulation to superficial mechanoreceptors by temporal control of suction pressure. 1st Joint Eurohaptics Conference and Symposium on Haptic Interfaces for Virtual Environment and Teleoperator Systems, 18–20 March 2005,World Haptics, pp. 229–234.

[50] Makino, Y., Minamizawa, K. and Shinoda, H. (2005) Sensor networking using two-dimensional electromagneticwave. IEEJ 22nd Sensor Symposium, pp. 83–88.

[51] Makino, Y. and Shinoda, H. (2006) Wrist band type man–machine interface for two-dimensional measurement of mechanoreceptors. 23rd Sensing Forum, pp. 293–298.

[52] Kunsun Om, Doctaral thesis “Sheet-like Waveguide for Short-Range Wireless Communication and Its Applications,” 2011.

LIST OF PUBLICATIONS

Journal papers

1. Tran Thi Lan, Yuka Shinozaki, Takuya Okura, and Hiroyuki Arai, "A free access segmented coplanar waveguide for on-body communication," *IEEE Transactions on Antennas and Propagation*, 2018, "Accepted".
2. Tran Thi Lan and Hiroyuki Arai, "Propagation Loss Reduction between On-body Antennas by Using a Conductive Strip Line," *Antennas and Wireless Propagation Letters*, 2018, "Submitted".

International conferences

1. Tran Thi Lan, Yuka Shinozaki and Hiroyuki Arai, "A Flexible Transmission Line Using Coplannar Waveguide for On-body Link," *2017 ISAP*, Phuket, Thai Land.

2. Tran Thi Lan, and Hiroyuki Arai, "Applications of the Segmented Coplanar Waveguide for On-body Links," *2018 VJISAP*, Da Nang, VietNam.

3. Tran Thi Lan and Hiroyuki Arai, "A Performance Comparison between a Conductive Strip Line and the Transmission Line in Improving On-body Communication," *2018 ISAP*, Busan, Korea, (Accepted).

IECE General/ Society Conferences

1. Tran Thi Lan, Takuya Okura, and Hiroyuki Arai, "A Free Access Transmission Line Using Coplanar Waveguide Structure for BAN", *IEICE General Conference*, Fukuoka, Sep. 2016.

2. Tran Thi Lan, Takuya Okura, and Hiroyuki Arai, "Performance Evaluation of the Free Access Transmission Line Using Coplanar Waveguide Structure for BAN", *IEICE Society Conference*, Hokkaido, Sep. 2016.

3. Tran Thi Lan, Yuka Shinozaki, and Hiroyuki Arai, "Transmission Improvement of the Free Access Transmission Line Using Coplannar Waveguide Structure for BAN", *IEICE General Conference*, Nagoya, Mar. 2017.